INVESTIGATION OF FIBER OPTIC EMBEDDING PROCESSES WITHIN DIFFERENT TYPES OF MATERIALS

BY

HAMMAM SAEED RIZQ DARAGHMA

A Thesis Presented to the

DEANSHIP OF GRADUATE STUDIES

KING FAHD UNIVERSITY OF PETROLEUM & MINERALS

DHAHRAN, SAUDI ARABIA

In Partial Fulfillment of the
Requirements for the Degree of

MASTER OF SCIENCE

In

MECHANICAL ENGINEERING

MAY 2017

KING FAHD UNIVERSITY OF PETROLEUM & MINERALS

DHAHRAN- 31261, SAUDI ARABIA

DEANSHIP OF GRADUATE STUDIES

This thesis, written by **Hammam Saeed Rizq Daraghma** under the direction his thesis advisor and approved by his thesis committee, has been presented and accepted by the Dean of Graduate Studies, in partial fulfillment of the requirements for the degree of **MASTER OF SCIENCE IN MECHANICAL ENGINEERING**

Dr. Samir Mekid
(Advisor)

Dr. Zuhair Qasem
Department Chairman

Dr. Saheb Nouari
(Member)

Dr. Salam A. Zummo
Dean of Graduate Studies

18/12/17
Date

Dr. Salem Bashmal
(Member)

2017

Dedicated

*To hometown **PALESTINE***

*To **JERUSALEM***

*To **AL-AQSA***

*To whom stationed in **AL-AQSA MOSQUE***

*Not forget **GAZA**'s heroes*

*To all Muslim **MARTYRS** and **PRISONERS** especially **PALESTINIAN***

*To who support and pray for me all the time my FATHER (**SAEED**), my MOTHER (**DALAL**)*

*To my BROTHERS (**BAKR, SOHAIB, AHMAD**) and My lovely SISTER (**ATHEER**).*

To My father's grandchildren

*To my life partner, my love, who carry that brilliant smile '**my wife (TASNEEM)**'*

ACKNOWLEDGMENTS

First and foremost. I have to thank, Almighty ALLAH for all things in my life and all the blessings that he has given.

(الحمد لله رب العالمين) سورة الفاتحة

Secondly, I would like to grab the chance to express profound, and deepest appreciation to my second father, advisor not in academic path even in the life, for his full support, encouragement, and guidance throughout the thesis

Prof. Samir Mekid

All my thanks to my committee members **Dr. Saheb Nouari** and **Dr. Salem Bashmal**. Also, thanks for KFUPM for providing me an opportunity to get M.Sc. Degree.

Also, I would like to acknowledge the National Science, Technology and Innovation Plan (NSTIP) for the financial support they provided. Moreover, my thanks to all technical staff who help me during my experimental work.

Finally, thanks to friends and Palestinian community at KFUPM. Especially, my brothers **Saif Najmeddin, Fadi Abu Samra, Amjad Abu Hassan, Bilal Karaki, and Iswan Pradiptya.**

TABLE OF CONTENTS

ACKNOWLEDGMENTS ..... **V**

TABLE OF CONTENTS ..... **VI**

LIST OF TABLES ..... **IX**

LIST OF FIGURES ..... **XI**

LIST OF ABBREVIATIONS ..... **XVI**

ABSTRACT ..... **XVII**

ملخص الرسالة ..... **XIX**

CHAPTER 1 INTRODUCTION **1**

1.1 BACKGROUND 1

1.2 STRUCTURAL HEALTH MONITORING (SHM) 3

1.2.1 Intelligence and smartness in materials *4*

1.2.2 Optical fibers *8*

1.3 FIBER OPTIC EMBEDDING 9

1.4 PROBLEM STATEMENT 10

1.5 WORK APPROACH: 11

1.6 MOTIVATION OF THE PRESENT WORK 12

1.7 WORK OBJECTIVES: 13

1.8 REPORT STRUCTURE 14

CHAPTER 2: LITERATURE REVIEW 15

2.1 FIBER OPTIC CHARACTERISTICS 15

2.2 HOST MATERIALS 17

2.3 ULTRASONIC CONSOLIDATION (UC): 19

2.3.1 Theoretical background 22

2.3.2 A literature review of UC process: 25

2.3.3 Fiber embedding using UC 27

2.4 POWDER METALLURGY (PM): 28

CHAPTER 3: FIBER OPTIC AND HOSTING MATERIAL: CHARACTERIZATION BEFORE EMBEDDING 31

3.1 FIBER CHARACTERIZATION BEFORE EMBEDDING: 31

3.1.1 Temperature resistance tests: 31

3.1.2 Temperature characterization of FBG 35

3.1.3 Pressure test 37

3.1.4 Checking fiber cross section 39

3.2 EMBEDDING IN THE HOST USING (USW) 39

3.2.1 Embedding power estimation 40

3.2.2 Experimental work 43

CHAPTER 4: FIBER OPTIC EMBEDDING USING ULTRASONIC CONSOLIDATION 46

4.1 FIBER EMBEDDING 46

4.1.1 Indirect ultrasonic consolidation 46

4.1.2 Direct ultrasonic consolidation 49

4.2 POWER LIGHT TEST 58

4.2.1 Indirect ultrasonic consolidation 58

CHAPTER 5: ALTERNATIVE METHODS FOR EMBEDDING (POWDER METALLURGY) 61

5.1 INTRODUCTION 61

5.2 DIE DESIGN 62

5.3 FINITE ELEMENT ANALYSIS (FEA) FOR THE BEAM 62

5.3.1 Modeling 63

5.4 COLD COMPACTION 71

5.4.1 Experimental Work 71

5.4.2 Power light test 79

5.5 SPARK PLASMA SINTERING (SPS) 80

CHAPTER 6: RESULTS AND DISCUSSION 91

6.1 CHARACTERIZATION OF THE EMBEDDING PROCESS PARAMETERS: 91

6.2 POWER LIGHT TRANSMISSION 96

CHAPTER 7: CONCLUSION AND RECOMMENDATIONS 98

7.1 CONCLUDING REMARKS 98

7.2 ACCOMPLISHMENTS 98

7.3 FUTURE WORK 99

REFERENCES 100

VITAE 108

LIST OF TABLES

Table 3.1: Heat test records 32

Table 3.2: Polyimide coated fiber properties [60] 35

Table 3.3: The amplitude and the corresponding generated power 43

Table 3.4: Preliminary results for welding hosting material 44

Table 4.1: Fiber embedding between two sheets 48

Table 4.2: Embedding using smaller friction area 50

Table 4.3: Embedding using larger friction area 51

Table 4.4: Test for one spot welding 59

Table 4.5: Test for two spot welding 59

Table 4.6: Test for three spots welding 60

Table 5.1: Meshing convergence 65

Table 5.2: Comparison of the analytical results and the ANSYS results 70

Table 5.3: First trial for compaction 71

Table 5.4: First sintering parameters 72

Table 5.5: Preliminary results of compaction and sintering 73

Table 5.6: Last test to define the proper compaction and sintering parameters 74

Table 5.7: Compaction and sintering test results 75

Table 5.8: Power light test comparison..... 80

Table 5.9: SPS parameters 84

Table 5.10: Microscopic picture for the cross section 88

LIST OF FIGURES

Figure 1.1 The nervous system of human body [1] 2

Figure 1.2: Self-Health Monitoring System [5] 4

Figure 1.3: Material classification [8] 5

Figure 1.4: Classification of smart material [12] 6

Figure 1.5: Basic structure of the optical fiber [16] 8

Figure 1.6: Typical cross section for a) multimode fiber 50/125 b) multimode fiber 62.5/125 c) single mode [18] 9

Figure 2.1: Basic principle of ultrasonic consolidation [38] 20

Figure 2.2: Ultrasonic welder with rotatory sonotrode [41] 20

Figure 2.3: Effects of reflecting and passing properties of the materials [42] 21

Figure 2.4: Weldability between the various metals [44] 26

Figure 2.5: Compaction stage 29

Figure 2.6: Schematic of SPS process [59] 30

Figure 3.1: Heat test a) labeled fibers b) fiber inside the furnace 32

Figure 3.2: Lab setup showing connections and instruments/apparatus used 36

Figure 3.3: (a) spectra of wavelength shift with varying temperature (°C)

(b) linear response of wavelength shift to temperature variation [60]..... 37

Figure 3.4: Experiment setup for a pressure test..... 38

Figure 3.5: Measured strain during pressure sensitivity test for fiber 38

Figure 3.6: Cut fiber a) using cleaver b) using scissor 39

Figure 3.7: Ultrasonic spot welding machine 40

Figure 3.8: Modified friction area a) large area b) small area 41

Figure 3.9: Initial experimental configuration..... 44

Figure 4.1: Initial configuration for embedding process a) with Al- foils b) without

Al-foils..... 47

Figure 4.2: Embedded fiber a) with Al-foils b) without Al-foils..... 47

Figure 4.3: Direct ultrasonic consolidation..... 49

Figure 4.4: The profile of the generated energy by the machine a) welding time (0-10)

sec b) welding time (0-1) sec..... 54

Figure 4.5: The profile of the energy flux due to small areaa) welding time (0-10) sec b) welding time (0-1) sec 55

Figure 4.6: The profile of the energy flux due to large area a) welding time (0-10) sec b) welding time (0-1) sec 56

Figure 4.7: Energy flux due to both area a) welding time (0-10) sec b) welding time (0-1) sec 57

Figure 4.8: Power Light Transmission Test configuration 58

Figure 5.1: Die Design a) Initial design b) Second design 62

Figure 5.2: The geometry of the beam 63

Figure 5.3: Meshing the beam 64

Figure 5.4: Von Mises stress distribution 66

Figure 5.5: Stress distribution on the cross section 67

Figure 5.6: Total strain distribution 67

Figure 5.7: Strain distribution on the cross section 68

Figure 5.8: Stress and strain distribution for cross bar a, b) bending load c, d) torsion load 68

Figure 5.9: SEM picture for compacted samples 40 sec a) 25000 Ib b) 35000 Ib..... 72

Figure 5.10: Pressure profile..... 77

Figure 5.11: Temperature profile..... 78

Figure 5.12: Broken samples 79

Figure 5.13: Compacted sample 79

Figure 5.14: Graphite dies..... 81

Figure 5.15: Modified die 81

Figure 5.16: Spark Plasma Sintering process 82

Figure 5.17: Spark Plasma Sintering machine..... 82

Figure 5.18: Flushing out of the powder from the die 83

Figure 5.19: Pressure and Temperature profiles for SPS samples..... 87

Figure 5.20: Measured relative density..... 89

Figure 5.21: Measured hardness 90

Figure 6.1: Progressive embedding of the fiber inside aluminum at high allowance level of energy using both areas (Afr)s and (Afr)l..... 92

Figure 6.2: Problem Configuration with Model 93

Figure 6.3: a) Temperature (ºC) distribution at 20 kHz frequency, 8.4 µm amplitude and 50 MPa load on sonotrode, b) Experimental test with the same parameters on the machine..... 93

Figure 6.4: Measured temperature a) before US welding, b) zoomed at the time of US welding..... 94

Figure 6.5: Powder Metallurgy a) resulted sample b) cross section (magnification 10x) c) cross section (magnification 20x)..... 95

Figure 6.6: SEM for SPS sample with different sintering time a) one hour b) half-hour. 96

LIST OF ABBREVIATIONS

BGs	:	Bragg Gratings
FBGs	:	Fiber Bragg Gratings
FEA	:	Finite Element Analysis
NDT	:	Non-Destructive Test
PM	:	Powder Metallurgy
SM	:	Smart Material
SMA	:	Shape Memory Alloy
SPS	:	Spark Plasma Sintering
SS	:	Smart Structure
UC	:	Ultrasonic Consolidation
VI	:	Visual Inspection

ABSTRACT

Full Name : Hammam Saeed Rizq Daraghma

Thesis Title : Investigation of Fiber Optic Embedding Processes within Different Types of Material

Major Field : Mechanical Engineering

Date of Degree : May 2017

Both functional and monitored mechanical structures need to have sensors embedded inside the material. Metallic materials are mostly dominant. This work aimed at embedding fiber optics inside various types of materials e.g. powder based materials and aluminum.

The embedding processes were investigated for appropriateness depending on the host materials. Various trials with full process control have been carried out in ultrasonic consolidation for fiber optics to be embedded in aluminum, and normal insertion inside powder based materials. Finite Element Modeling has been carried out to identify and quantify triggering process parameters to support experiments.

These parameters include processing time, wavelength amplitude and contact area. The study of the effect of these parameters on the process has been investigated. The experimental tests have shown that progressive embedding is achieved using specific combined sets of parameters in the process and specifically full embedding of the fiber is

reached with welding time towards one second combined with a wavelength amplitude of 50% with small area of contact and for large area of contact with amplitude larger than 60% and welding time less than 1 sec.

The end process will result in the fiber embedded inside the material. The next concern is to check the integrity of the sensors in post process and also to verify that the sensor reproduces properly the behaviour of the material. Both integrity and reliability of reporting behaviour seem to be adequate and serve the purpose of measurement.

In powder based materials as host, cold compaction and Spark Plasma Sintering (SPS) were used to fabricate the material while the fiber optic was initial placed at the time of filling the die with the powder. The material has been prepared under different known conditions of compaction and sintering since care has to be observed on the embedded fiber e.g. high compaction pressure and sintering temperature can damage the fibers. Practical values in cold compaction technique were: 155 MPa compaction load and 450 ˚C sintering temperature applied for 6 hours. Regarding SPS, load of 20 MPa, and temperature of 400 ˚C applied for half-hour have been used.

This work has characterized the embedding process i.e. Ultrasonic Consolidation in aluminum and insertion of fibers in powder based materials to secure proper reading and protection of the sensors from delicate environment.

ملخص الرسالة

الاسم الكامل : همام سعيد رزق دراغمة

عنوان الرسالة : التحقيق في عمليات تضمين الألياف البصرية داخل أنواع مختلفة من المواد

التخصص : الهندسة الميكانيكية

تاريخ الدرجة العلمية : نيسان، 2017

تحتاج كل من الهياكل الميكانيكية الوظيفية و المستخدمة في المراقبة إلى وجود أجهزة استشعار مضمنة داخل المادة. يهدف هذا العمل إلى تضمين الألياف البصرية داخل أنواع مختلفة من المواد مثل مسحوق المواد والألومنيوم.

تم التحقيق في عمليات التضمين للحصول على تضمين ملائم اعتمادا على نوع المادة المستضيفة. وقد اجريت تجارب مختلفة مع تحكم كامل في العملية باستخدام الموجات فوق الصوتية لتضمين الألياف داخل الألمنيوم، وطريقة الإدراج العادي داخل مسحوق المواد. وقد تم وضع نموذج باستخدام تحليل العناصر المحدودة من أجل تعريف وتحديد متغيرات العملية لدعم التجارب. وتشمل هذه المتغيرات وقت المعالجة، واتساع الموجة ومنطقة الاتصال. وقد تم دراسة تأثير هذه المتغيرات على العملية. أظهرت الاختبارات التجريبية أن التضمين التدريجي يتحقق باستخدام مجموعات مترابطة ومحددة من المتغيرات المؤثرة في العملية وتحديدا تم الحصول على تضمين كامل للألياف باستخدام مساحة الاتصال الصغيرة بزمن مقداره تقريبا ثانية واحدة مرتبط باتساع موجي مقداره 50%، بينما عن طريق

استخدام مساحة الاتصال الكبيرة كانت المتغيرات 60% اتساع موجي مرتبط بزمن اقل من ثانية واحدة.

العملية النهائية سوف تنتج ألياف بصرية مضمنة داخل المواد. التحقق من سلامة أجهزة الاستشعار ما بعد العملية هو محل الاهتمام التالي لعملية التضمين وأيضا التأكد من قدرة أجهزة الاستشعار من اعادة عرض سلوك المادة بشكل صحيح. سلامة الألياف والعرض النسبي لسلوك المادة يكون كافيا ويخدم الغرض من القياس.

في عملية استخدام مسحوق المواد كمادة مستضيفة، تم استخدام تقنية الضغط على درجات حرارة طبيعية وتقنية SPS لتكوين المواد حيت تم بداية وضع الألياف البصرية داخل القالب الذي يملأ بمسحوق المواد. وقد تم إعداد المواد في ظل ظروف مختلفة معروفة من الضغط والتلبيد حيث يجب مراعاة الألياف البصرية المضمنة أثناء العملية، على سبيل المثال: الضغط العالي المستخدم في العملية وكذلك درجة الحرارة العالية يمكن أن تتسبب في الحاق الضرر بالألياف.

كانت القيم العملية للمتغيرات المستخدمة في عملية الضغط على درجات طبيعية: 155 MPa حمل الضغط ، ودرجة حرارة تلبيد 450 °C لمدة 6 ساعات. فيما يتعلق ب SPS: تم استخدام حمل ضغط 20 MPa، ودرجة حرارة 400 °C لمدة نصف ساعة.

وقد تميز هذا العمل عملية التضمين : باستخدام الموجات فوق الصوتية في الألمنيوم وإدخال الألياف في مسحوق المواد لضمان قراءة سليمة لمتغيرات البيئة الخارجية وحماية أجهزة الاستشعار من البيئة الخارجية الحساسة.

CHAPTER 1

INTRODUCTION

1.1 Background

The repeated changes (stimuli) that occur inside or/and outside the mechanical structures affect and could cause some damages to that structures. The structures should have a stable state and a safe operating condition during their operation time, so it is worthy to be improved by sensing and reacting to the surrounding stimuli. Responding to such stimuli in a proper way provides ground to avoid or at least reduce the occurrence of damages. Not all the structures can feel and respond to these stimuli. Missing capabilities i.e. sensing and responding are the reasons behind the inability of the structures to deal with the surrounding stimuli. Conventional structures are structures that have no response to the stimuli. By looking around, most of the structures in our life are passive. Another type of structures could have sensors and actuators, which rarely exist, can be called nervous structures. These structures like the human body can trigger response to different stimuli as shown Figure 1.1. These variations of structures is based on their characteristics.

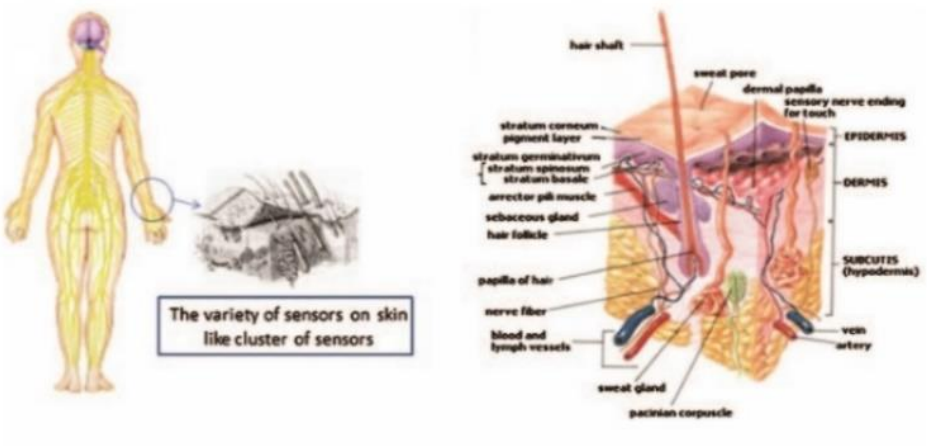

Figure 1.1 The nervous system of human body [1]

Unexpected changes should be followed-up during the operating and non-operating state of the structure. Monitoring is the proper method to achieve the inspections to detect any unusual stimuli i.e. a general assessment of the structure and perceiving unusual stimuli which could have an impact on the structure and cause a sudden damage.

Previously, the Visual Inspections (VI) which is based on the human observation and use of some primary inspection tools were the main methods for the monitoring. But, such methods do not give a complete overview and assessment of the structure. Furthermore, it is missing a clear explanation in the case of any sudden failure. Later, a new powerful technique i.e. Nondestructive testing (NDT) is used in such inspections, because of its ability to evaluate the state of the structure without causing damages. Also, the structure can be inspected during the operating or non-operating state.

These capabilities for the (NDT) increase its chance of being used in a very wide range of applications either in the mechanical or another type of structures [2], [3]. For example, Structural Health Monitoring (SHM) uses the (NDT) technique to evaluate the functionality of the structures.

1.2 Structural Health Monitoring (SHM)

Structural Health Monitoring (SHM) aims to apply a functional assessment for every part of the structure and the whole structure at every moment of the structure's life either in operation or non-operation state. In these regards, the structure should have the ability to sense and respond the different stimuli, achieving its need by itself is becoming a more advanced concept.

(SHM) has different applications in many types of structures such as bridges and aerospace applications [4]–[7].

A novel technique of monitoring and continuing assessment of the structure is introduced by using the smartness concept. This concept is based on using a sensorial material as well as nervous material. Smartness are used to achieve the purpose of monitoring the structure using online data acquisition or information technology [4].

As mentioned before, a conventional structure cannot achieve any action by itself. The challenge is to equip the structure with a monitoring system that allows self-structural monitoring. To overcome the challenge, sensor or/and actuator should be a part of the hosting structure without changing its material properties. Including sensor within hosting structure gives the sensorial property to it. Therefore, the potential of the hosting structure can be increased by introducing the actuator. The actuator reduces or prevents extensive deformation of the host structure. Hence, the concept of delaying failure and preventing damage helps develop a type of structure called in this case a smart structure.

Figure 1.2 shows an example of using the smartness in the structures i.e. an impact damage monitoring for the filament wound composite structure in the rocket motor.

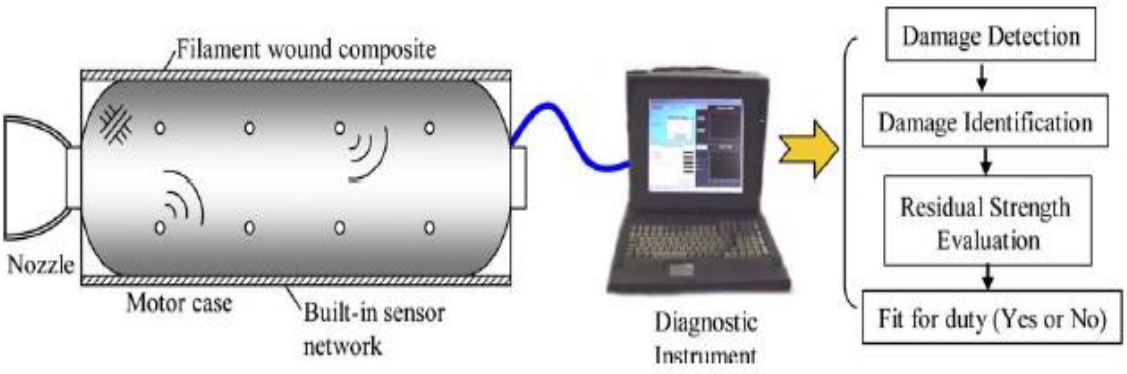

Figure 1.2: Self-Health Monitoring System [5]

1.2.1 Intelligence and smartness in materials

Intelligence and smartness added to the material are becoming a need in our life and is an important field of research. The materials can serve itself to operate, control, and follow-up, which leads reducing the effort and care by the humans for a structure having such material. In the next sub-sections, a brief introduction is presented about the smart material and smart structures:

1.2.1.1 Smart material (SM)

Material scientists classified the materials due to the chemical bonds between their atoms into different types such as metals, polymers, ceramic. Another classification is done based on its application. Figure 1.3 shows some of these materials that used nowadays in many applications.

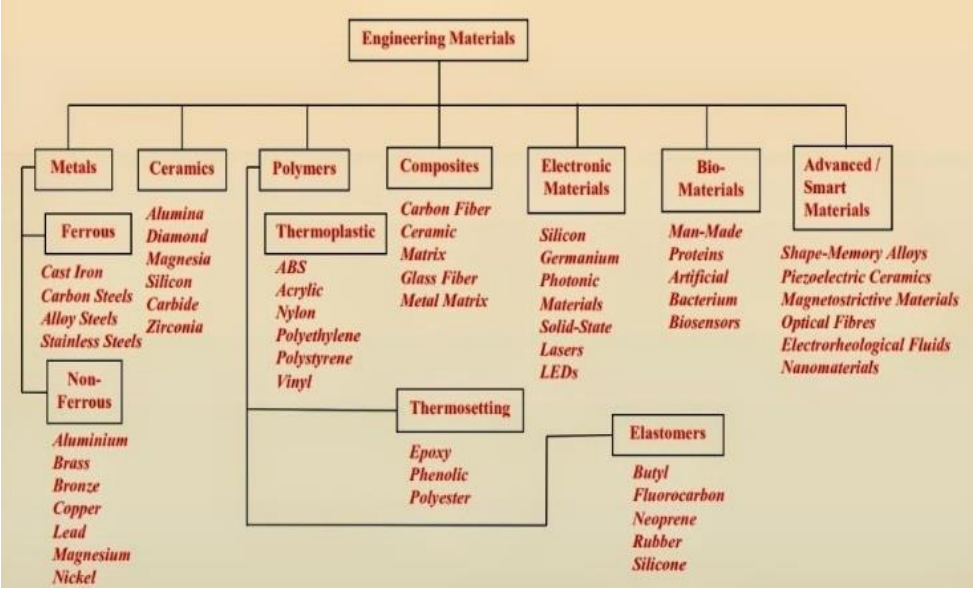

Figure 1.3: Material classification [8]

Smart Material (SM) is a material that has the intrinsic and extrinsic capabilities to respond to external stimuli in a functionally useful manner, and are sometimes called functional material, where it can sense the environmental stimuli, monitoring by itself, make a decision and act through a response [6], [7], [9]. (SM) takes a significant place in such modern classification due to the high potential of its application.

Figure 1.4 shows the (SM) classification; which is based on the input and the output. The material is exposed to an input from the surrounding environment and response as an output for the surrounding environment. For example, the piezoelectric material is exposed to a deformation to give an output of electrical charges and could be exposed to an electrical supply to change its shape, another example is the shape memory alloy which is deformed if it is exposed to temperature. Electrostrictive, magnetostrictive, thermo-electric, thermo-chromic, fiber optic; these are other types of (SM) that can be used as sensors and actuators [10], [11].

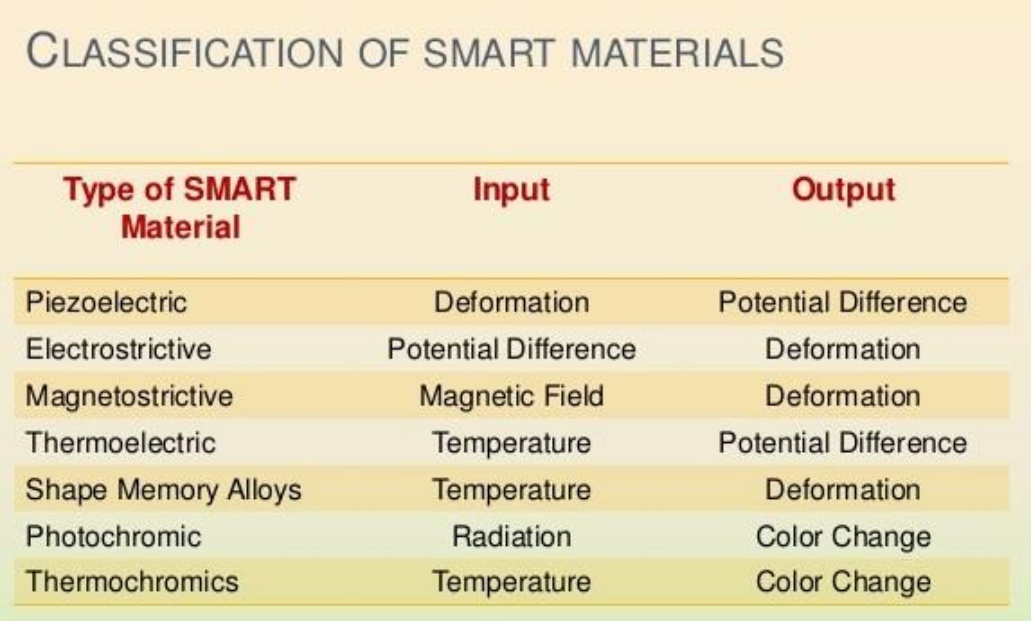

CLASSIFICATION OF SMART MATERIALS

Type of SMART Material	Input	Output
Piezoelectric	Deformation	Potential Difference
Electrostrictive	Potential Difference	Deformation
Magnetostrictive	Magnetic Field	Deformation
Thermoelectric	Temperature	Potential Difference
Shape Memory Alloys	Temperature	Deformation
Photochromic	Radiation	Color Change
Thermochromics	Temperature	Color Change

Figure 1.4: Classification of smart material [12]

Generally, (SM) have numerous applications in structural engineering (either civil or mechanical structure), biomedical applications and other applications [13]–[15].

1.2.1.2 Smart structure (SS)

Smart structure (SS) have one or more smart materials which leads to deal and adapt to the stimuli coming from the surrounding environment with the positive reaction. Having such material helps in securing the integrity of the structure and continuing to achieve its functions. Where the non-smart structure cannot deal, or adapt to the changes coming from the surrounding environment. This inability of the reacting to the stimuli could influence the structure with an adverse effect and may cause a failure.

So, the (SS) should contain two main elements (sensors and actuators) in addition to controlling strategies, and power electronics [10], the following four points show the function of each part:

1- Sensors: to monitor environment changes and generate signals proportional to the changes measured.
2- Actuators: used to change the properties of the structure to overcome the changes and achieve the desired response.
3- Control strategies: in this part, continuous monitors should be done for the sensor and processing information to decide whether any action is required, to give the signal for the suitable actuator.
4- Power electronics: it is used to organize and control the electrical power in the system.

Based on the previous introduction, we need in this work to investigate the ability to enrich the structure with sensors. In this regard, the fiber optic was chosen to accomplish this purpose because of its higher potential, size aspects and advantages compared with other existence conventional sensors in (SHM) applications [16].

For starting up this investigation, a single mode fiber i.e. SMF-28 has been used to get this enrichment in this work. The physical and operating specifications of this fiber could be found in [17]. The success with the single mode fiber can also be used to gain insight into more advance fibers.

1.2.2 Optical fibers

Fiber optic is a flexible, transparent fiber made of glass (silica) with a very low diameter slightly thicker than a human hair, used to transmit the light for very long distance at high bandwidth. The structure of the fiber is a cylindrical shape as shown in Figure 1.5.

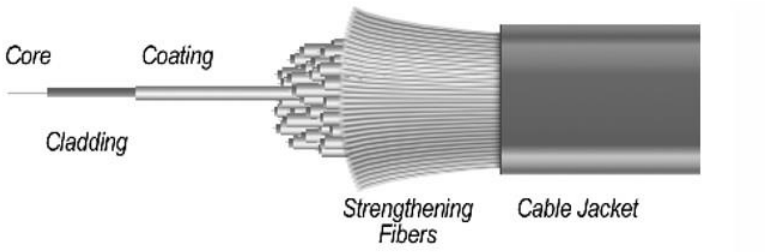

Figure 1.5: Basic structure of the optical fiber [16]

Mainly, the fiber consists three layers:

A) Core: the main part of the fiber made of glass (silica) to transmit the light, its diameter measured in microns e.g. 9, 50, and 62.5 micrometer.

B) Cladding: dielectric material (glass or plastic) with known reflection index, its reflection index should be less than the core material to achieve its purpose of keeping the transmission of the light and avoid scattering losses, its diameter almost fixed of 125 microns.

C) Buffer/ coating: the last layer used to protect the fiber from the surrounding environment, its diameter is 250 microns. Some fiber cover with the fourth layer called jacket has 400 microns in diameter.

Based on the diameter of the core, the optical fiber is divided into two types: single mode fiber (SMF) has 8-10/125 core to cladding diameter ratio where the multimode fiber (MMF) has 50/125 or 62.5/125. The single-mode fiber allows the light to propagate in one mode, where the multimode fiber allows the light to propagate in more than one mode. The typical cross section for both single mode and multimode fibers shown in Figure 1.6.

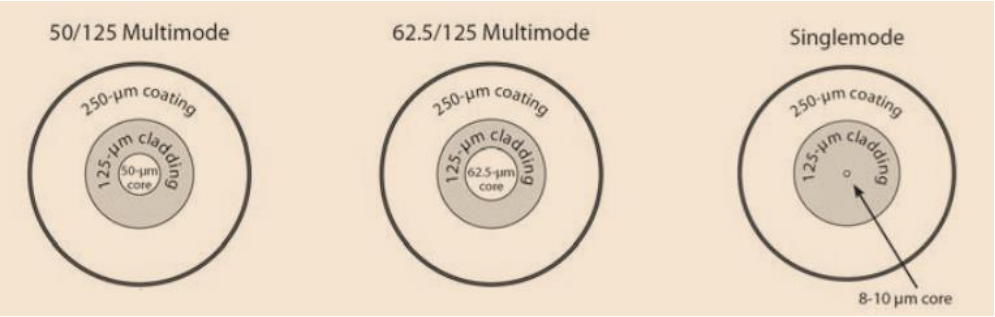

a) **b)** **c)**

Figure 1.6: Typical cross section for a) multimode fiber 50/125 b) multimode fiber 62.5/125 c) single mode [18]

1.3 Fiber optic embedding

Enriching the sensory property of the structure needs attaching the fiber optic with the structures that ensure proper measurements match with the actual changes exposed by the structure. Hence, the fiber optic should be part of the structure, so it will be affected by the same stimuli.

Different ways can be used for attaching the fiber with the structure such as: gluing the fiber either on the surface of the structure or by making slot on the sub-surface, but compatibility issue will arise due the change of the thermal and mechanical properties between the glue and hosting material which cause unreliable measurements for the stimuli. Also, in the case of operating the structure in a difficult surrounding environment, the fiber optic will be under more risk conditions

which could damage the fiber. Thus, the best way of involving the fiber is to be embedded inside the structure. The embedding will protect the sensor from any external effects and ensure the safety of the fiber.

In this regard, two main issues should be considered in the embedding: the structural and functional integrity of both the host material and the embedded fiber over the time. In addition to, ensuring a well sticking between the fiber and host material secure the compatibility needs to get proper measurements.

1.4 Problem statement

The fiber optics are chosen to be embedded inside the material with the purpose to become a sensorial material. Hence, the integrity of the fiber optic becomes important. With the common environment conditions, the current coating of the core fiber may be sufficient to resist these conditions, but it is not enough for harsh environment where the temperature can reach 75˚C accompanied with humidity and other effects. Medium and large mechanical structures need the fiber to be embedded inside at the subsurface of the material without damaging both sensor and the host material.

This embedding can help in developing sensorial materials that have sensors embedded within the structure, as well as smart materials for embedding actuators. Successful embedding will guarantee the compatibility between them. Therefore, the sensor and actuator will be affected by the same stimuli from the environment.

The contribution of this work will be to investigate embedding processes in two different based materials i.e. metal and powder based materials.

1.5 Work approach:

The work was carried out in various stages, these stages are:

A. Characterization the fiber to be embedded.

Because of the pressure and heat that the fiber will be exposed to during the embedding process using either Ultrasonic consolidation (UC) or Powder metallurgy (PM). A heat test and pressure test were carried out to evaluate the resistance of the fiber to such loads. These tests will indicate the limits of the fiber to overcome such the mechanical and thermal loads. These tests, in addition to material characterization before embedding will be mentioned at the beginning of Chapter 3.

B. Preparation of the host material where the fiber will be embedded.

Aluminum sheet and Aluminum powder were used as hosting material in the Ultrasonic consolidation (UC) and Powder Metallurgy (PM) techniques, respectively. During the building of the material, the fiber will be embedded within the material without changing the physical properties of the whole structure i.e. the sensor or the hosting material. The main technique (UC) will be presented in Chapter 4 in addition to the alternative technique (PM) in chapter 5.

C. Characterization the host material and the fiber after the embedding.

To check the integrity of both hosting material and sensor by taking microscopic scale pictures for the interface between the fiber and the host material. The pictures were taken using the optical microscope and the scanning electron microscope (SEM). This characterization aims to define the process control in building the material with the sensor, to avoid any damaging and to confirm the

compatibility between the host material and fiber before testing the functionality of the fiber. The challenges in this stage are: to keep the integrity of the fiber in addition to ensuring the compatibility between the host material and the fiber to sense true measurements.

Next step is to check the functionality of the fiber by using power light transmission test, where the fiber transparent the light without missing all the light as result of the embedding.

D. Ultrasonic consolidation (UC) process characterization

To clarify the process parameters and its effect on the process, also quantify the process parameters that are needed to get full embedding.

E. To report the details of the study.

Chapter 6 present the main results of the present work, discussion of these results, and conclusion of the work with a recommendation for the future work.

1.6 Motivation of the present work

Defining the process parameters for a sub-surface embedding for the fiber will open the way to extend the work by using a superior optical fiber called Fiber Bragg Gratings (FBGs). Bragg gratings (BGs) which are inscribed in fiber optics are an extremely enabling technology where hundreds of sensors can be inscribed in the fiber optic to measure various physical properties such as temperature, displacement, pressure. The inscribed (FBGs) reflect a certain wavelength of the transmitted light and pass the others. These reflections affected by the surrounding environment stimuli that can make a shift in the wavelength of the light. Such fiber with high potential is used

to achieve a fundamental role in different applications mainly to design smart material e.g. Structural Health Monitoring (SHM).

Also, it can be used in various applications at small and large scale, where the fiber optics in these cases can be long distances and hence need to be added to mechanical systems and protected against surrounding harsh environment.

1.7 Work objectives:

Ultrasonic consolidation (UC) has been considered in this work to embed the fiber optics, in addition to Powder Metallurgy (PM) as an alternative method. During the process, the fiber is embedded to be part of the hosting material; this leads to allow the ability to sense and monitoring the structure by using the principle of light transmission, and it is a reflection. To accomplish, the following sub-objective:

A. An efficient embedding of the fiber by doing the characterization of the sample, where the compatibility between the fiber and the structure is the essential point to give outputs appropriate the stimuli affect the structure.
B. Checking the functionality of the fiber after embedding, using power light transmission test.

1.8 Report structure

The content thesis will be split into seven chapters:

Chapter 1 brief introduction to the topic and the need for this work.

Chapter 2 literature survey about the methods used in the embedding.

Chapter 3 test the fiber, and checking its integrity in extreme condition i.e. Temperature and Pressure, and define the parameter of building the host material.

Chapter 4 characterizing the embedding process using (Ultrasonic Consolidation).

Chapter 5 alternative method using (Powder Metallurgy) for embedding.

Chapter 6 Results and Discussion

Chapter 7 Conclusion of the work with recommendation for the future work

CHAPTER 2:

LITERATURE REVIEW

Conventionally, the main idea of embedding the fiber within host material is to increase the strength and the hardness of the material by creating matrix composite with different material properties. Different fibers polymers and other conventional fibers used for this purpose [19]–[21]. For example, fiber-reinforced polymer (FRP) used to for strengthening civil engineering infrastructures [22]. The functionality of the matrix could be improved using more advanced fiber such as shape memory alloys (SMA) embedded within host material leads to increase the potential of that material [21], [22]. The sensorial material can be achieved with the embedding an optical fiber. Embedded fiber optic provide can measurements for the behavior changes due to the basic principle of reflecting light inside the core of the fiber.

2.1 Fiber optic characteristics

Implementing the nervous structures is based on the development and integration of the sensors within the host material [9]. The size, weight, and stability of the sensing are essential merits for the sensor to be embedded within the host material. Unique advantages compared with conventional sensors give the propriety for the fiber optic to be used in this process of embedding [23]–[25]:

1. Easily to be embedded and it does not affect the material i.e. wounds during embedding due to its small geometry.
2. Resist high temperature and pressure during the embedding process due to its material properties.
3. Many fiber optic sensors can be multiplexed in a single line.
4. Compatibility for the fiber optic data link, where a different bandwidth can be provided for many sensors.
5. Dielectric property of the optical fiber can give an immunity to electromagnetic effects.

Generally, three main types of sensor can be considered in this aspect: interferometric, distributed and grating-based sensors [26], due to its principle of work:

1. Interferometric sensor: reacts as phase change of the two interfering light signals when it is exposed to physical changes [27]. An example of this sensor is a Fabry–Perot interferometric sensor which achieved a maximum strain resolution of 0.15 με. Typically, the strain is measured with the range of ±1000 με, and can be extended to ±5000 με. Also, it can be embedded within the materials without any effects due to its small size where it can be impacted to 1-20 mm length. The disadvantage of this type of sensor the low capability for multiplexing.
2. Distributed fiber optic sensor:

   Optical time-domain reflectometry (OTDR), Raman optical time-domain reflectometry (ROTDR) and Brillouin optical time-domain reflectometry (BOTDR), these are the main types of the distributed fiber optic sensor, the principle of operation of these fibers are different for each.

3. Grating-based sensor

   FBG is one of the widely used sensors in various applications due to a special merit such as light weight, immunity to electromagnetic interference, stability and little signal loss over very long distances [28]. The principle of work for this type of sensors depend on the back reflection of the light signal which comes with specified wavelength i.e. Bragg wavelength. The grating pitch and refractive index of the fiber are the main parameters used to determine the Bragg wavelength. So, any external changes affect the fiber cause these parameters to be changed, monitoring these changes leads to measure different measurements such as: temperature, strain, vibration, etc.

   Low cost, compact size, good linearity as well as the multiplexing capability for one fiber to have different wavelengths are the attractive properties for the FBG to get well embedding.

2.2 Host materials

Different material can be considered as hosting material to have the FBG sensor embedded with different condition within its geometry.

1. Embedding in composite structures:

   The FBG sensor can be embedded easier in polymer matrices than other hosting material [29]–[31]. Minakuchi and Takeda [29] presented a general review for the research work in different applications of structural health monitoring where the optical fiber sensors are used. Regarding measuring the strain in the composite material, Luyckx and co-authors [30] reviewed the part of the technical issues for embedding FBG within composite

materials. The resulting embedded FBG was related to the strain of the material through monitoring the change of the material. During measuring the strain using the FBGs the author considered the temperature compensation. Embedding FBGs within polymer matrices was explored and promised good results within 70˚C, also wavelength shift and spectral bandwidth change of the polymer FBG can be observed and it is affected by the temperature and thermal effects [32], [33].

2. Embedding in metals and alloys

   The metals are widely used in the industries either heavy or light industries, but the embedding in metallic based material is more difficult due to its effects on the grating and the sensitivity loss at high temperature for the FBG [34]. The embedding of FBGs in metals was explored by Li et al [35] where they used the ultrasonic welding for embedding FBGs in Aluminum and Copper foils with very low thickness. The results showed the possibility of embedding the bare fiber in copper, also it showed the effect of the high hardness of copper in the embedding.

   The FBG fiber coated through a chemical-electroplating method was successfully embedded in aluminum with observed shift in wavelength. An electro-less plating method was used in [36] to coat FBG sensors, and hence, the observed common changes of the FBG spectrum after metalizing were reduced through a stress control technology, which enabled retention of the optical properties of the metal-coated FBGs. In this research [34] has developed a high thermal sensitivity optical FBG sensor with bi-material coating, which can be embedded into a smart tool.

The type of the hosting material as well as the fiber to be embedded constraint the way of embedding. Hence, a brief literature survey of the two methods is done to help in understanding the basics of these methods. Ultrasonic consolidation (UC) is the main method, which based on using the ultrasonic waves and the energy generated from these waves to get an embedding of the fiber within a metal based hosting material. Powder compaction (PC) was the alternative method; this method belongs to the Powder Metallurgy (PM) science that uses the powder as based material exposed to pressure and heat to formulate the structure, in this method the fiber is inserted inside the powder during the process of pressing the powder.

2.3 Ultrasonic consolidation (UC):

(UC) is a manufacturing process used to build 3D structures by combining low thickness layers one above another [37]. Figure 2.1 shows the basic principle of this method [38], where the energy generated from the ultrasonic waves has the possibility to be transferred as sonic energy with a slight portion compared to the heat produced due to the friction between the metals.

The process of (UC) is affected by different parameters e.g. the setup used, the type of material to be welded, and the direction of waves propagation i.e. Solid materials need horizontal waves propagation as shown in Figure 2.1, where plastic materials need vertical waves propagation [39].

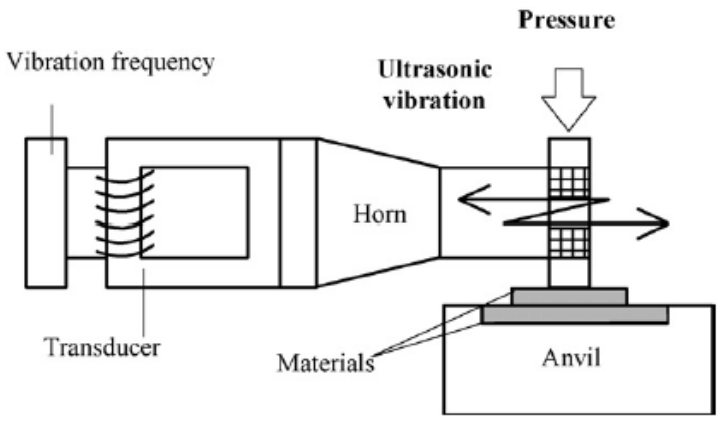

Figure 2.1: Basic principle of ultrasonic consolidation [38]

Also, the sonotrode shape plays the main role in the (UC): the spot, seam, and butt are different methods of ultrasonic metal welding [40]. These various welding ways based on the diversity of the sonotrode shape. The spot and seam welding are the most popular way of welding; the sonotrode on the spot welder has very narrow cross section area. In the seam welder, the welder is rotating sonotrode as shown in Figure 2.2. This type of welder being proposed to use for fiber optics consolidation over the length of the hosting part.

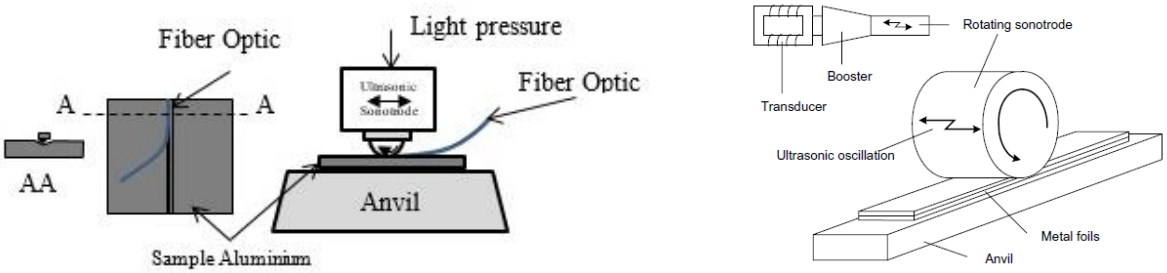

Figure 2.2: Ultrasonic welder with rotatory sonotrode [41]

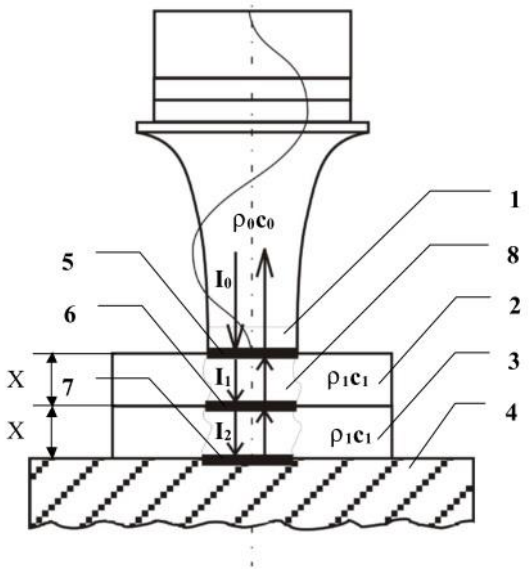

Figure 2.3: Effects of reflecting and passing properties of the materials [42]

In addition to the previous parameters, Figure 2.3 shows the effects of reflecting and passing properties of the materials at the contacting area energy transferred during the (UC) process [42].

The following formulas are governing these effects of reflecting and passing [42]:

$$I_0 = 2\pi^2 f^2 {A_0}^2 \rho_0 c_0 \quad (1)$$

$$\eta = \left(\frac{\rho_0 c_0 - \rho_1 c_1}{\rho_0 c_0 + \rho_1 c_1}\right)^2 \quad (2)$$

$$d = 1 - \eta \quad (3)$$

Where, I_0 is ultrasonic waves intensity

$Z = \rho c$ is an acoustical impedance

A is the contacting area

f is the frequency of wave

η is a reflection coefficient

d is a transmission coefficient

Without going deeply, this work considers the general mechanism of the (UC) that illustrated in the following sub-section.

2.3.1 Theoretical background

(UC) is depending on the energy transfer from the mechanical energy generated by the vibrations to heat energy due to friction between the sonotrode and the materials to be welded. The mechanism of the welding process can be summarized with a few steps. First, the contact surface of the welded material is cleaned from the contaminants and oxides due to friction, which increases the contact area of pure material [43]–[45]. The continuity of the friction by ultrasonic vibrations leads to heat generation, and transfer it to the material depending on its thermal properties. These vibrations lead to create the temperature gradient through the materials and increase the temperature at the surfaces, with the existence of the applied pressure a new bond starts to form between the contacted surfaces.

To illustrate this mechanism, it is needed to be clarified with the following four next points:

1. The power generation by the ultrasonic waves.
2. The power transfer from the ultrasonic waves to heat.
3. The temperature gradient in the material.
4. Process control which is determined by the parameters of this process.

2.3.1.1 Power generated

The power flux $\grave{P}$ due to friction force during the process is governed by the following relations:

$$\grave{P} = \frac{P}{A_{fr}} = \frac{Fr * V_{avg}}{A_{fr}} \quad (4)$$

Where $Fr = \mu * F_N$ Friction force

$V_{avg} = 4 * \lambda_w * f_r$ Cosine average velocity

$$\dot{P} = \frac{F_N * \mu * 4 * \lambda_w * f_w}{A_{fr}} \quad (5)$$

Where, F_N is the normal applied Force

μ Friction coefficient between the surfaces

λ_w the amplitude of the waves

f_w the frequency of the wave

A_{fr} friction contact area

Introducing the welding time t_w with the relation leads to the energy flux during the process

$$\dot{E} = \dot{P} * t_w \quad (6)$$

Where, $\dot{E}$ is the energy flux during the process.

t_w the duration time of keeping the work of the waves

Finally, the power flux $\dot{P}$ and energy flux $\dot{E}$ depend on the following parameters

$$\dot{P} = f(F_N, \mu, \lambda_w, f_w, A_{fr}) \quad (7)$$

$$\dot{E} = f(F_N, \mu, \lambda_w, f_w, A_{fr}, t_w) \quad (8)$$

2.3.1.2 Energy transferred from mechanical to heat

The energy generated from vibration is transferred into heat energy, this transferring depends on:

- The material properties of the materials to be welded i.e. thermal conductivity k and heat capacity c_p.

- The needed area to be welded: which mentioned in the previous sub-section as A_{fr} contact area.
- The depth of the welding of the structure.

Since the interest is to embed the fiber within the structure, the depth of the welding is an important point to be discussed.

In the case of the embedding in the sub-surface of the bottom layer, there is a need for more deformation in the further side of the sonotrode contacting area. So, the material closest to the horn should conduct as much as possible of the generated heat (conducting material). Thus, this material should have a high thermal conductivity to conduct energy as much as possible, also to avoid any melting for this material the heat capacity should be optimized to reduce the consumed energy. To ensure the melting happened in the sub-surface, the melting temperature of the upper layer should be higher.

For a constant amount of power generated, the increase in friction contacting area reduces the efficiency of the embedding process i.e. does not give the needed temperature gradient to achieve the embedding due to dissipating the energy in a wider area.

2.3.1.3 Temperature gradient through the material

The partial differential equation governs the heat transfer in the (x, y) plane during the process is:

$$k\left(\frac{\partial^2 T}{\partial x^2}+\frac{\partial^2 T}{\partial y^2}\right)+Q-\rho * c_p * \frac{\partial T}{\partial x}=0 \quad (9)$$

Where Q Volumetric heat generation rate (W/mm^3)

k thermal conductivity

T Temperature gradient

ρ material density

c_p Specific heat

(x, y) the coordinate

The gradient of the temperature through the material is found by solving and modeling this equation. The energy dissipates in the material increases the temperature and leads the material either soften or melt. The following formula represents the amount of energy the material can have due to temperature gradient:

$$Heat\ energy = mass * specific\ heat * the\ change\ of\ temperature$$

$$Q = m * c_p * \Delta T \tag{10}$$

2.3.1.4 Process control of embedding parameters

Based on the theoretical background, two types of parameters can be controlled i.e. the material parameters (properties and dimensions) and the operating parameters (applied force, area, amplitude, and frequency of vibration) in addition to the welding time. Different setups have a different set of parameters can control the process to get the optimal amount of energy to achieve the purpose of embedding.

2.3.2 A literature review of UC process:

In the 1950s, despite using the ultrasonic welding for soft material welding i.e. aluminum, it had a broad range of applications in different welding material. Daniels in [44], after investigation the effect of the interactive dependence process parameters i.e. pressure, power, and the welding time. Due to the material properties, he concluded that physical or dimensional properties influence

ultrasonic welding process. His experiments confined to metal welding the following Figure 2.4 shows the weldability between different metals.

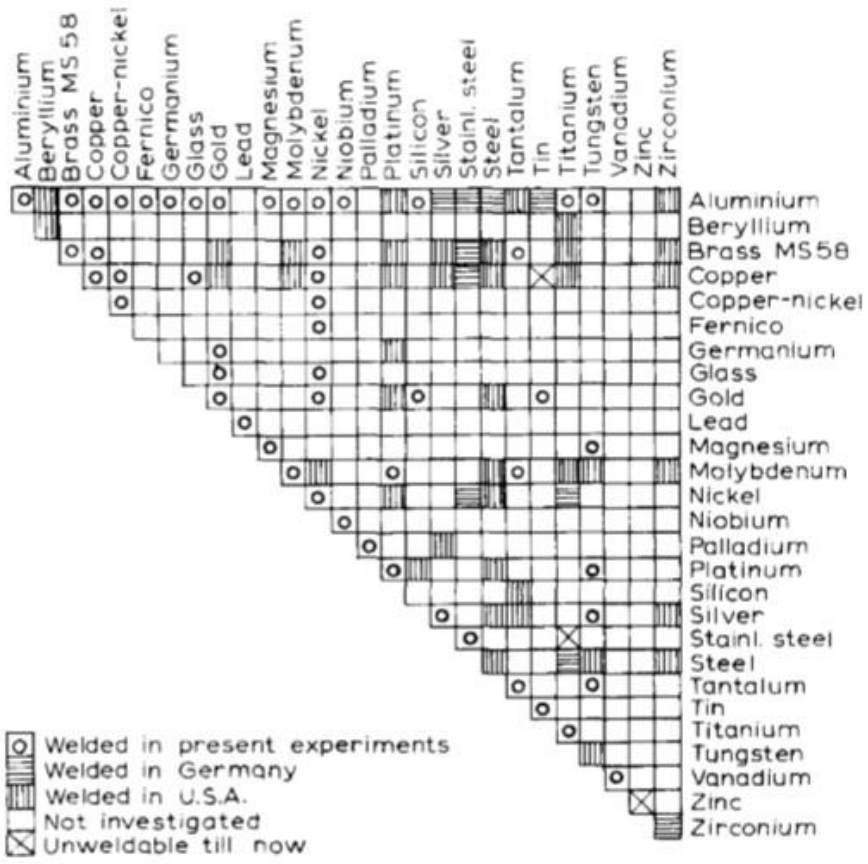

Figure 2.4: Weldability between the various metals [44]

Later, Tsujino et al. [46] proposed different welding methods using ultrasonic for different size of specimens e.g. butt welding used to weld thick and large samples; also two vibration systems crossed from the upper and lower sides used to weld medium specimens. In term of welding time, Allameh et al. [47] studied the microstructure analysis, and characterization of an aluminum sample welded ultrasonically. Investigating the control the parameter of (UC) of the material was

an important point to be studied. Ram et al. [37] and Kong et al. [41] reported the optimum parameters of the (UC) process of aluminum 3003 and aluminum alloy 6061 in [48].

2.3.3 Fiber embedding using UC

Kong et al.[49] and Kong and Soar [50] embedded different fibers in the metal substrate using ultrasonic consolidation process. Three different types of fibers embedded between two foils of aluminum 3003. Each foil of aluminum was 100 µm thick and 25 mm wide. As a first step, two foils of aluminum 3003 were welded together to form the substrate and the top foil, each of 200 µm thickness. The types of fiber used are Sigma silicon carbide (SiC), shape memory alloy (SMA) and optical fibers coated with the polymer without grated sensors. Three different embedding methods used named as a full load, partial load and no load. In the no-load method, full sized grooves were provided in the substrate to accommodate the fibers with no load on these from the sonotrode pressure. In partial load method, partial grooves were provided in both the substrate and top foil to relieve some pressure on the fibers. No grooves contained in the full load methods implying that the fibers bear the full load on sonotrode. The results show that ultrasonic consolidation is an effective process to embed SiC or SMA fibers in an aluminum matrix, even at full load conditions. However, optical fibers present a challenging scenario. The polymer coating disperses under full and partial loads, while it only distorted in no load conditions. If the polymer coating removed, then full consolidation is achieved, but the integrity of the fiber may compromise. A physical examination showed no cracking of glass cladding or core. However, no tests were conducted to ascertain the optical properties of the fiber. Building on previous work, Mou et al. [51] explicitly embedded fiber Bragg grating (FBG) in aluminum 3003 foils of 200 µm (obtained by pre-bonding two foils of 100 µm thickness each). Analysis of five specimens, in

which the FBG survived ultrasonic consolidation, showed varying degree of success although a blue-shifting of the Bragg peaks indicates that the gratings experienced a compression strain.

The previous work was focused on embedding fiber between two thin similar sheets i.e. Aluminum sheet using seam welder with rotating sonotrode. However, getting an embedding for the fiber in the sub-surface of bulk material was missed as per the literature shows.

So, the present work is done using spot welding machine to get fiber embedded within the sub-surface of bulk material. The latter need careful work due to the sensitivity of the fiber under direct source of power, also to define specific parameters for this embedding.

2.4 Powder Metallurgy (PM):

Powder metallurgy (PM) is a metal processing technology to produce parts from metallic powder with certain shapes, comes from the die which contains the powder. The technique has two stages: compaction stage done by exposing the particles to a high pressure which increases the green density of the material shown in Figure 2.5. The next stage is the sintering process which is a thermal treatment of the compacted powder to harden the material i.e. exposing the compacted powder to a temperature below the melting point of the main component to increase its strength and give the final shape. Due to the separation of the compaction from sintering, this process is called a cold compaction process. On the other hand, the compaction and sintering can be done simultaneously in a process called a hot compaction.

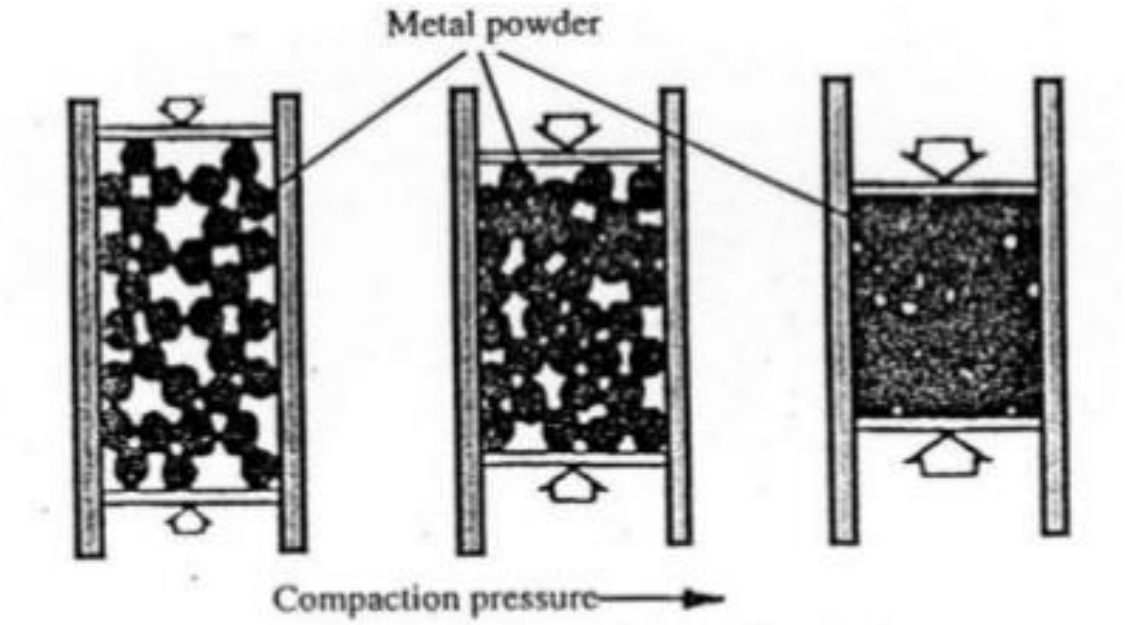

Figure 2.5: Compaction stage

The previous researches show that the powder metallurgy process based on the theoretical background. Akisanya et al. [52] studied the yield behavior during cold hydrostatic compaction process, Sirdhar and Fleck [53] investigated the behavior of powder composite i.e. aluminum with silicon carbide, also the lead-steel composite during the axisymmetric cold compaction process. Later, a fundamental analysis was done for the cold die compaction by Al-Qureshi et al.[54]. This process is constrained by the parameters of the process i.e. the material properties and the powder size affect the process parameters and the behavior of the material during the process also make the influence of the nature of the produced parts [55]–[58].

The (PM) is a very common technique use in many different applications e.g. the cutting tool design. Also, this technique used to build the different shape of the structure since it is based on using the powder which easily takes the form of the containing die. Regarding this capabilities, in our work, the (PM) was used to embed fiber within the powder-based material.

Nouari et al. in [59] did a review for the work puplished in the Spark Plasma Sintering (SPS). (SPS) is a (PM) technology which classified as a low temperature process Figure 2.6, so it is a novel technique can be used to embed the fiber within a metallic material.

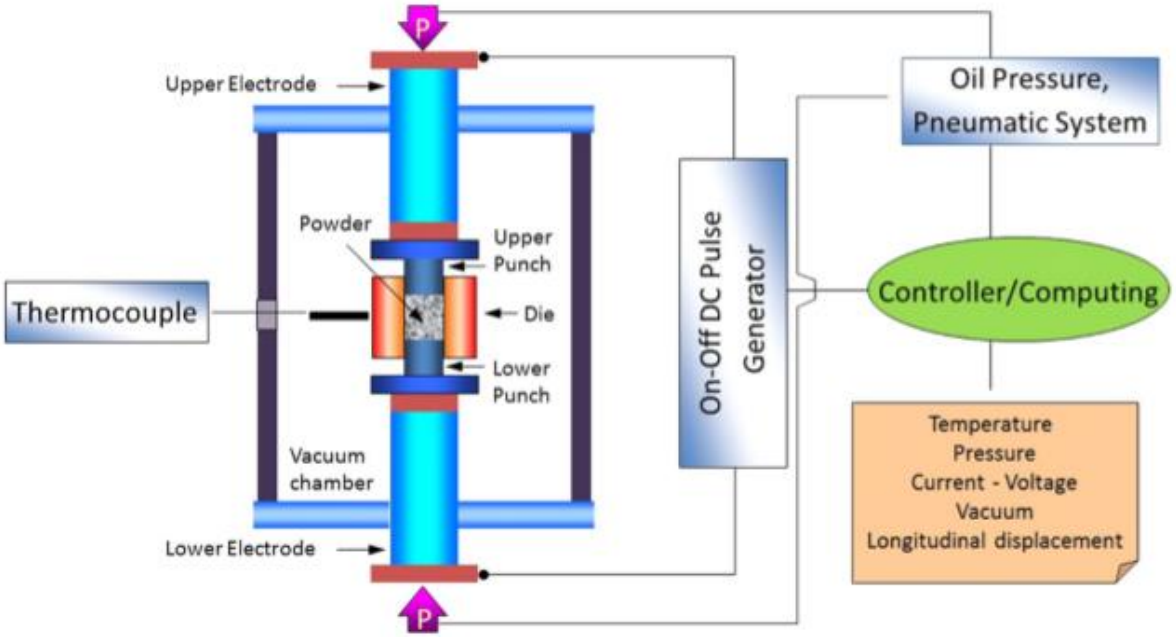

Figure 2.6: Schematic of SPS process [59]

CHAPTER 3:

FIBER OPTIC AND HOSTING MATERIAL:

CHARACTERIZATION BEFORE EMBEDDING

For the proposed methods of embedding the fiber, the fiber will be exposed to different types of loads during the process. So, characterizing the optical fiber before embedding followed by investigating the parameters of constructing the hosting material using Ultrasonic Spot Welding (USW) present in this chapter:

3.1 Fiber characterization before embedding:

In both methods, the fiber exposed to a mechanical load represented by pressure (P) and temperature gradient (ΔT) as a thermal load.

3.1.1 Temperature resistance tests:

Temperature gradient (ΔT) as a thermal load will be a main source of affecting the fiber during the embedding processes i.e. UC and PM. Hence, to check the capability of the fiber to resist such load, a separate experiment was conducted to characterize the fiber before embedding

3.1.1.1 Test setup

Heat test was done for the fiber to examine its resistivity to the heat and temperature changes during the embedding process. Ten fibers were labeled and put inside the furnace to be exposed to different temperature as shown in Figure 3.1. Temperatures from (100˚C) to (1000 ˚C), with an

average heat rate of 15.3 ˚C/ min, were applied to the fibers in steps (100˚C) for each to have ten fibers exposed to ten different temperatures. Each labeled fiber was tested with normal bend into three different locations along the fiber to check its ability to resist bending after it is heated.

a)

b)

Figure 3.1: Heat test a) labeled fibers b) fiber inside the furnace

3.1.1.2 Test results and discussion

Table 3.1: Heat test records

Temp. (˚C)	Time (min: sec)	In the Furnace	Pictures	Bending test
100	6:44	Nothing affect the integrity of the fiber	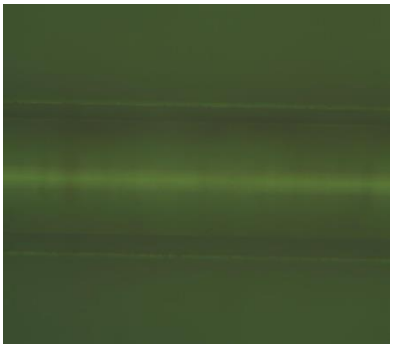	Not Broken

200	**12:13**	**Nothing affect the integrity of the fiber**	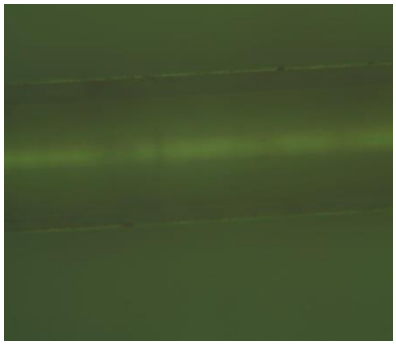	**Not Broken**
300	**18:00**	**The coating starts to burn, and the color is changed (Brown)**	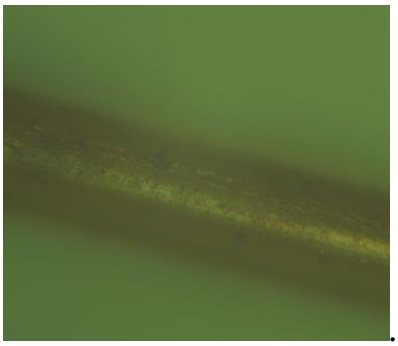	**Not Broken**
400	**23:54**	**Continue burning the coating, and the color is changed (black)**	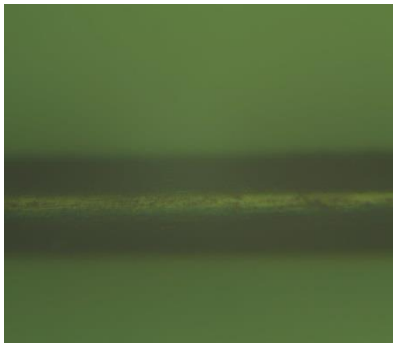	**Not Broken**
500	**31:03**	**Continue burning the coating, and the coating start removed**	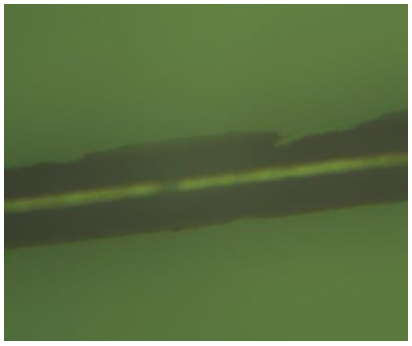	**Not Broken**

600	**37:35**	**Continue burning the coating, and the coating continue removed**	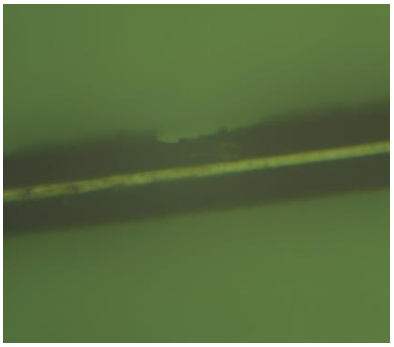	**Broken from 1 location**
700	**45:44**	**coating completely removed**	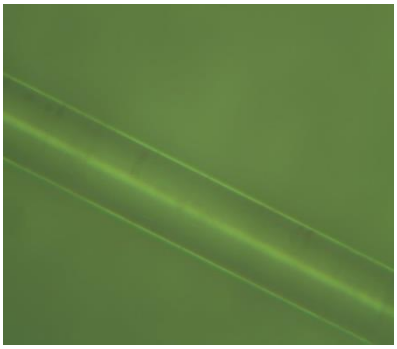	**Broken from 3 locations**
800	**56:02**	**The fiber entirely melted**	**No observation since the fiber was melted**	**No observation**
900	**1:08:14**	**The fiber entirely melted**	**No observation since the fiber was melted**	**No observation**
1000	**1:15:32**	**The fiber entirely melted**	**No observation since the fiber was melted**	**No observation**

Table 3.1 summarizes the results of the influence of temperature gradient on the fiber. The outer layer of the fiber is burned at a temperature of 300 ˚C, increasing burning leads the black color to appear on that layer and it is started to be removed at a temperature of 500 ˚C. The temperature of 700 ˚C is almost the maximum temperature the fiber can resist, beyond this temperature the cladding and the core material of the fiber will melt. Three different locations were chosen along

the fiber to check its flexibility after it exposed to the temperature gradient. The bending results show the fiber is keeping its flexibility with the range (0-500) ˚C where no breakage happened, then it is started to be effected at 600 ˚C with one broken and three broken for the fiber exposed to 700˚C. So clearly, the fiber lost its flexibility beyond 600 ˚C.

3.1.2 Temperature characterization of FBG

The other aspect of the fiber characterization includes the evaluation of the maximum temperature to the failure [60]. A single mode FBG inscribed SMF 28 is used in this test. The FBG inscribed SMF 28 is polyimide coated shown in Table 3.2:

Table 3.2: Polyimide coated fiber properties [60]

Test Parameters	***Specifications***
Geometrical Properties	
Cladding Diameter	125 ± 1.0 [µm]
Core Diameter	9.8 [µm]
Coating Diameter	145 ± 5 [µm]
Mechanical Properties	
Fiber proof test level	0.7 [GPa]
Operating Temperature Range	-50 to +430 [°C]
Short Term	+430[°C] (10Hrs) +400 [°C] (100 Hrs)
Optical Properties	
Attenuation	<0.5 [dB/km]
Cutoff Wavelength	<1300 ± 50 [nm]
Operating Wavelength	1300-1600 [nm]
Bend loss at 1550nm per 100 turns 25mm dia	<0.02 [dB]

3.1.1.1. Test setup

The experiment was performed to maintain reading, as the temperature increased, shifting of the FBG wavelength and the light transmission characteristics of the optical fiber in tandem were observed using the special setup for fiber optics. Both fibers were introduced through a top opening

of a Lindberg Blue box furnace with dimensions 30 x 30 x 30 cm and making a bend radius of approximately 1.5 cm, Figure 3.2.

Figure 3.2: Lab setup showing connections and instruments/apparatus used

3.1.1.2. Test results and discussion

Initially, the FBG central wavelength was recorded to be at 1538.5 nm at room temperature of 23°C. The test temperature was then raised with gradual steps, and a corresponding wavelength shift was observed as shown in Figure 3.3 (a). The wavelength was almost proportional to the increase of temperature as recorded in Figure 3.3 (b). The optical transmission loss remained negligible until the end of experiment with almost no sign of FBG wavelength peak at 956°C.

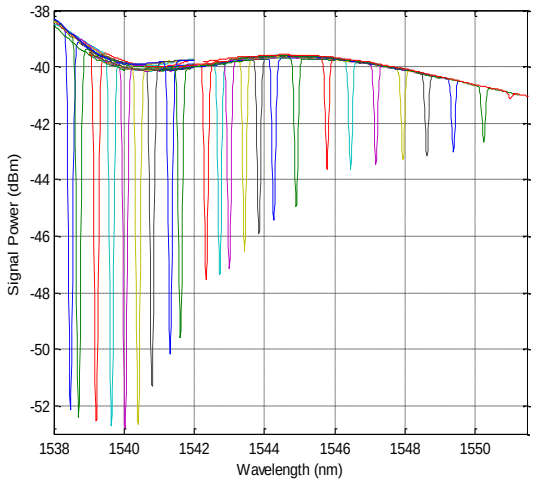

(a)

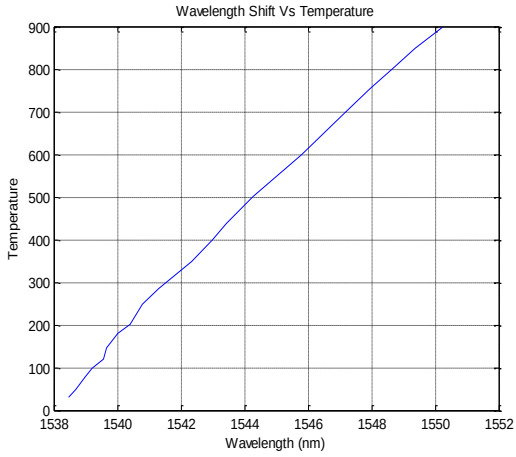

(b)

Figure 3.3: (a) spectra of wavelength shift with varying temperature (°C) (b) linear response of wavelength shift to temperature variation [60]

3.1.3 Pressure test

This test has been investigated with our research team to investigate the capability of the fiber to bear the pressure [60]. The test was part of the pressure test to study the sensitivity of the fiber to the applied pressure using the strain and its effect of the wavelength of the light pass through the

fiber. Figure 3.4 shows the setup which was utilized in this test. The fiber was kept in metal fitting; then water pump developed a pressure that applied to the fiber.

Figure 3.4: Experiment setup for a pressure test

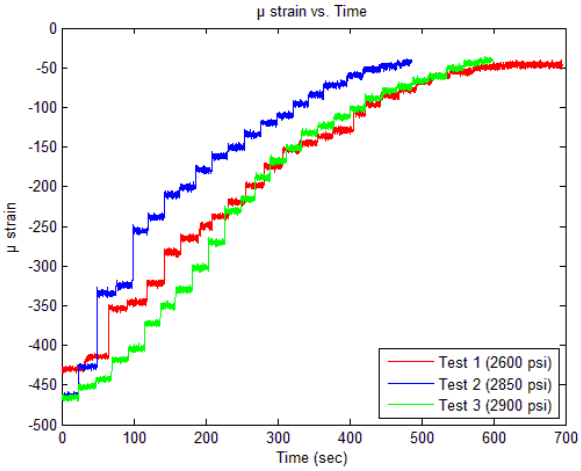

Figure 3.5: Measured strain during pressure sensitivity test for fiber

Figure 3.5 presents some results of using three different value of pressure i.e. 2600, 2850, and 2900 psi and its effect on the strain. For consideration of the main purpose of the test, a maximum pressure of 2900 psi (20 MPa) used. Although, the fiber has the capability to bear high pressure more than 2900 psi (20 MPa).

3.1.4 Checking fiber cross section

A short test was carried out on the fiber cross section using different tools i.e. cleaver and scissor to check the structure of the fiber. The next Figure – 3.6 present the two-cut fiber:

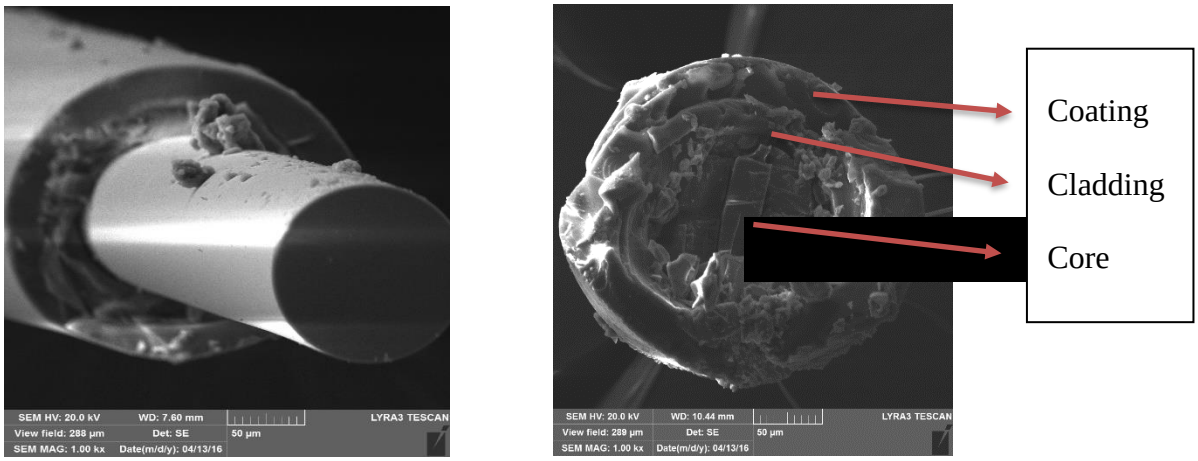

a) **b)**

Figure 3.6: Cut fiber a) using cleaver b) using scissor

The figure 3.6 shows that the fiber has two layers i.e. coating and jacket, covering the cladding and the core. Also, high damage of the fiber due to use the scissor compared to the fiber cut by a cleaver.

3.2 Embedding in the host using (USW)

Building the hosting material was done in stages starting with building the host material without fiber using Ultrasonic Spot Welding (USW). These preliminary tests to study the effect of the parameters in which the fiber will be checked in term of the integrity of host material and sensors and to get the specific parameters needed to have acceptable embedding. The next stage, in next chapters, was involving the fiber within the hosting material during the process.

3.2.1 Embedding power estimation

Regarding the theoretical background presented in chapter two, the parameters that control the ultrasonic spot welding are: physical parameters (properties and dimensions), the operating parameters (applied force, area, amplitude, and frequency), and the welding time.

Figure 3.7 shows the setup that is used to carry out this experiment. The limitations of the setup has enforced the experiments to have a specified trend. Since the frequency is limited in this machine to 20kHz and the applied force in terms of the applied pressure and area of the pneumatic system is also determined to have certain values. Thus the only parameters that can be changed are the amplitude; which is given as a percentage of the output power of this machine which varying (0- 4200) Joule, and the welding time.

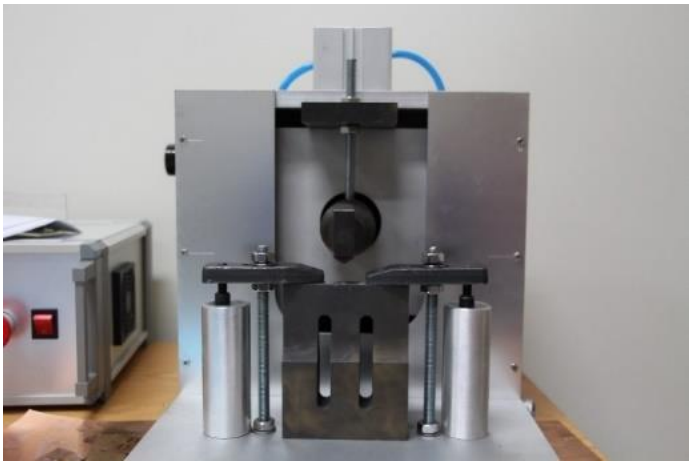

Figure 3.7: Ultrasonic spot welding machine

Through the equation (4), power is inversely proportional to the area of friction A_{fr}. Since there is limitation of the generated power, the horn friction area was modified to have a variety of the heat flux in term of the ratio between the friction areas.

Next figure 3.8 shows modified areas of friction:

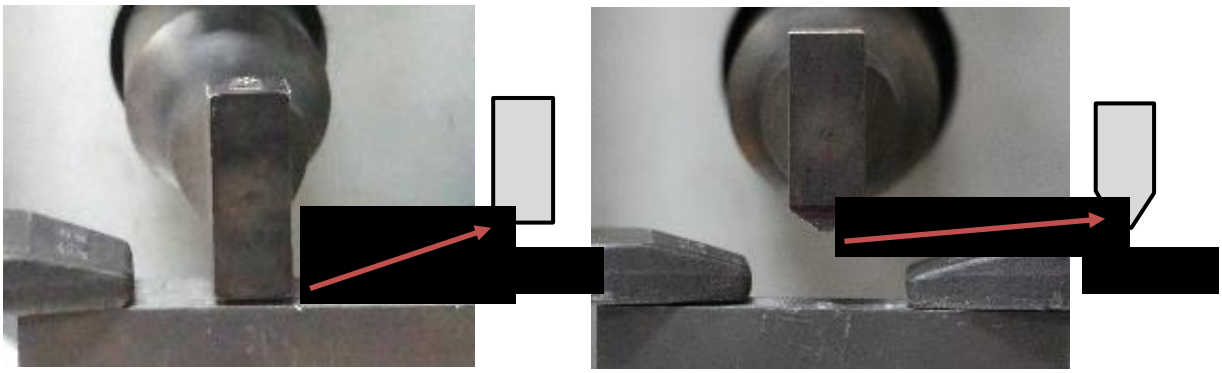

a) b)

Figure 3.8: Modified friction area a) large area b) small area

Characterization of the power generated by the machine was done using the following parameters for the used setup:

a) Operating applied pressure of the machine $Pr.$ = 0.3 – 0.4 Mpa. (stick to 0.3 Mpa)

b) The cross section area of the pneumatic system $A = \frac{\pi}{4} \times (6 \times 10^{-2})^2 = 2.83 \times 10^{-3}\ m^2$

c) The frequency f_w = 20 kHz.

d) Amplitude λ_w = (50%-100%).

e) Welding time t_w = 0-10 sec.

f) Input power factor ≥ 80% (= 85%)

g) Modified Friction areas $(A_{fr})_s$ =2×11= 22 mm^2

$$(A_{fr})_l = 16 \times 11 = 176 \text{ mm}^2$$

The range of power i.e. 0, and 4200, which corresponding to the welding time related to 0, and 10 sec, respectively. Thus, using equations (4) - (6) with the known power range will help to quantify the amplitude corresponding to each percent:

The maximum percentage of 100% is corresponding to the maximum power of 4200×0.85= 3570 joule, this value corresponding to the maximum welding time of 10sec; this leads to having an amplitude of 17.52 µm.

The minimum percentage of 50% is corresponding to the minimum power 2100×0.85= 1785 joule, this value corresponding to the maximum welding time of 10sec; leads to having an amplitude of 8.76 µm.

A linear relation was formulated for the output power generated by the machine based on the amplitude percentage. From Equation (5) we get the power generated can be written as follow:

$$P = F_N * \mu * 4 * \lambda_w * f_w$$

Moreover, by using the following value of parameters:

$$Pr. = 0.3\ Mpa, A = 2.83 \times 10^{-3}\ m^2$$

$$F_N = 0.3e6\ x\ 2.83\ e-3 = 849\ N$$

$$f_w\ =\ 20\ kHz, \mu = 0.3$$

The power generated can be represented as a function of amplitude by the following formula:

$$P = 3.57 \times \lambda_w(in\ \%)\ = 20.37 \times \lambda_w(in\ \mu m) \quad (11)$$

Including the welding time will give the energy generated by the ultrasonic machine:

$$E = 3.57 \times t_w \times \lambda_w(in\ \%)\ = 20.37 \times t_w \times \lambda_w(in\ \mu m) \quad (12)$$

Table 3.3 shows the value of the amplitude and the corresponding generated power:

Table 3.3: The amplitude and the corresponding generated power

Amplitude λ_w (%)	Amplitude λ_w (μm)	Power Generated (Watt)
50	8.76	178.49
60	10.51	214.15
70	12.26	249.80
80	14.01	285.47
90	15.77	321.33
100	17.52	356.99

3.2.2 Experimental work

The experiment started to construct the hosting material by welding two similar materials. Aluminum sheets of grade 6063 T6 separated by two aluminum foils were used in the experiments as shown in figure 3.9. Repeated experiments lead to the optimum value of the useful parameters i.e. amplitude and welding time.

Figure 3.9: Initial experimental configuration

Table 3.4: Preliminary results for welding hosting material

λ_w(in %)	t_w (sec)	$Cross-cut\ picture$	$Remarks$
75	0.85		Two sheets are welded together energy = 227.59 Joules energy flux= 10.35e6 Joules/m^2
80	0.65		Not good welding energy = 185.64 Joules energy flux= 8.44e6 Joules/m^2

80	0.7		Good welding energy = 199.92 Joules energy flux= 9.09e6 Joules/m^2
80	0.75	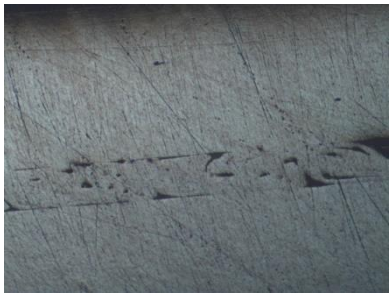	Good welding energy = 214.2 Joules energy flux= 9.74e6 Joules/m^2
85	0.85		Good welding energy = 257.93 Joules energy flux= 11.72e6 Joules/m^2

Generally, the previous table 3.4 shows the minimum energy needed for creating real bonds between the aluminum sheets and aluminum foils using the small friction area $(A_{fr})_s$. An energy of 200 Joules was enough to weld the two sheets with energy flux of 9.1e6 Joules/m^2. This value of energy can be extended to give the pairs of amplitude and welding time parameters for the used machine e.g. 75% amplitude with 0.85sec welding time gives value of 227.59 Joule give well bonding between the sheets. Where 80% amplitudr with 0.65sec welding time dose not creat actual bond also a big pore a pear in the contacting area of the two sheets.

CHAPTER 4:

FIBER OPTIC EMBEDDING USING ULTRASONIC CONSOLIDATION

After the characterization of the power needed to weld two similar sheets carried out in chapter 3. This chapter will present the embedding process of the fiber using (USW). Followed by testing the fiber with power light transmission:

4.1 Fiber embedding

Two configurations have been examined in this process. First, the fiber embedded between two similar sheets in a process called indirect ultrasonic consolidation. Second, is the direct ultrasonic consolidation where the fiber is embedded in the sub-surface of the sheet.

4.1.1 Indirect ultrasonic consolidation

4.1.1.1 Test configuration

The fiber was hosted in a sandwich between two sheets of Aluminum sheets (5 x 5 x 0.06 cm). First, two aluminum foils were added between the fiber and the Aluminum sheets to save the fiber during the process. The second case was without using aluminum foils to see the difference between both cases. Figure 4.1 shows the graphic drawing for both cases.

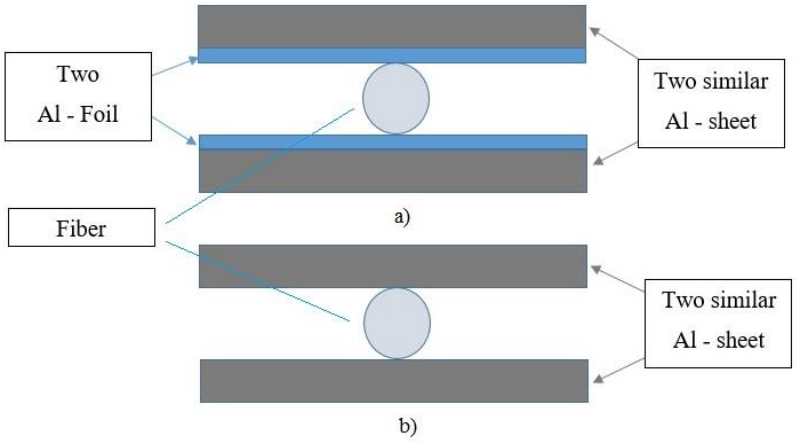

Figure 4.1: Initial configuration for embedding process a) with Al- foils b) without Al-foils

Two identical parameters i.e. amplitude of 75% and welding time of 0.85 sec, were used. The preliminary results indicate that the foils will affect the process i.e. will dissipate some energy to be able to embed the fiber as shown in figure 4.2. Lower embedding for the fiber was noticed using Al-foils, where some of the energy dissipated and cause damage for the foils.

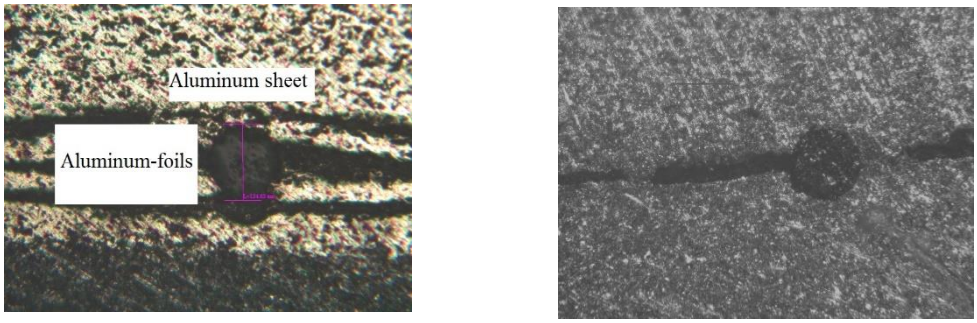

a) **b)**

Figure 4.2: Embedded fiber a) with Al-foils b) without Al-foils

Embedding of the fiber was started using the minimum power for welding the aluminum sheets i.e. 200 Joules, with a different pair of parameters (amplitude and welding time).

4.1.1.2 Test results and discussion

The result of three separate value of energy is presented in the following Table 4.1.

Table 4.1: Fiber embedding between two sheets

λ_w(in %)	t_w (sec)	$cross-cut\ picture$	$Remarks$
70	0.85	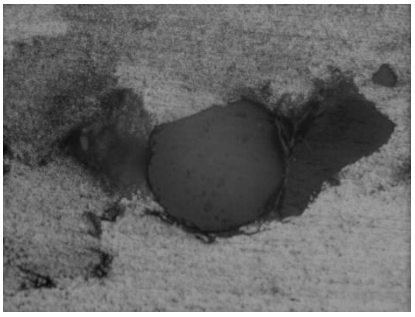	Partially embedding with some defects energy = 212.42 Joules energy flux= 9.66e6 Joules/m^2
75	0.85	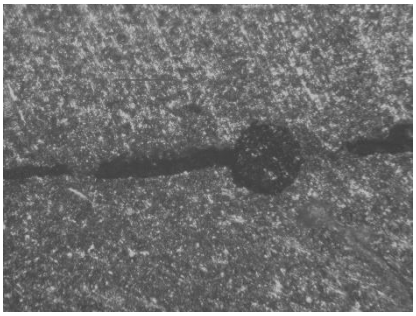	Good embedding energy = 227.59 Joules energy flux= 10.35e6 Joules/m^2
80	0.85	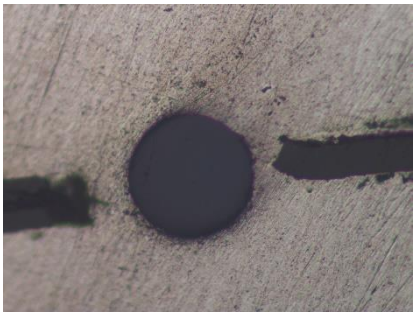	Embedding is done energy = 242.76 Joules energy flux= 11.03e6 Joules/m^2

Table 4.1 shows that the minimum value of welding two sheet of aluminum, found in the previous chapter, is not enough to embed the fiber within two aluminum sheets. Where the first picture in the same table shows the pores around the fiber i.e. no well sticking between the fiber and the host material. The value of 227.59 joules in the second picture, in the previous table 4.1, also is not enough to get the proper embedding. It is noticed that the embedding between two sheets achieved using the energy of 242.76 Joules energy flux of 11.03e6 Joules/m^2 as shown in the last picture. This value of energy can be generated using a different pair of changeable parameters.

4.1.2 Direct ultrasonic consolidation

4.1.2.1 Test configuration

The fiber is in sandwich and direct contact with the host aluminum sheet. Aluminum sheets used as hosting material, with dimensions 5 x 5 x 0.06 cm and copper sheets of thickness 0.04 cm, as heat conducting material, to transfer the energy to the hosting material as shown in Figure 4.3:

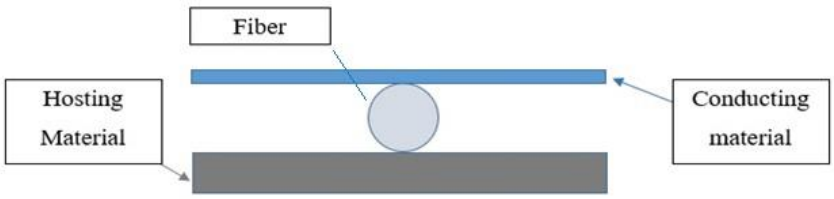

Figure 4.3: Direct ultrasonic consolidation

The experiment was carried out with two different friction surfaces mentioned before. The reason was to have a large range of power not only by the amplitude and welding time that are limited in ranges in this machine but also from friction area.

4.1.2.2 Test results and discussion

The following Table 4.2 presents the result of using the smaller friction area:

Table 4.2: Embedding using smaller friction area

λ_w(in %)	t_w (sec)	$cross-cut\ picture$	$Remarks$
50	0.65	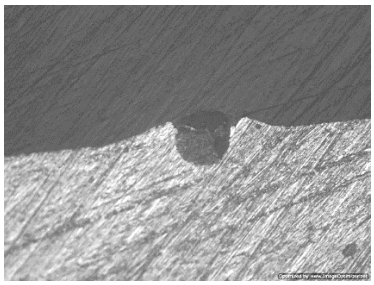	75% quarter embedding energy = 116.03 Joules energy flux = 5.274e6 Joules/m^2
50	0.75	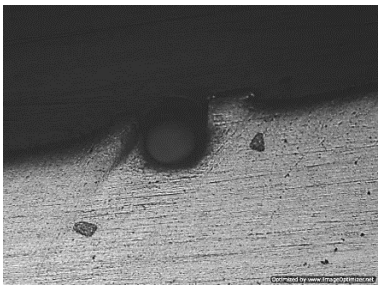	80% embedding energy = 133.88 Joules energy flux = 6.09e6 Joules/m^2
50	0.85	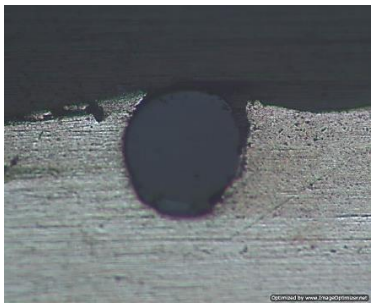	90% embedding energy = 151.73 Joules energy flux = 6.89e6 Joules/m^2

The previous table 4.2 shows the fiber embedding using the small area of friction. It is noticed the embedding is almost achieved using low parameters i.e. 50% amplitude and 0.85sec welding time.

These results do not give the graduation of the embedding for a large range of parameters; the reason that the power is directed in a small area due to use of smaller area of friction. So, the larger friction area was used with different parameters to show the effect of the friction area on the embedding process, Table 4.3:

Table 4.3: Embedding using larger friction area

λ_w(in %)	t_w (sec)	$cross-cut\ picture$	$Remarks$
60	0.25	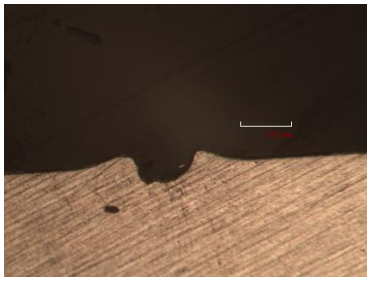	25% quarter embedding energy = 53.55 Joules energy flux = 3.04e5 Joules/m^2
60	0.5	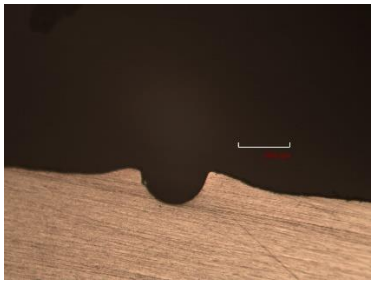	50% embedding energy = 107.1 Joules energy flux = 6.08e5 Joules/m^2
60	0.75	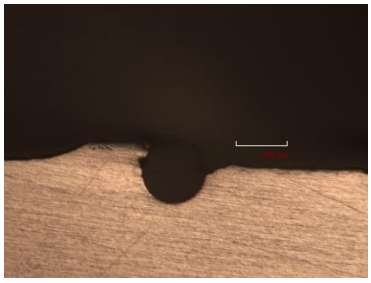	75% embedding energy = 160.65 Joules energy flux = 9.13e5 Joules/m^2

60	1	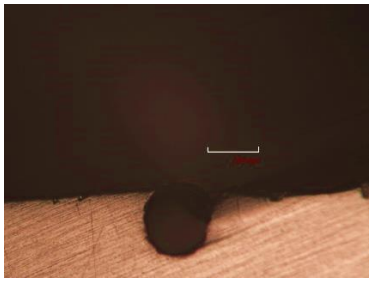	90% embedding energy = 214.2 Joules energy flux = 1.22e6 Joules/m^2

From the previous tables 4.2 and 4.3, smaller friction area leads to rapid embedding using a lower value of amplitude. The energy generated increased by increasing the welding time. So, the depth of embedding increased with increasing the energy.

Regarding the embedding, it is noticed that that both energy and energy flux determine the depth embedding e.g. for small friction area 50% and 0.85 sec gives almost the same embedding depth for 60% and 1 sec using larger friction area. The energy was 151.73 Joules for 50%, and 214.2 Joules for 60%. Energy flux was 6.89e6 Joules/m^2, and 1.22e6 Joules/m^2 for 50% and 60%, respectively. So, different areas produce different embedding with the same process parameters

For all previous experiment, a common observation was noticed during the embedding that the coating of the fiber was always melted because of the temperature gradient the fiber is exposed to. The melting of the coating leads the fiber to be weaker and could not resist the direct mechanical loads. The heat test done before gives the explanation for this event. Also, the needed time for the embedding does not exceed the 1 sec welding time.

The following figures summarize the energy generated from the machine and the power behavior for the process using both friction areas i.e. small and large area.

4.1.2.3 Generated power estimation

The energy generated by the machine and the resulted energy flux is affected by the used parameters; the following figures show the total power generated from the machine, and the energy flux induced through the material due to different friction areas.

The next figures 4.4, 4.5, 4.6, and 4.7 show the effect of changing the friction area; the same amount can be transferred faster by reducing the friction area, leads to developing faster temperature gradient and then a localized heating in a shorter time.

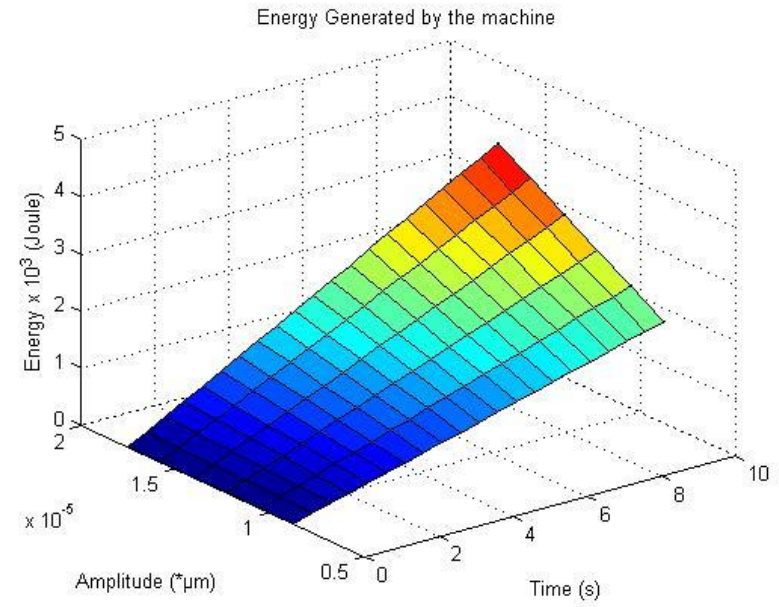

a)

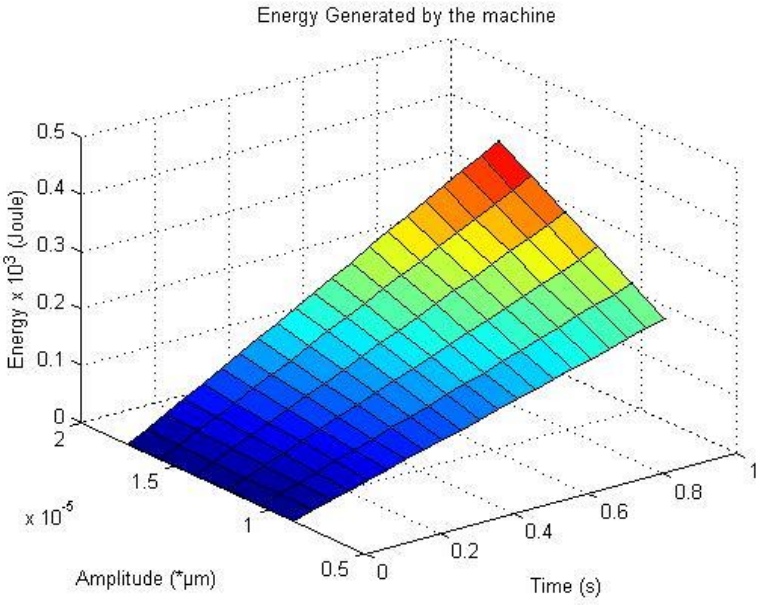

b)

Figure 4.4: The profile of the generated energy by the machine a) welding time (0-10) sec b) welding time (0-1) sec

The flux due to small friction area is shown in Figure 4.5:

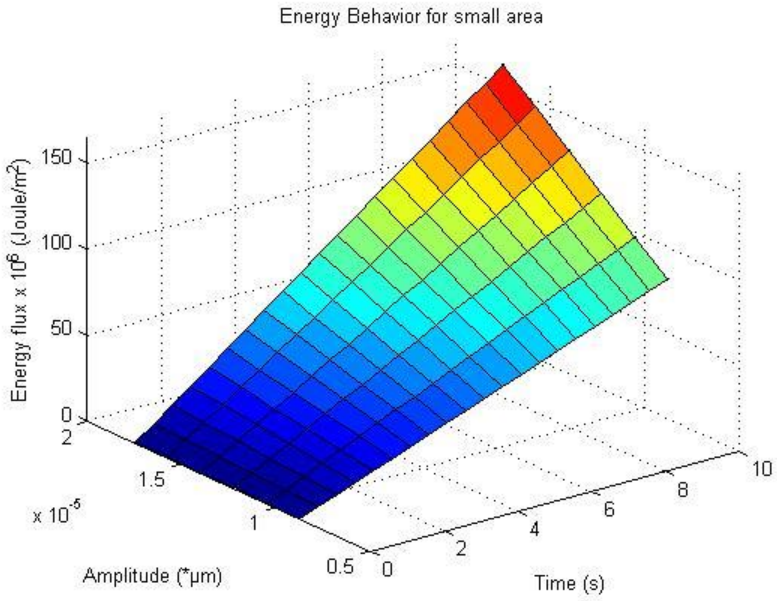

a)

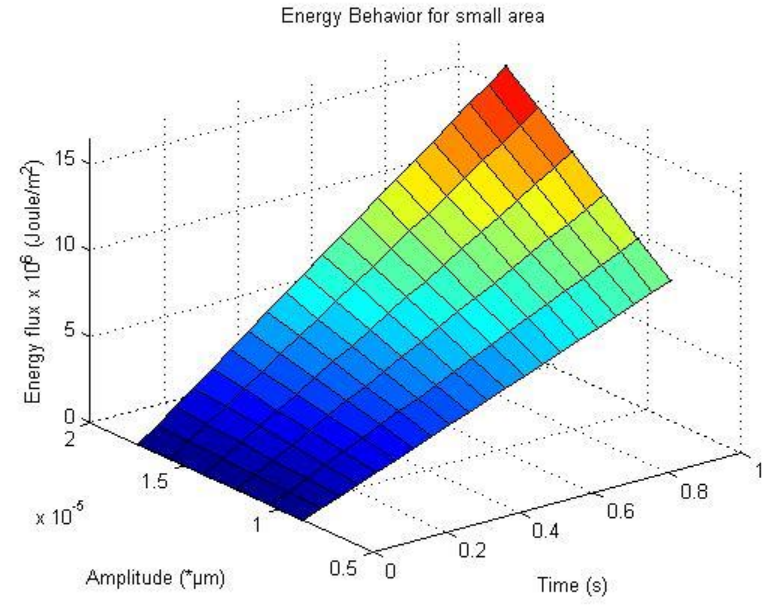

b)

Figure 4.5: The profile of the energy flux due to small area a) welding time (0-10) sec b) welding time (0-1) sec

The flux due to large friction area is shown in Figure 4.6:

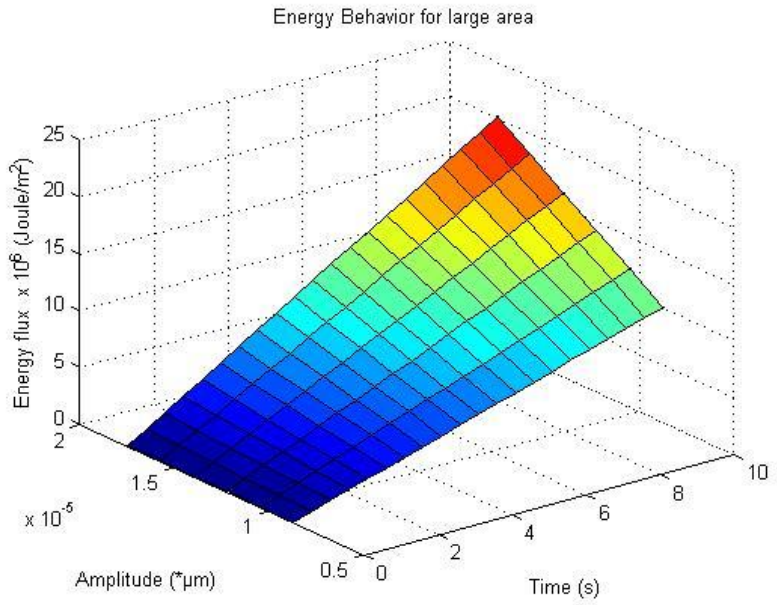

a)

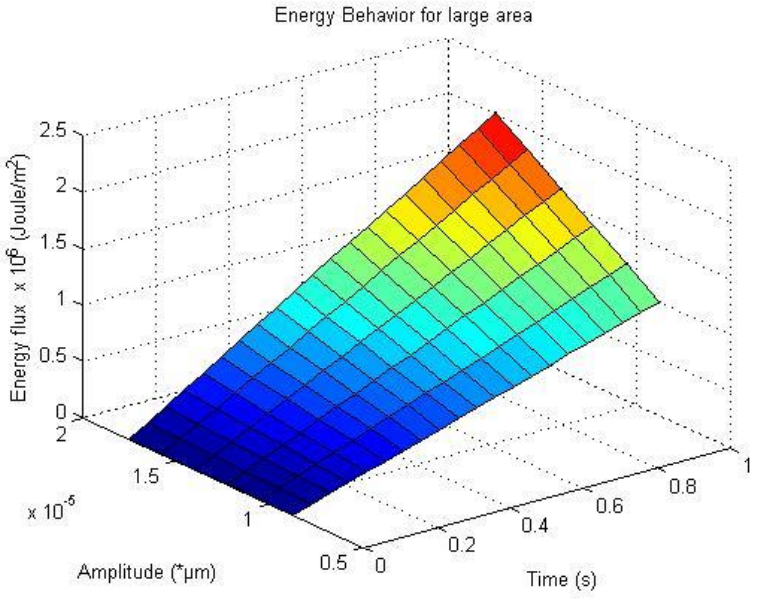

b)

Figure 4.6: The profile of the energy flux due to large area a) welding time (0-10) sec b) welding time (0-1) sec

Figure 4.7 shows the big difference between the energy flux due to small and large friction area:

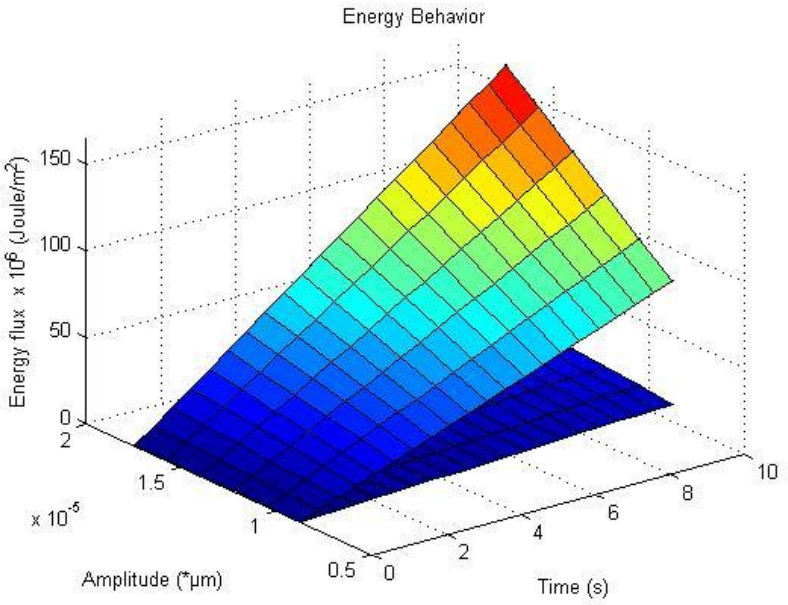

a)

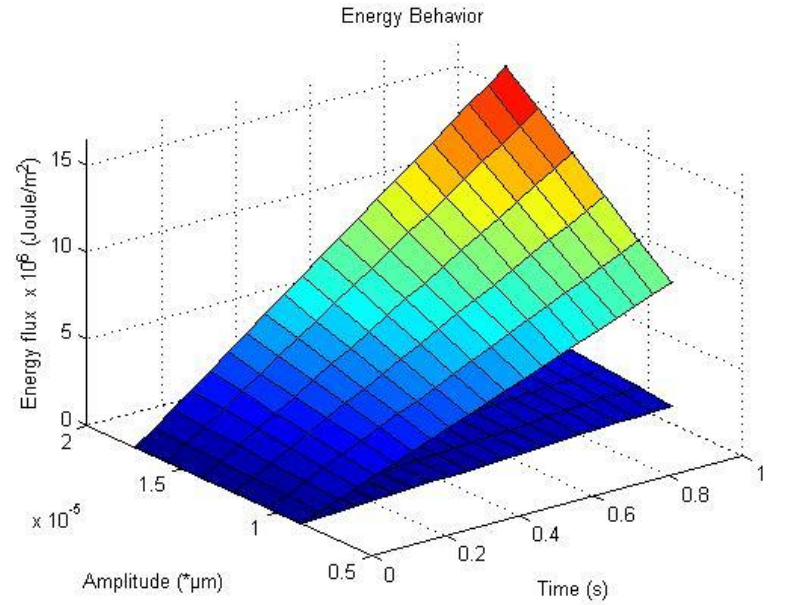

b)

Figure 4.7: Energy flux due to both area a) welding time (0-10) sec b) welding time (0-1) sec

4.2 Power light test

The power light will characterize the fiber and the host material followed by checking the integrity of the fiber after embedding. It is based on the concept of reflecting the light through the fiber without scattering i.e. the ability of transmission the light with minimum losses. Securing the functional integrity for embedded fiber lead to be used as a sensor in (SM). Regarding indirect ultrasonic consolidation, tests were achieved for the sample with three stages. However, unfortunately, in the indirect ultrasonic consolidation method, the fiber was broken due to mechanical load, since the coating is melted and deformed because of the thermal load during the process.

4.2.1 Indirect ultrasonic consolidation

The purpose of the test is to check the signal for the light in the embedded state and compare it with a reference value of the power to see the effect of the embedding on the transmission. The operation parameter of the embedding was (65% amplitude and seven sec. welding time). The test was done for the fiber with three stages: one, two and three spot welding with two level of light power (Low and High). The following Figure 4.8 shows the configuration of the test.

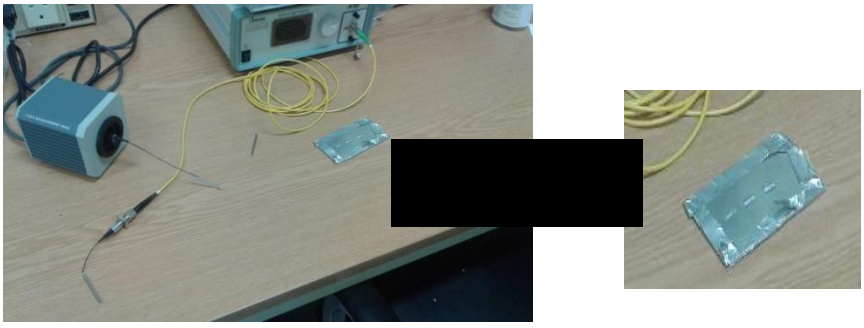

Figure 4.8: Power Light Transmission Test configuration

The total losses due to splicing were 0.16 dBm (≈ 1.0375 mW). Moreover, the losses due to configuration were 0.73 dBm (≈1.183 mW). Since the configuration losses included in the reference value of the power no need to be considered to calculate the error.

The following tables 4.4, 4.5 and 4.6 show the result of the tests:

Table 4.4: Test for one spot welding

POWER LEVEL	REF.		SAMPLE		SAMPLE LOSSES		% LOSSES	
	dBm	mW	dBm	mW	dBm	mW	dBm	mW
LOW	-7.505	0.1776	-19.579	0.01101	12.074	0.16659	160.9	93.8
HIGH	2.087	1.617	1.458	1.3986	0.629	0.2184	30.1	13.5

Table 4.5: Test for two spot welding

POWER LEVEL	REF.		SAMPLE		SAMPLE LOSSES		% LOSSES	
	dBm	mW	dBm	mW	dBm	mW	dBm	mW
LOW	-7.48	0.1786	-20.167	0.009622	12.687	0.168978	169.6	94.6
HIGH	2.085	1.616	0.914	1.234	1.171	0.382	56.1	23.6

Table 4.6: Test for three spots welding

POWER LEVEL	REF.		SAMPLE		SAMPLE LOSSES		% LOSSES	
	dBm	mW	dBm	mW	dBm	mW	dBm	mW
LOW	-7.515	0.1772	-55.5	3.17E-06	47.985	0.177197	Very high	99.9
HIGH	2.062	1.6075	-35.555	2.82E-04	37.617	1.607218	Very high	99.9

The error of the test using the high-power source almost is lower than using the low source of energy. These significant losses can be interpreted due to the high reflection index of the hosting material. One of the properties of the fiber that the cladding should have less reflection index than the core. The source of the error comes from the changing of the reflection index due to coating removal i.e. the coating of the fiber is removed, and the cladding is affected by the mechanical load, so the reflection index is changed. Using the high power could overcome this changing of the index, but the low power could not. The error due to using a different unit of power come from the large difference in scale between the two units.

For Direct Consolidation, no extend fiber was gotten due to the repeated broken during the process. So, the power light test was not achieved for this consolidation.

CHAPTER 5:

ALTERNATIVE METHODS FOR EMBEDDING

(POWDER METALLURGY)

5.1 Introduction

The Powder Metallurgy (PM) technique is considered relatively as lower power process, so it was proposed to be used for embedding the fiber within the powder based material, so the aim of this part of the work is to find the effective parameters that can be used to get the proper embedding using this method. The work started by designing the die that contains the powder to be compacted and the die will give the final shape to the sample. Deciding the location of the fiber embedded within the material is an important aspect that should be considered, a numerical analysis using Finite Element Analysis (FEA) was done to determine the proper location of the fiber to be embedded within the structure. The software ANSYS 15.0 was utilized in this analysis.

The analysis followed by a preliminary experiment, Aluminum powder i.e. Al-6061 powder was used, to define the compaction and sintering parameters. The process was done in two stages: the powder is filled into a steel die, then it is compacted at high pressure to give the green density of the sample. For sintering, the sample is solidified by exposing it to heat source with a regular cycle in the furnace using an inert gas (Argon).

5.2 Die design

The pressure which is used in the compaction process needs a hard material to make the die, so carbon steel was selected for this purpose. Figure 5.1a shows the configuration that used for the initial die design. The first test displayed two main problem that the die was not strong enough due to low hardness i.e. 50 HRC and side parts do not have the capability to withstand multi compaction with trials to build several samples. A second die redesigned as shown in Figure 5.1b with 62 HRC hardness and side parts with enclosure.

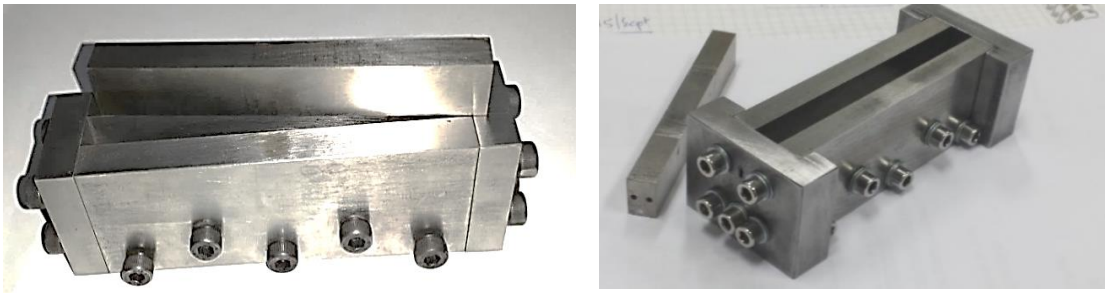

a) b)

Figure 5.1: Die Design a) Initial design b) Second design

5.3 Finite Element Analysis (FEA) for the beam

(FEA) was used to investigate the stress and strain distribution for the structure, this investigation helps define the proper location where the sensor will be embedded during the process of embedding. A simple structural element i.e. beam was used in this investigation because it is easy to be validated with the analytical solutions, the validating for simple structure leads to model a complex one i.e. cross bar structure.

5.3.1 Modeling

5.3.1.1 Material modeling

To have compatibility with aluminum sheet in the process of (UC), an Aluminum 6061 T6 was chosen in this analysis; the following properties belong to this grade of Aluminum:

a) Modulus of elasticity E = 6.9e10 Pa.
b) Poisson's ratio v =0.33
c) Density $\rho = 2700\ kg/m^3$
d) Yielding strength S_Y = 2.75e8 Pa
e) Ultimate Tensile Strength S_T = 3.1e8 Pa

5.3.1.2 Geometry modeling:

Like the die cavitation, the cross section was taken as a uniform rectangular shape of 10x10 mm, and the length is 100 mm. The beam was modeled as a cantilever beam loaded with end point load. Next Figure 5.2 shows the geometry of the beam:

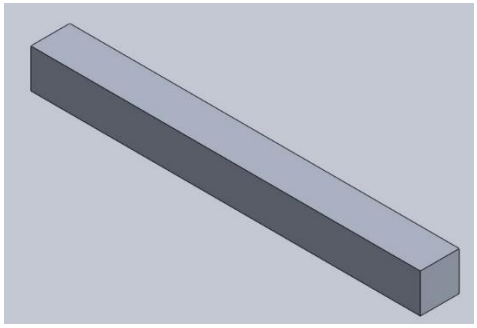

Figure 5.2: The geometry of the beam

Brick solid element with eight nodes (SOLID 185) was prefered to be used because it gives a uniform distribuiton for loading in adition to the advantages of directness, then it is meshed using

mapped meshing due to its uniform shape. For more accurate result, different sizes of meshing were tried to get the convergence of the result to be reasonable. The convergence was based on the maximum deflection that measured in the tip for the cantilever beam.

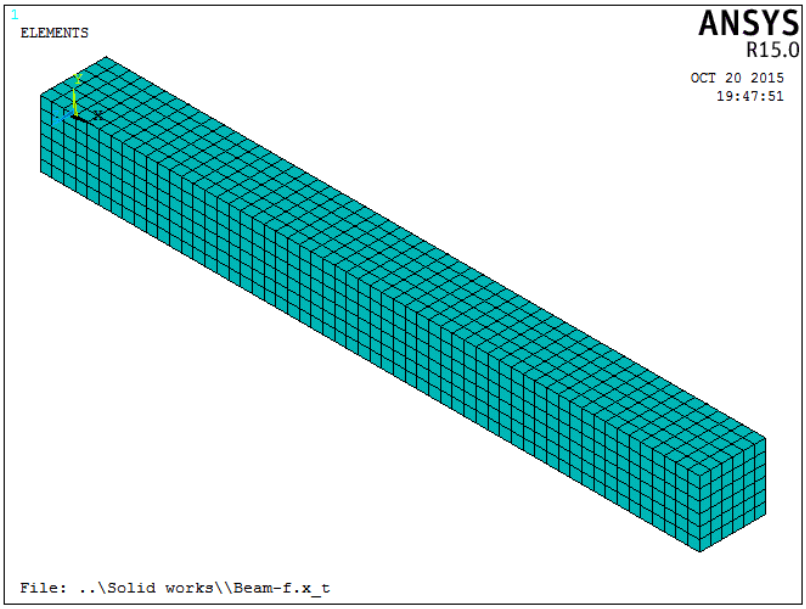

Figure 5.3: Meshing the beam

Next table 5.1 shows this convergence; The convergence is done for element size of 0.0018 m and number of elements of 2016, where the result of the stress and the max. deflection starts to have a constant value, which means increasing the element number will not give any chance of changing the stress and deflection:

Table 5.1: Meshing convergence

Element size	Number of element	Von Mises stress (*e8 Pa)	Max Deflection (*e-3 m)
0.005	80	0.258	0.277
0.004	225	0.271	0.282
0.003	544	0.281	0.285
0.002	1250	0.283	0.282
0.0019	1908	0.292	0.288
0.0018	2016	0.292	0.289
0.0017	2129	0.293	0.289

5.3.1.3 Load modeling

Different loads of 50, 100, 150, 200, 250, 300, 380, and 400N are applied on the end tip of the beam. Stress and strain distributions are plotted to define where the sensor will be embedded,the following figures present the Stress and strain distributions.

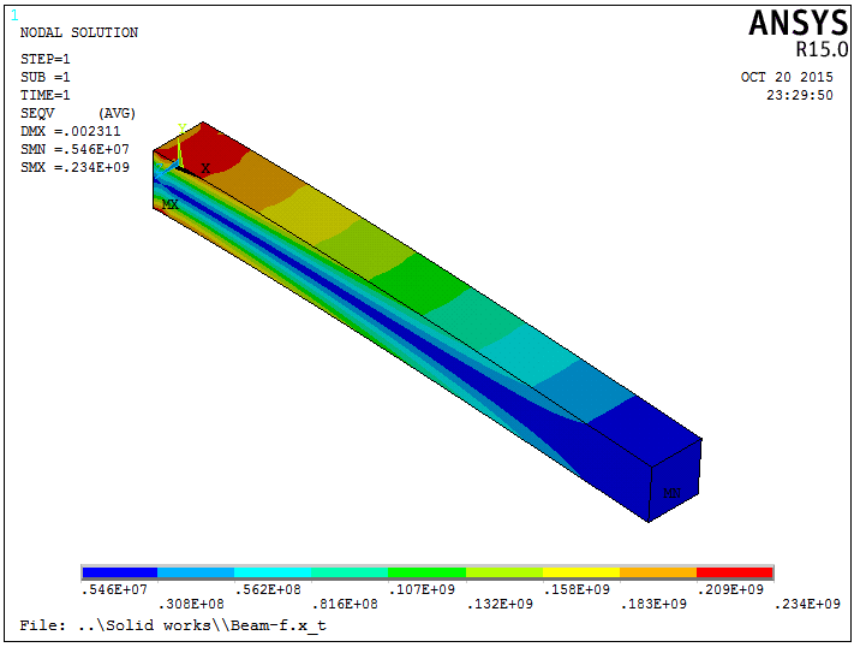

Figure 5.4: Von Mises stress distribution

Figure 5.4 present the stress developed along the beam due to the applied pressure and developed stress along the neutral axis has negligible value compared to other reading in other locations of the beam, also Figure 5.5 shows that variation on the cross section of the beam. The strain has the same trend of the stress either along the beam or in the cross-section view shown in Figures 5.6, and 5.7.

The proper location for the fiber to be embedded is the sub-surface, where different readings for the strain can be measured along the beam. The embedded fiber will be affected with the same strain developed in the beam. So, extracting the data from the reflecting light pass through the fiber will reflect the effect of the load on each point of the beam.

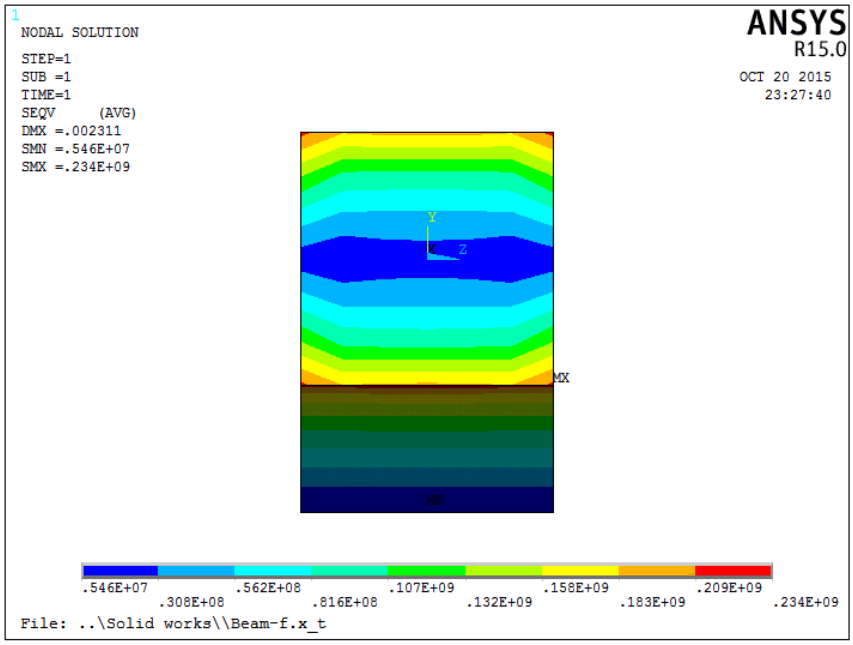

Figure 5.5: Stress distribution on the cross section

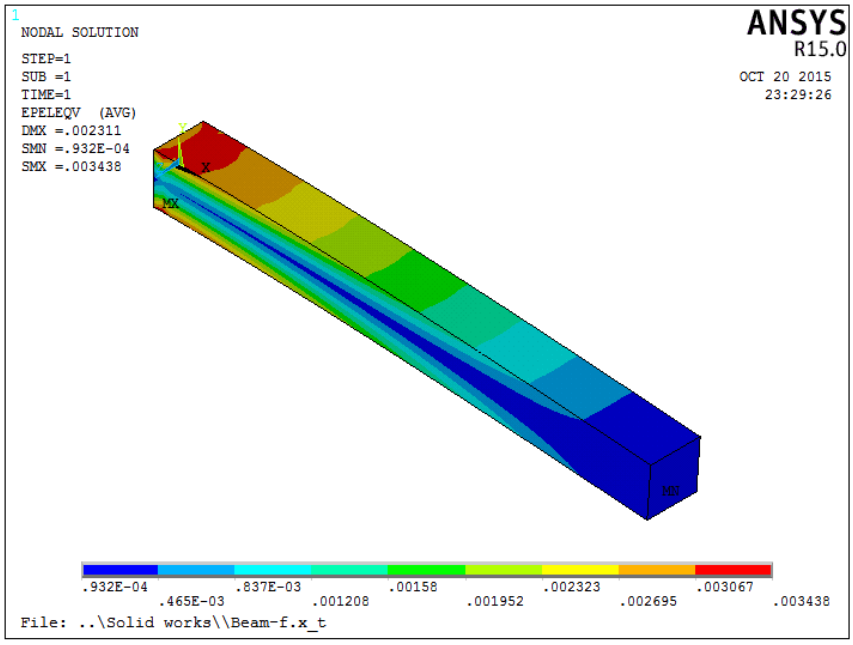

Figure 5.6: Total strain distribution

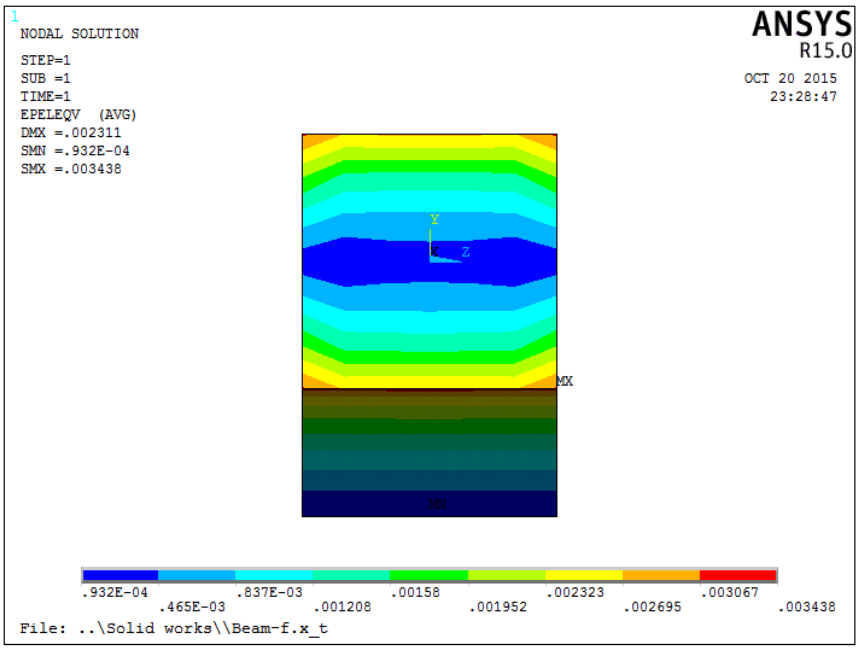

Figure 5.7: Strain distribution on the cross section

For more complicated structure a cross bar was simulated with two loads i.e. bending and torsion to show the stress and strain distribution through all the structure to help of defining the proper place of embedding as shown in Figure 5.8:

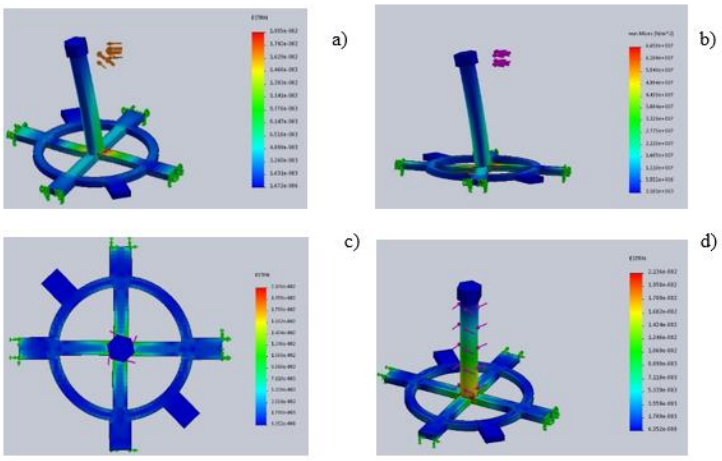

Figure 5.8: Stress and strain distribution for cross bar a, b) bending load c, d) torsion load

5.3.1.4 Validation of the FEM model

For validation, the results obtained from the FEM model of the beam were compared to the results of the von Mises yield criterion. The resulted value of the stress, strain and deflection were compared to the analytical result of this formula:

$$\boldsymbol{\sigma_{von}} = \sqrt{\frac{\mathbf{1}}{\mathbf{2}}\left[((\boldsymbol{\sigma_x} - \boldsymbol{\sigma_y})^2 + (\boldsymbol{\sigma_y} - \boldsymbol{\sigma_z})^2 + (\boldsymbol{\sigma_z} - \boldsymbol{\sigma_x})^2) + \mathbf{6}(\boldsymbol{\tau_{xy}}^2 + \boldsymbol{\tau_{yz}}^2 + \boldsymbol{\tau_{xz}}^2)\right]} \qquad (13)$$

Where:

$$\boldsymbol{\sigma_x} = \frac{-\boldsymbol{F} * \boldsymbol{x} * \boldsymbol{y}}{\boldsymbol{I}}, \qquad \boldsymbol{\tau_{xy}} = \frac{-\boldsymbol{F} * (\boldsymbol{c}^2 - \boldsymbol{y}^2)}{\mathbf{2} * \boldsymbol{I}} \{\boldsymbol{\tau_{xy\ @y=c}} = \mathbf{0}\}$$

$$\boldsymbol{\sigma_y} = \boldsymbol{\sigma_z} = \boldsymbol{\tau_{yz}} = \boldsymbol{\tau_{xz}} = \mathbf{0}$$

and

$$\boldsymbol{\varepsilon_{von}} = \frac{\mathbf{2}}{\mathbf{3}} * \sqrt{\left[\frac{\mathbf{3}\left(\boldsymbol{\varepsilon_x}^2 + \boldsymbol{\varepsilon_y}^2 + \boldsymbol{\varepsilon_z}^2\right)}{\mathbf{2}} + \frac{\mathbf{3} * ((\mathbf{2} * \boldsymbol{\varepsilon_{xy}})^2 + (\mathbf{2} * \boldsymbol{\varepsilon_{yz}})^2 + (\mathbf{2} * \boldsymbol{\varepsilon_{xz}})^2)}{\mathbf{4}}\right]} \qquad (14)$$

Where:

$$\boldsymbol{\varepsilon_x} = \frac{-\boldsymbol{F} * \boldsymbol{x} * \boldsymbol{y}}{\boldsymbol{E} * \boldsymbol{I}}, \boldsymbol{\varepsilon_y} = \frac{-\boldsymbol{v} * \boldsymbol{F} * \boldsymbol{x} * \boldsymbol{y}}{\boldsymbol{E} * \boldsymbol{I}}, \boldsymbol{\varepsilon_{xy}} = \frac{-\boldsymbol{F} * (\boldsymbol{c}^2 - \boldsymbol{y}^2)}{\mathbf{2} * \boldsymbol{I} * \boldsymbol{G}} \{\boldsymbol{\varepsilon_{xy\ @y=c}} = \mathbf{0}\}$$

$$, \boldsymbol{\varepsilon_z} = \mathbf{0}, \boldsymbol{\varepsilon_{yz}} = \mathbf{0}, \boldsymbol{\varepsilon_{xz}} = \mathbf{0}, \boldsymbol{\delta_{max}} = \frac{\boldsymbol{F} * \boldsymbol{l}^3}{\mathbf{3} * \boldsymbol{E} * \boldsymbol{I}}$$

Next table 5.2 shows the comparison between the analytical results and the results from the ANSYS 15.0 software for different loads. By looking at the table, it is clear that the percentage of error for the ANSYS result are acceptable except that the strain has high error of almost 15%. So, the FEA model clarifies the stress and strain distribution within the beam shape, also locating the fiber within the structure which will be produced using the (PM) technique. Clearly, location of the fiber could be any location within the beam, but the neutral axis should be avoided since there

is no strain or stress developed in this axis, this will secure to have some wavelength shift reading in case of any deformation happened for the beam

Table 5.2: Comparison of the analytical results and the ANSYS results

Load	Von Mises stress (Pa)			Von Mises strain			Max Deflection		
	Analytical	ANSYS	*100 % error	Analytical	ANSYS	*100 % error	Analytical	ANSYS	*100 % error
50	3E+07	2.9E+07	0.02667	0.00037	0.00043	0.15026	0.00029	0.00029	0.00295
100	6E+07	5.9E+07	0.025	0.00075	0.00086	0.15026	0.00058	0.00058	0.00295
150	9E+07	8.8E+07	0.02556	0.00112	0.00129	0.14937	0.00087	0.00087	0.00295
200	1.2E+08	1.2E+08	0.025	0.0015	0.00172	0.14959	0.00116	0.00116	0.00295
250	1.5E+08	1.5E+08	0.02667	0.00187	0.00215	0.14972	0.00145	0.00144	0.00364
300	1.8E+08	1.8E+08	0.02778	0.00224	0.00258	0.14981	0.00174	0.00173	0.00353
380	2.3E+08	2.2E+08	0.02632	0.00284	0.00327	0.14956	0.0022	0.0022	0.00313
400	2.4E+08	2.3E+08	0.025	0.00299	0.00344	0.14959	0.00232	0.00231	0.00338

5.4 Cold Compaction

For cold compaction process, the process was set to get good green compaction for the sample and defining the proper parameters to get a compacted sample. Based on these results, few parameters would be used to have the fiber inserted within the sample during the compaction process.

5.4.1 Experimental Work

First, the work was aimed to define the parameters that should be used in the process to get proper embedding. Two considerations are needed, the compacted sample and an appropriate embedding. So, two different loads were used in this process 25000 Ib and 35000 Ib. Like the first trial, different samples were compacted as shown in the following Table 5.3:

Table 5.3: First trial for compaction

Sample #	Fiber	Load (Ib)	Time (sec)
1	without	25000	40
2	without	35000	40
3	with	25000	40
4	with	35000	180

The early observation for these samples that the load of 25000 Ib was not enough to achieve the compaction i.e. sample #3 containing the fiber, also there are some cracks happened on sample #2 that compacted using 35000Ib. Next figure 5.9 shows a picture for the cross section of the compacted sample without the fiber. The high load of 35000 lbs gives proper compaction compared with 25000 lbs.

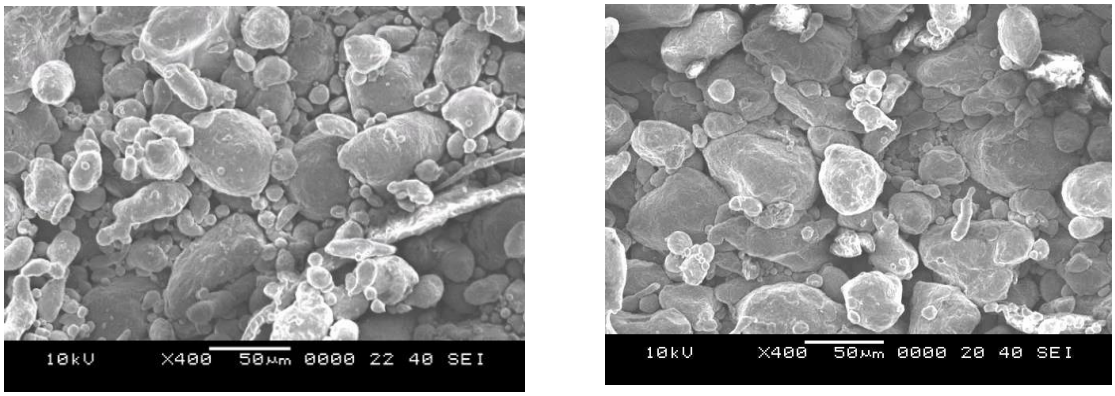

a) **b)**

Figure 5.9: SEM picture for compacted samples 40 sec a) 25000 Ib b) 35000 Ib

For more investigation of the compaction and sintering process, some of the remaining samples were sintered. The following Table 5.4 presents the parameters used for sintering, followed by the cross-sectional pictures for the resulted samples:

Table 5.4: First sintering parameters

Trial #	Sintering Temperature (˚C)	Sintering time (hour)	Load (Ib)	Time (sec)	Sample name
1	200	4	25000	40	A
2	250	4	25000	40	B
3	300	4	25000	40	C
4	300	4	35000	180	D

Table 5.5: Preliminary results of compaction and sintering

Sample Name	Parameters	Pictures	
A	25000 lbs, 200 ˚C, 4 Hours	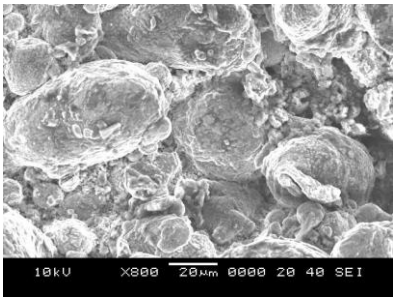	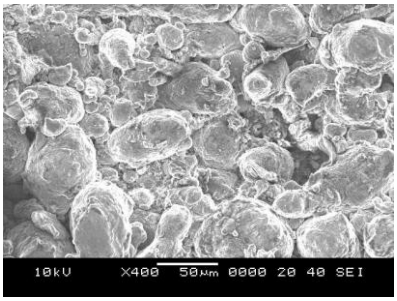
B	25000 lbs, 250 ˚C, 4 Hours	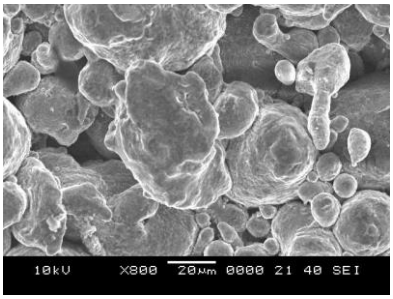	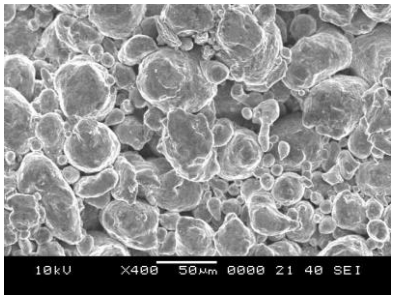
C	25000 lbs, 300 ˚C, 4 Hours	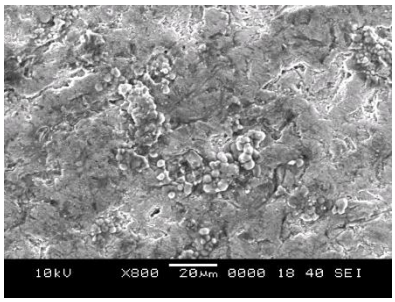	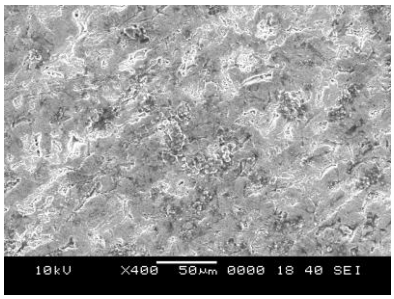

D	35000 lbs, 200 ˚C, 4 Hours	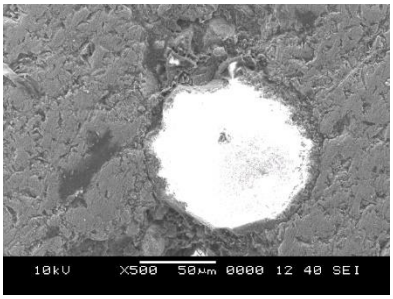	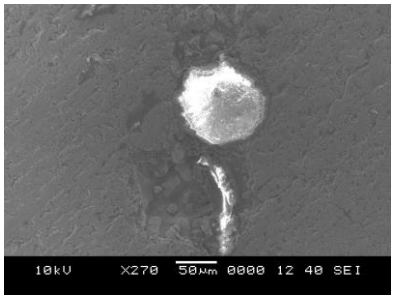

The result in table 5.5 proves that sintering temperature of 300˚C dose not give the needed sintering, also using 25000 lbs compaction load does not lead to suitable compaction. So, in the next stage, the sintering temperature was fixed at 450 ˚C with changing the time i.e. 4, 6, and 8 hours using different compaction loads (25000 lbs, 35000 lbs). Table 5.6 shows the last test to define the proper parameters of compaction and sintering:

Table 5.6: Last test to define the proper compaction and sintering parameters

Load (lbs)	compaction time (min)	T(˚C)	Sintering time (hour)	Sample name
35000	5	450	4	E
35000	5	450	6	F
35000	5	450	8	G
25000	5	450	4	H
25000	5	450	6	I
25000	5	450	8	J

Table 5.7 shows the results of the tests summarized in the previous table 5.6:

Table 5.7: Compaction and sintering test results

Sample Name	Parameters	Pictures	
E	35000 lbs, 450 ˚C, 4 Hours	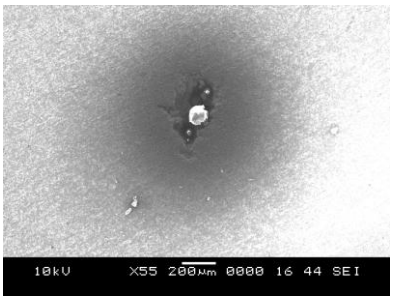	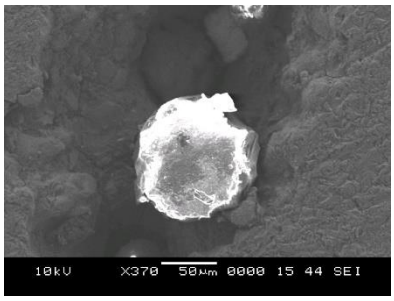
F	35000 lbs, 450 ˚C, 6 Hours	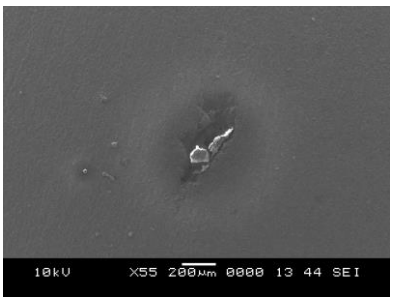	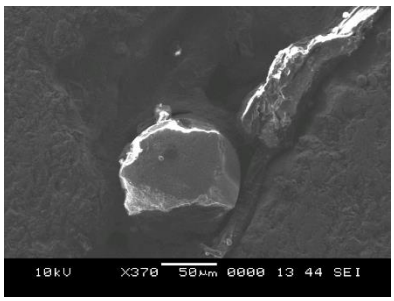
G	35000 lbs, 450 ˚C, 8 Hours	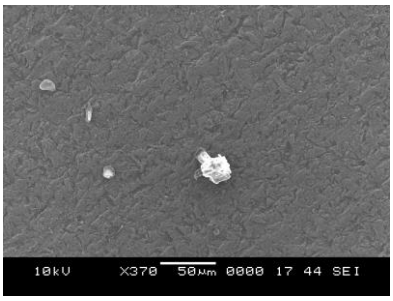	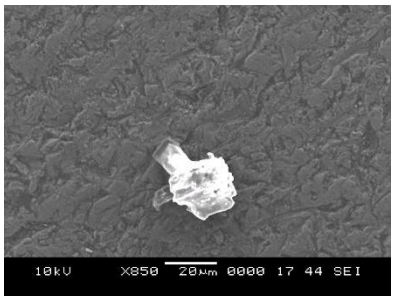

H	25000 lbs, 450 ˚C, 4 Hours	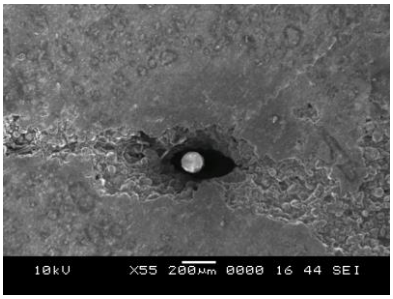	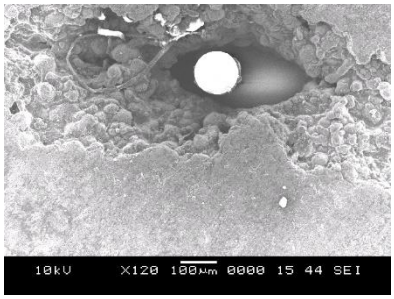
I	25000 lbs, 450 ˚C, 6 Hours	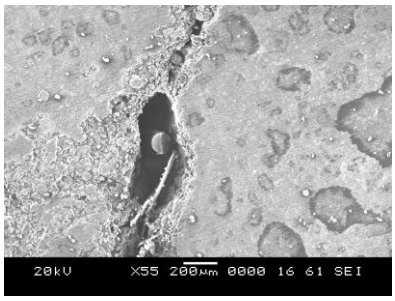	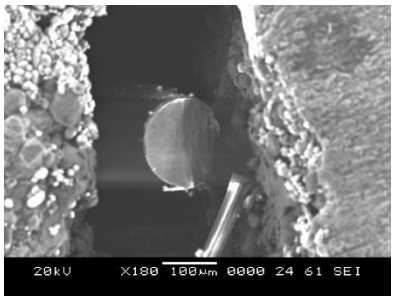
J	25000 lbs, 450 ˚C, 8 Hours	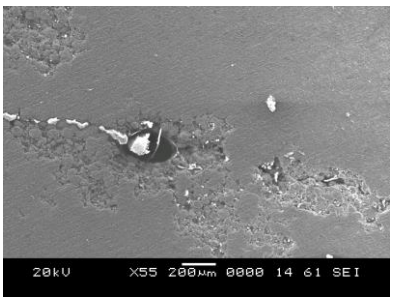	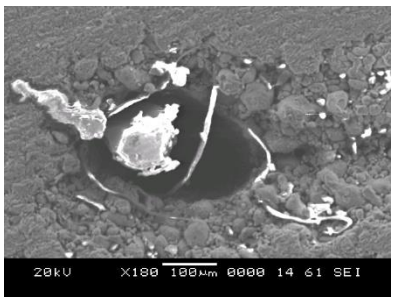

The results show that using the load of 25000 lbs will not give a good compaction for the material, so it is better to use a load of value greater than 25000 lbs. Regarding the sintering temperature, 450˚C was enough to obtain the proper sintering, after 6 hours which has shown better sintering compared with using 4 hours. 8 Hours sintering time affects the fiber by some deformation and melting as shown in sample J, Table 5.7. The oval shapes around the fiber do not give a good expression for the interface between the fiber and the material, and the expected reason for this

shape is the way of cutting the sample. In the beginning, the disc cutter was used to have the sample to be characterized. Later, EDM wire was used to cut the sample. However, the repeated experiments showed that the preparation of the sample i.e. grinding and polishing may affect due to the oscillatory motion of the fiber during the process.

The profile for the pressure and temperature used in the process of compaction and sintering explaind below.

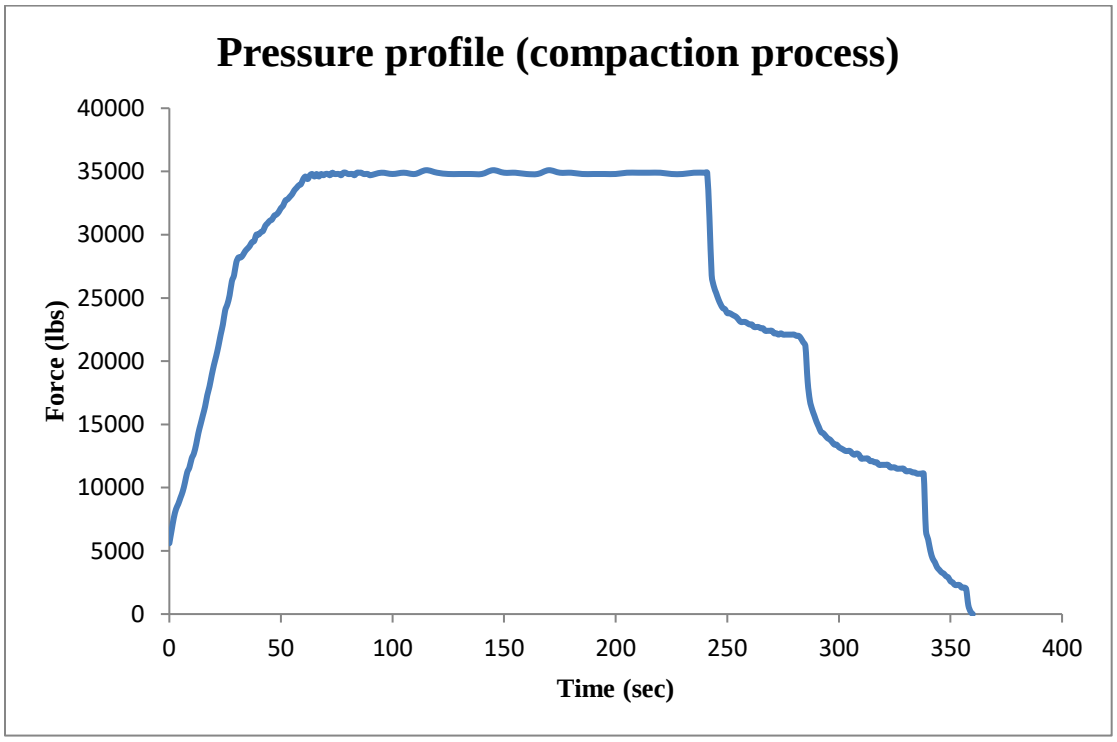

Figure 5.10: Pressure profile

Regarding the compaction machine, the compaction was gradually increasing then it takes a constant value and then de-compacted by steps Figure5.10, where the sintering takes the trend of the regular cycle of heating and cooling Figure5.11.

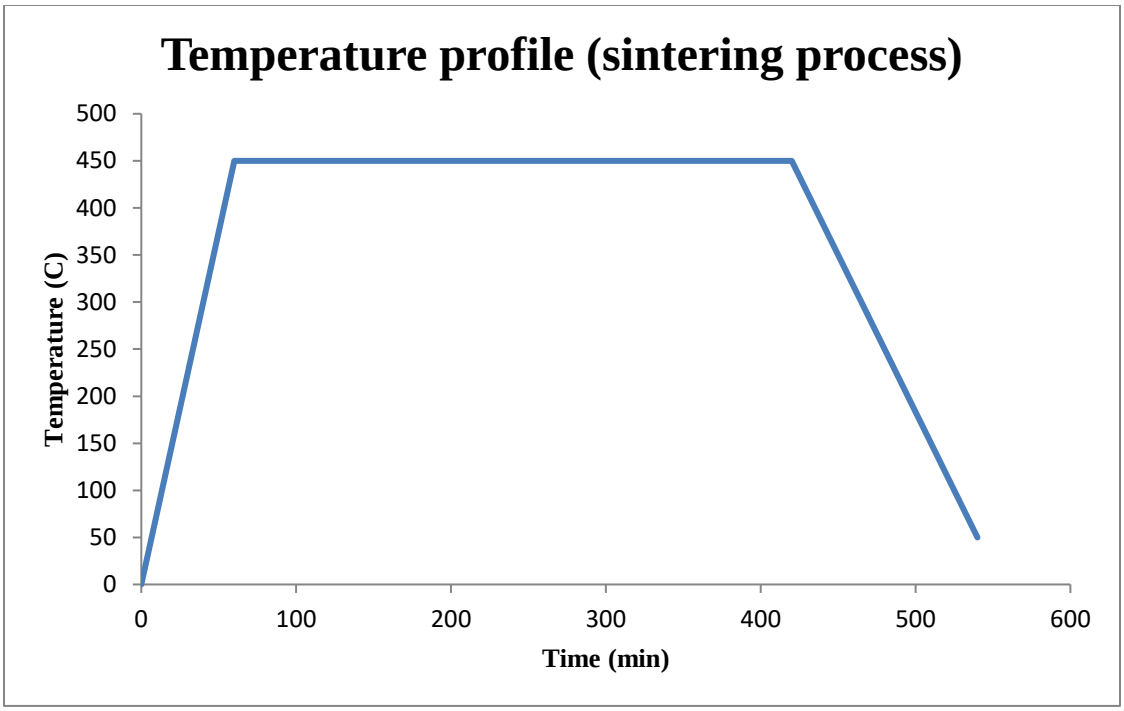

Figure 5.11: Temperature profile

The second method of compaction multi-stage compaction i.e. compact the sample in more than one stage was used to achieve a different purpose which keeps both sides of the fiber extends outside the sample to be tested in the power light test. However, the problem of having broken fiber is developed due to this method. Figures 5.12a shows the sample has a crack in the upper side before removing it from the die, the other two Figures 5.13b,c show the upper side is broken after the sample is removed where The broken part had a layer shape due to compact the sample in multi-stage.

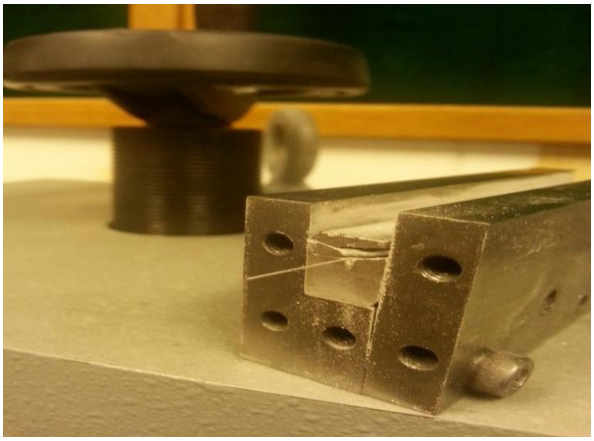

a)

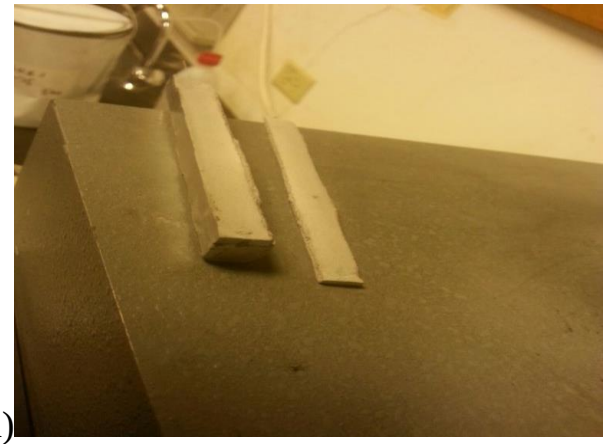

b)

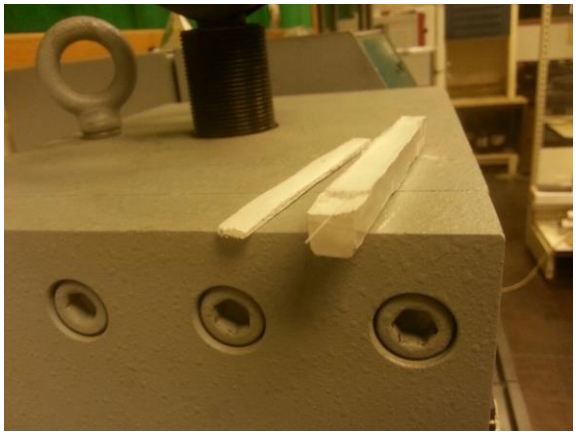

c)

Figure 5.12: Broken samples

5.4.2 Power light test

The functionality of the fiber was tested for the compacted sample shown in Figure - 40:

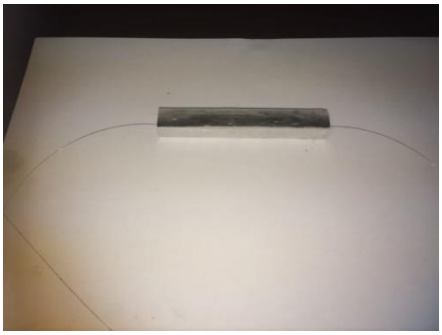

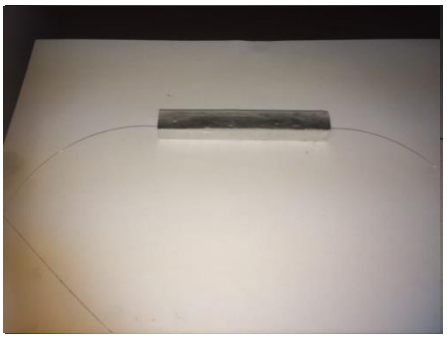

Figure 5.13: Compacted sample

The result of the test shown in Table 5.8, also it is compared with the other method of hosting structures i.e. ABS and PLA materials built using 3D printing.

Table 5.8: Power light test comparison

Power level	Host material	Reference		Sample		Loss		%Loss	
		mW	dBm	mW	dBm	mW	dBm	mw	dBm
Low	PLA	0.18	-7.54	0.14	-8.42	0.04	0.88	22.2	11.7
	Aluminum	0.17	-7.76	0.09	-10.66	0.08	2.9	47	37.4
	ABS	0.18	-7.72	0.05	-13.4	0.13	5.36	72.2	69.4
High	PLA	1.66	2.05	1.36	1.13	0.30	0.92	18	44.9
	Aluminum	1.66	2.05	0.78	-1.41	0.88	3.46	53	168.7
	ABS	1.67	2.22	0.66	-3.44	1.01	5.66	60.5	255

The table shows an intermediate result for the sample of compacted powder compared with the other two materials i.e. PLA and ABS.

5.5 Spark Plasma Sintering (SPS)

Spark Plasma Sintering (SPS) belongs to the powder metallurgy (PM) method to construct the structure. The pressure load and sintering temperature are applied simultaneously on the powder. The temperature induced by internal heat generation source represented by pulse DC electrical current. The current pass through special graphite dies shown in Figure 5.14, to heat up the powder and later sintering the sample. The resulting samples have a cylindrical shape.

Figure 5.14: Graphite dies

The trial was to make holes in the die to insert the fiber inside the powder to have an extended fiber outside the die shown in Figure 5.15.

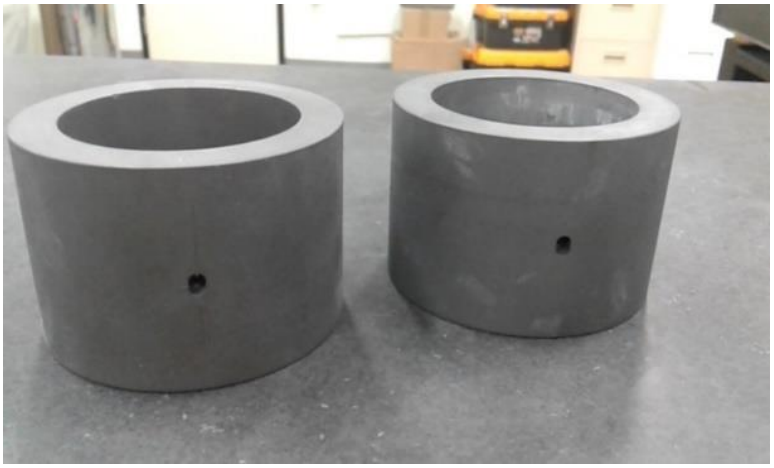

Figure 5.15: Modified die

But, the spark plasma sintering (SPS) machine has a sophisticated setup which limited the possibility of getting a sample to be tested in power light transmission test, Figure 5.16 shows the operational setup for the process. This complication comes from the need of vacuum chamber during the machine Figure 5.16.

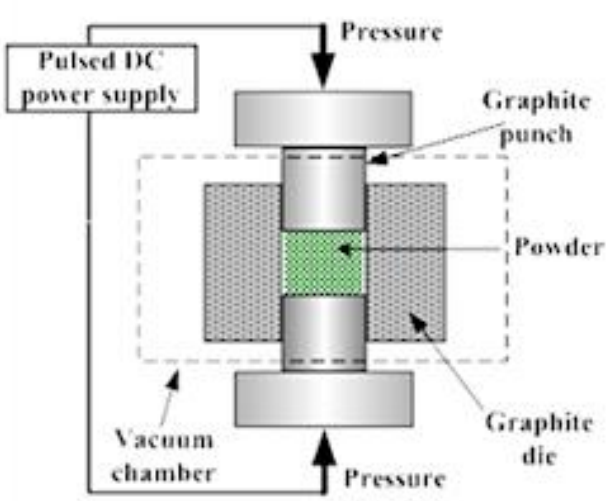

Figure 5.16: Spark Plasma Sintering process

Figure 5.17: Spark Plasma Sintering machine

The vacuum developed inside the chamber causing flushing out the powder from the die that is shown in Figure 5.18.

Figure 5.18: Flushing out of the powder from the die

In term of operating parameters, the process governed by the following parameters:

Heat rate (K). (˚C/min)

Dwell temperature (T). (˚C)

Time (t). (min)

Applied pressure (P). (Mpa)

Three cylindrical samples, using a circular die, were prepared using SPS. The dimension of the sample is 50 mm in diameter, 5 mm in height, and the amount of the powder used was calculated based on the density of the aluminum 2.7 gm/cm^3 to be 26 gm of powder.

The following Table 5.9 shows the parameters used for each sample:

Table 5.9: SPS parameters

	Sample 1	Sample 2	Sample 3
Heat rate(˚C/min)	50	50	50
Temperature (˚C)	400	400	400
Time (min)	30	30	60
Pressure (Mpa)	20	10	20

The following figures show the pressure and temperature profiles for each sample based on the data given from the SPS machine. Since, the SPS process is applying the pressure and temperature at the same time. The process starts pressing the powder at low pressure of 2 MPa and low temperature of 25 ˚C nearly for 3 minutes, this step followed by increasing the pressure, within 4 minutes, to the maximum value as per the programming of the process e.g. 20 MPa for sample #1. With the heat rate of 50 ˚C/min, the temperature reached the maximum e.g. 400 ˚C, the pressure and temperature remain constant until the process is finished, the pressure is removed and temperature gradually decreased. The same procedure is done for all sample with different process parameters to give the following Figure 5.16.

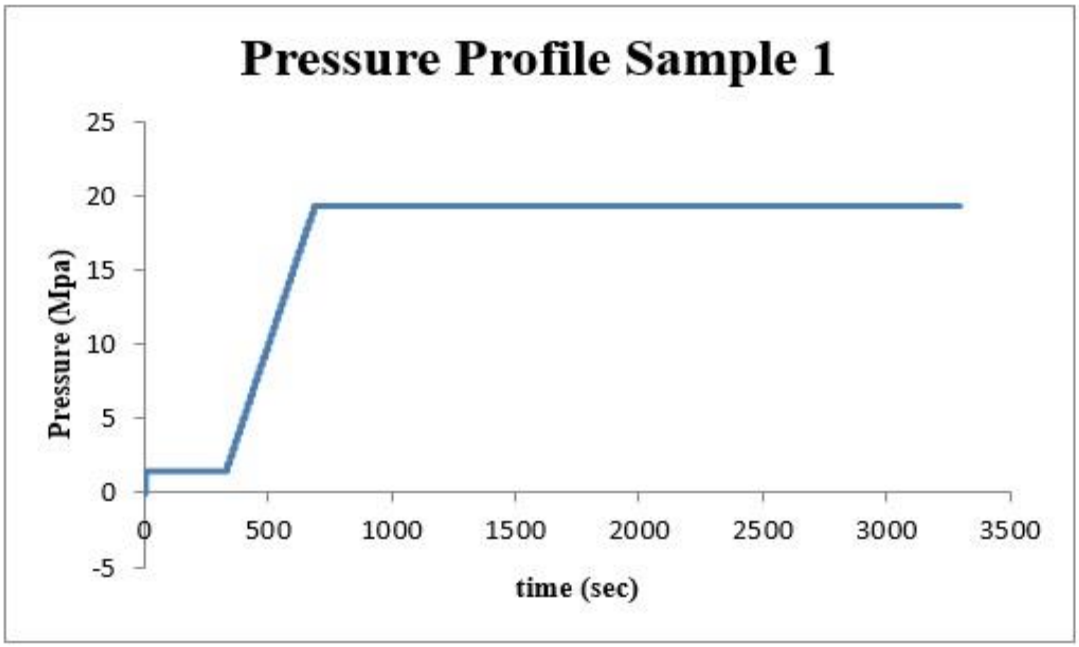
Pressure Profile Sample 1
Pressure (Mpa)
25
20
15
10
5
0
-5
0
500
1000
1500
2000
2500
3000
3500
time (sec)

a)

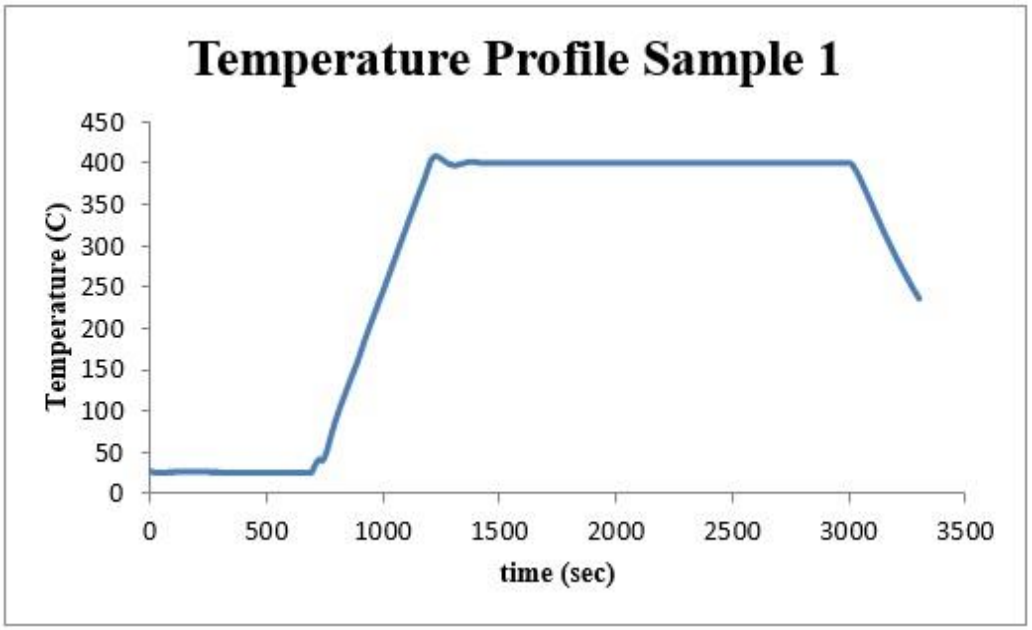
Temperature Profile Sample 1
Temperature (C)
450
400
350
300
250
200
150
100
50
0
0
500
1000
1500
2000
2500
3000
3500
time (sec)

b)

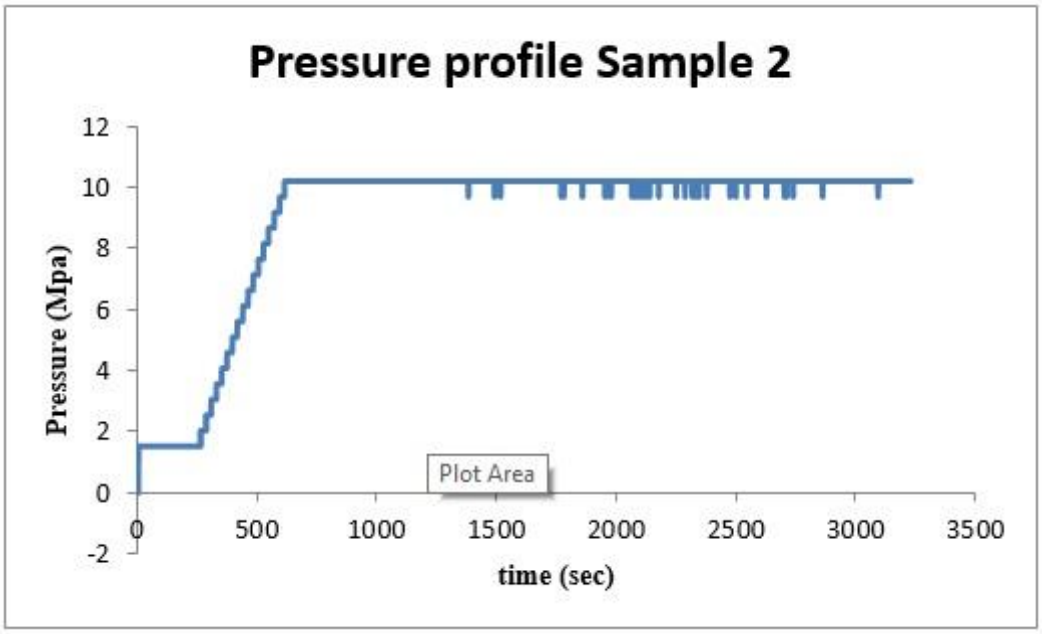
Pressure profile Sample 2
Pressure (Mpa)
12
10
8
6
4
2
0
-2
0
500
1000
1500
2000
2500
3000
3500
time (sec)
Plot Area

c)

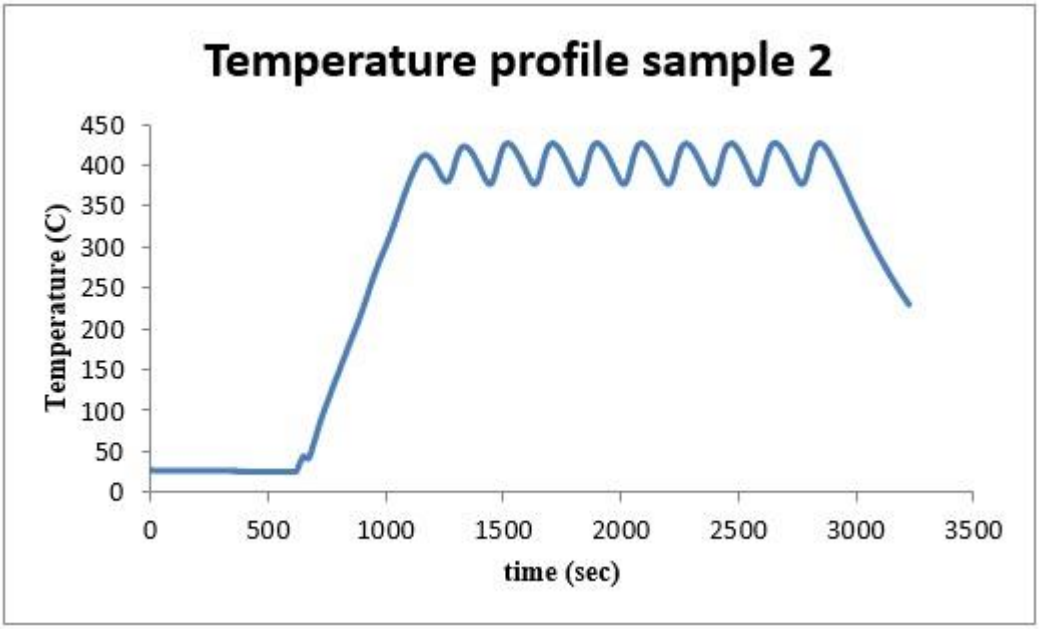
Temperature profile sample 2
Temperature (C)
450
400
350
300
250
200
150
100
50
0
0
500
1000
1500
2000
2500
3000
3500
time (sec)

d)

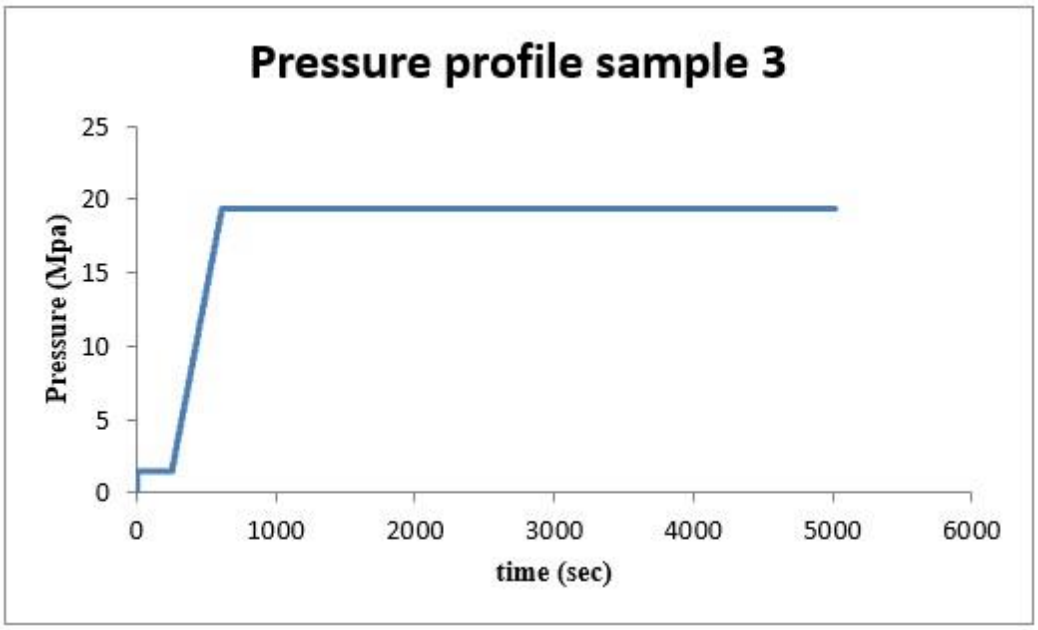

e)

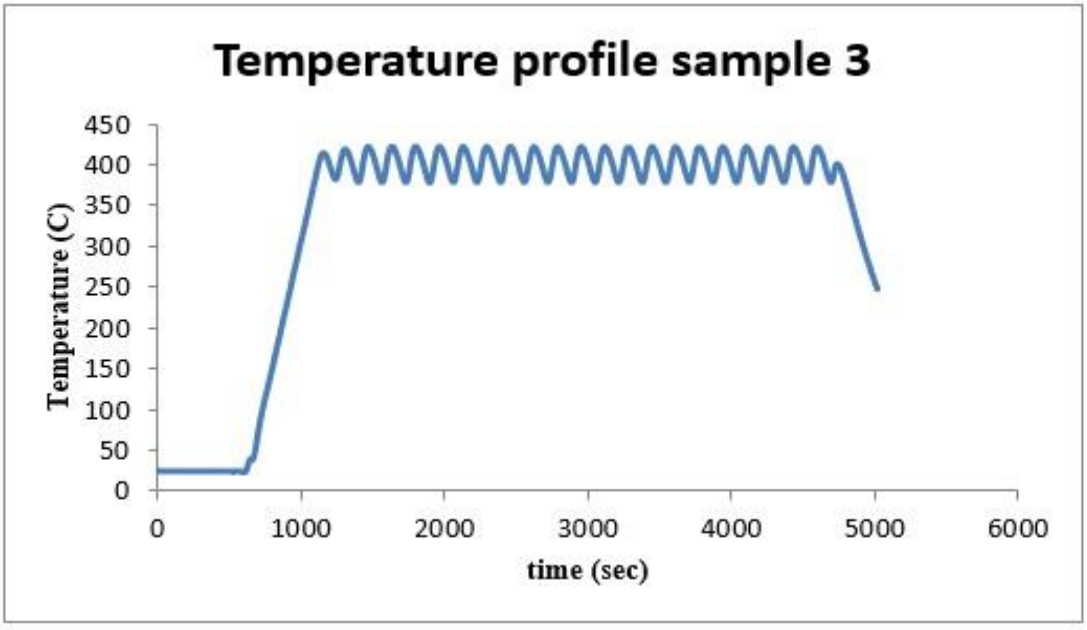

f)

Figure 5.19: Pressure and Temperature profiles for SPS samples

The resulted samples were characterized by taking microscopic pictures for the cross section, the results of these tests are presented in Table 5.10. The density was measured for the resulted samples using densimeter, and hardness using Vickers hardness tester.

Table 5.10: Microscopic picture for the cross section

Sample#	Pictures		Remarks
1	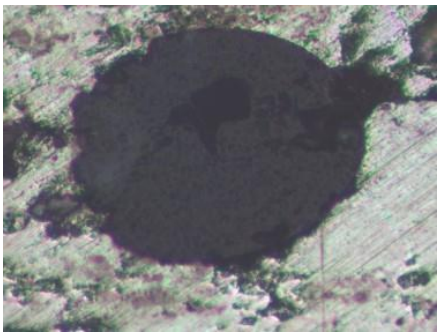		Material well Sintered Little deformation for the fiber
2			Not-well compacted for the material.

3	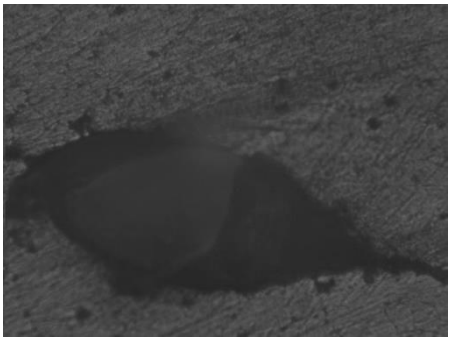	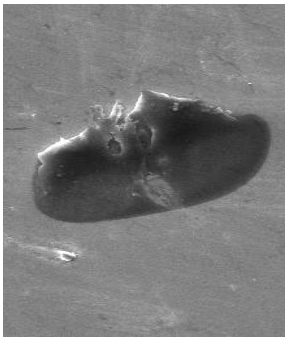	High deformation for the fiber (elliptic shape). Material well Sintered

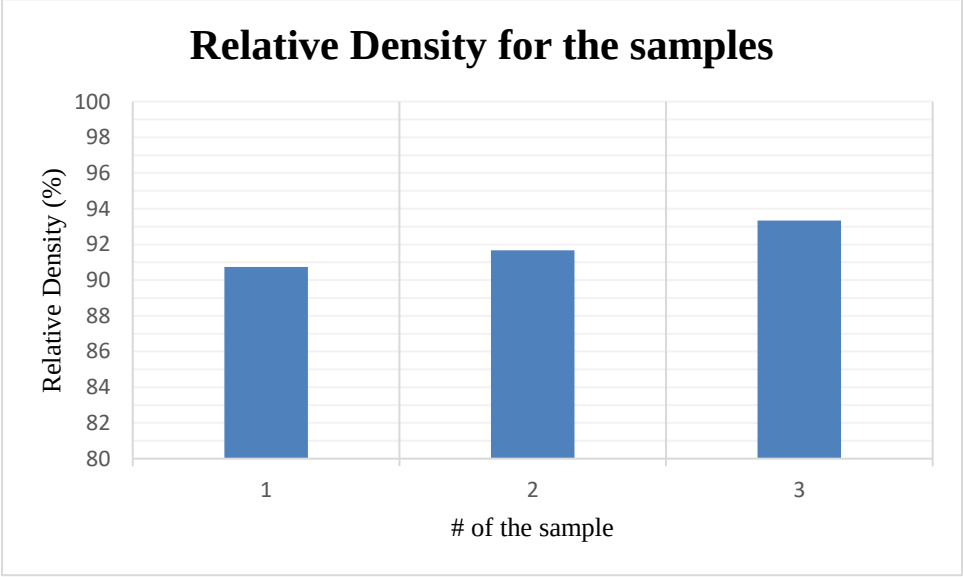

Figure 5.20: Measured relative density

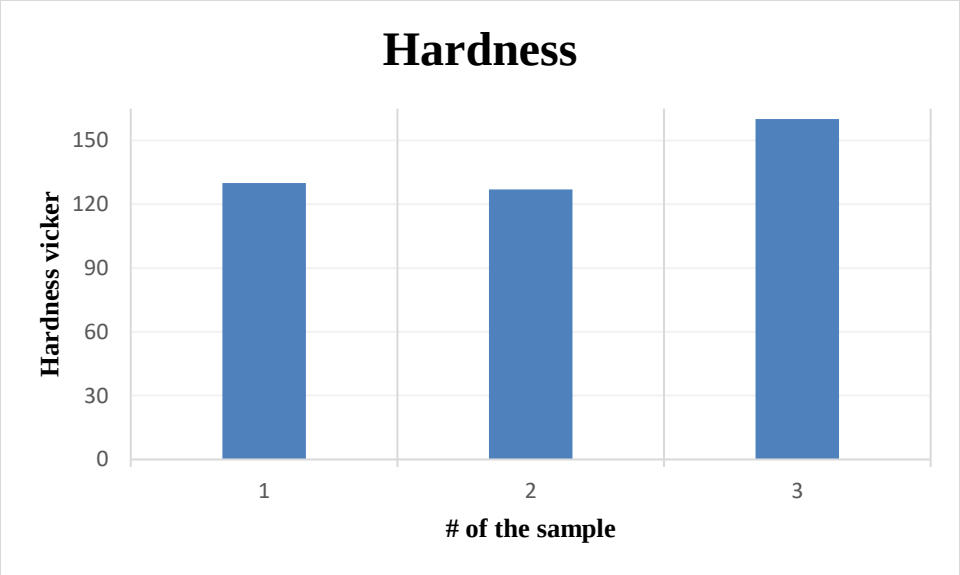

Figure 5.21: Measured hardness

The results of the relative density i.e. theoretical density is 2.7 gm/cm^3, and hardness are show in Figures 5.17,5.18, sample #3 have a high relative density of 93.3 % and high hardness of 160 HV, which is reasonable due to the high pressure and long sintering time. Sample #1 and #2 do not have significant differences in the hardness i.e. 127 HV, 130 HV, densities are 91.7% and 90.7%, respectively.

CHAPTER 6:

RESULTS AND DISCUSSION

The results of this work can be concluded into two major categories:

Characterizing the parameters for both embedding methods i.e. Ultrasonic Consolidation (UC), and Powder Metallurgy (PM), and Achieving the embedding using both methods.

Partially, testing the light transmission through the embedded fiber.

6.1 Characterization of the embedding process parameters:

The UC process is governed by two main operating parameters i.e. amplitude and welding time depending on the ultrasonic available machine. Quantifying the frequency amplitude of the machine that is related to each assigned percentage given by the machine is shown in Table 3.4. Based on that characterization of the power a different test was done to quantify the minimum energy needed to secure the embedding in both indirect and direct ultrasonic consolidation.

The resulting experiments have exhibited the behavior of the fiber embedding from start to full embedding depending on the selected parameters range of values. Based on the previous experiments, the progressive embedding achieved has been summarized by various combinations of the two main parameters i.e. welding time and wavelength amplitude and the effect of having small or large friction area. Figure 6.1 gives an overview of the embedding progress when both parameters are increasing. Full embedding is reached with welding time towards one second combined with a wavelength amplitude of 50% with small area friction and for large area of contact with amplitude larger than 60% and less than 1 sec.

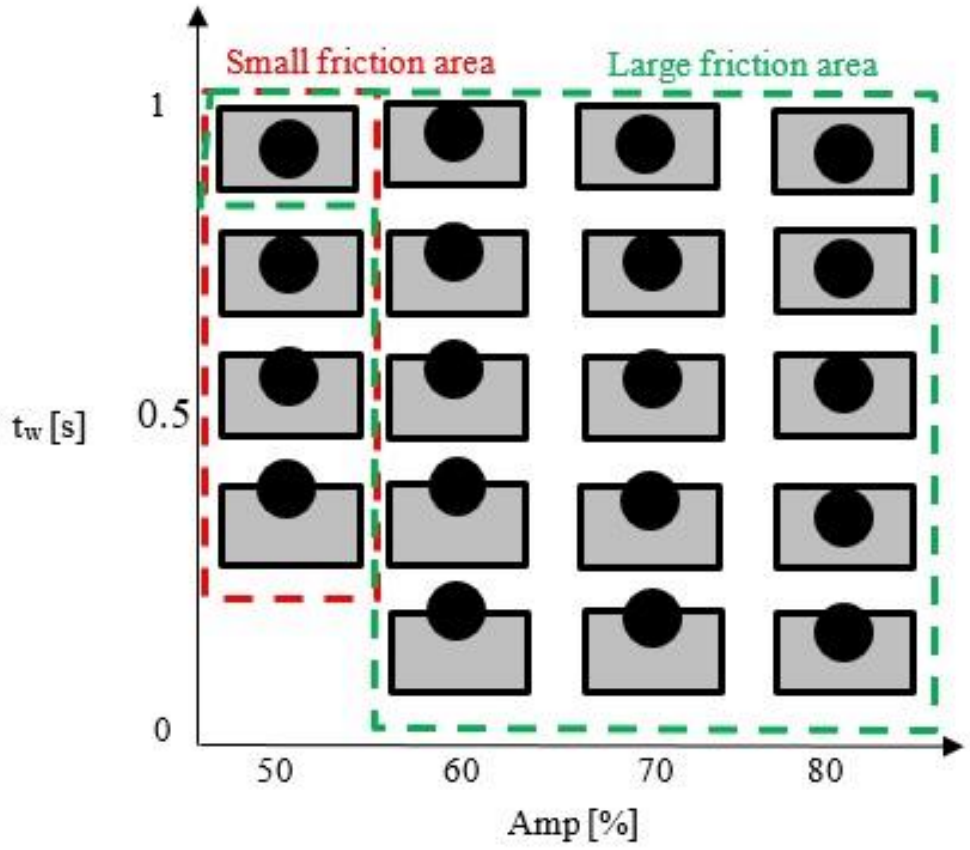

Figure 6.1: Progressive embedding of the fiber inside aluminum at high allowance level of energy using both areas $(A_{fr})_s$ and $(A_{fr})_l$

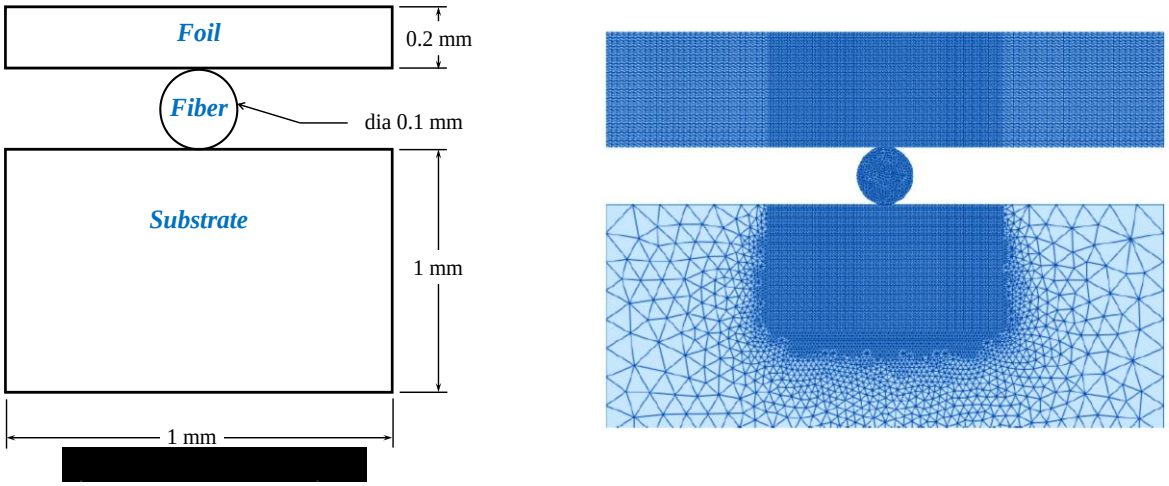

Figure 6.2: Problem Configuration with Model

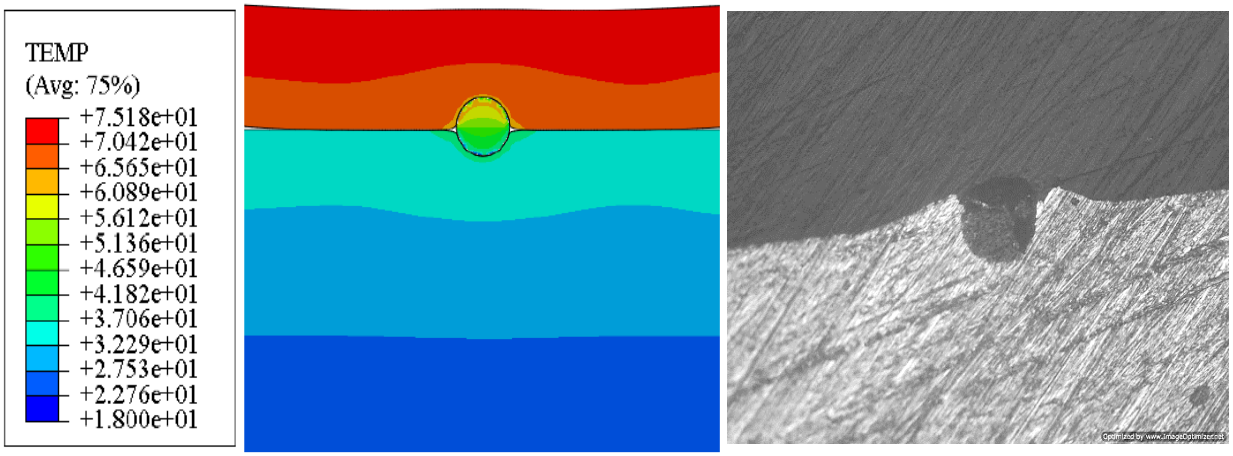

Figure 6.3: a) Temperature (°C) distribution at 20 kHz frequency, 8.4 µm amplitude and 50 MPa load on sonotrode, b) Experimental test with the same parameters on the machine

a) 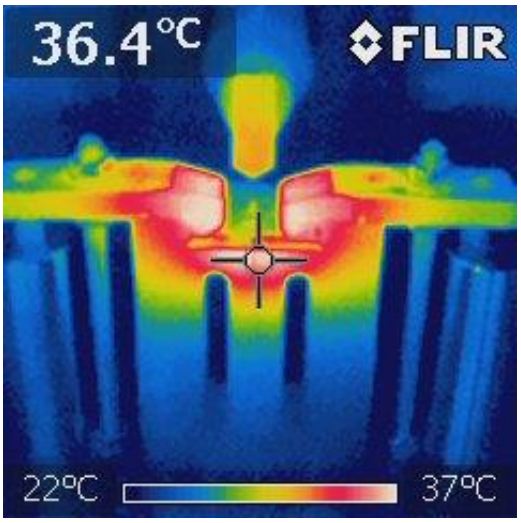

b) 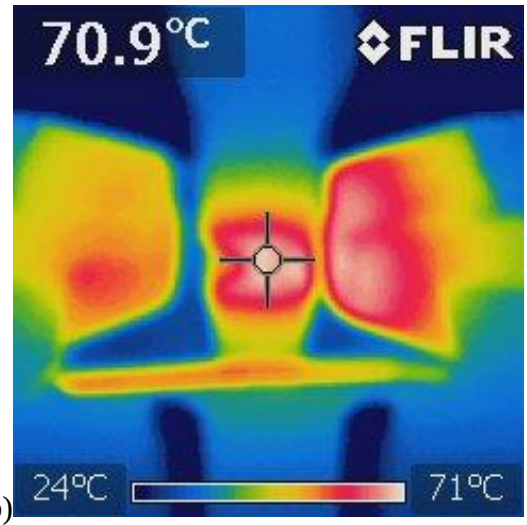

Figure 6.4: Measured temperature a) before US welding, b) zoomed at the time of US welding

The experiment was compared with the simulation done by [62] where the process was modeled by the concept of plastic flow rule with an isotropic hardening model; the previous figures 6.3 and 6.4 show the model used and the comparison between the simulation result and the experiment result which shows good agreement.

Regarding PM, the pressure applied and the sintering temperature combined with the time of sintering were the main parameters governing the process of embedding the fiber. The tests defined the proper parameters of this process result were 35000 lbs as a compaction pressure and the sintering temperature of 450 ˚C applied for 6 hours. Figure 6.5 shows the sample result and cross section of the sample realized using these parameters.

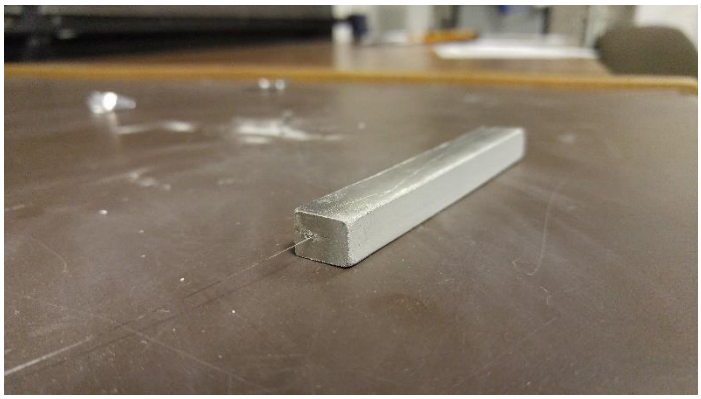

(a)

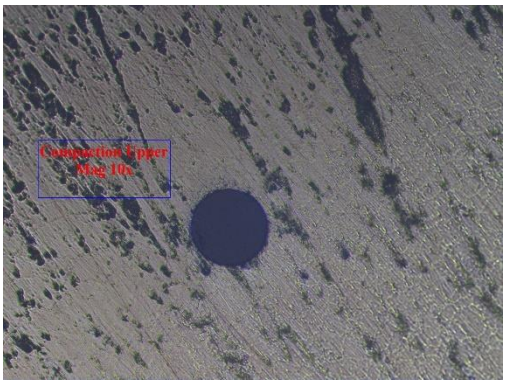

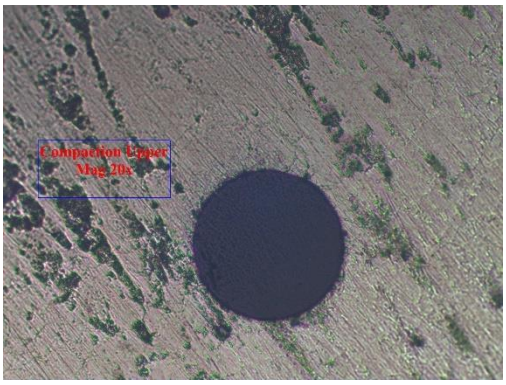

(b) (c)

Figure 6.5: Powder Metallurgy a) resulted sample b) cross section (magnification 10x) c) cross section (magnification 20x)

The SPS process produces different samples, as shown in Figure 6.6, with different mechanical properties depending on the operating parameters e.g. heating rate of 50 ˚C/min, temperature of 400 ˚C and pressure of 20 MPa.

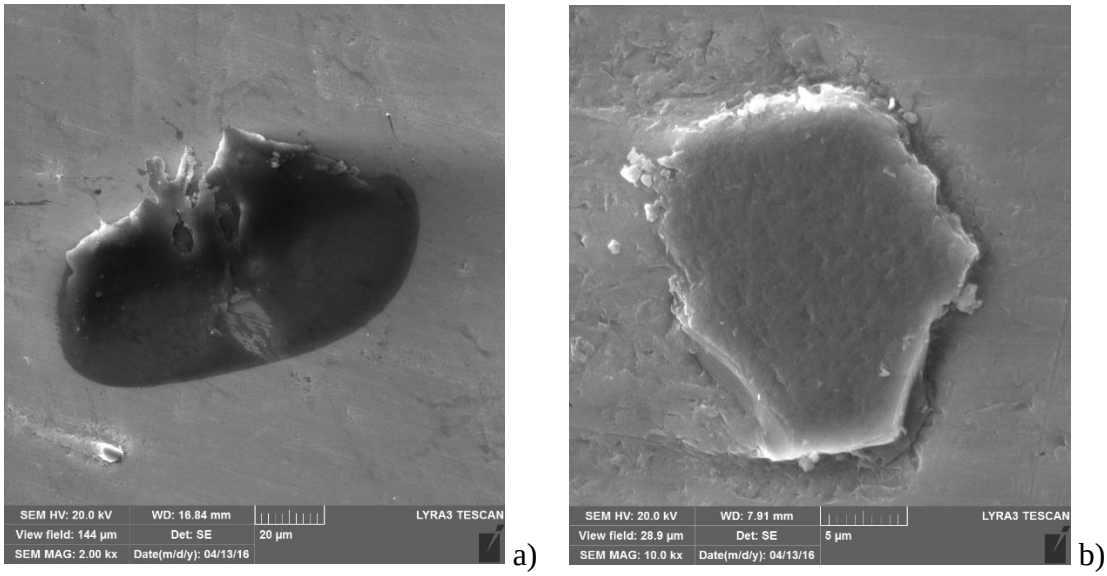

Figure 6.6: SEM for SPS sample with different sintering time a) one hour b) half-hour

In this process, the samples produced were not able to be tested for power light test. The samples do not have extended fiber due to the sophistication preparation process and the processing machine.

6.2 Power light transmission

This test is done for the indirect ultrasonic consolidation, where the light was passed through the fiber after embedding it but with high error due to the change of reflection index of the hosting material compared with that needed from the cladding. This error is produced due to the diffraction of the light which let the low amount of light to be passed through the fiber. In the direct ultrasonic consolidation, despite embedding the fiber, it was noticed that the fiber was broken due to the direct force applied to the fiber. The reason behind is that the fiber has lost its coating because of the combined loads i.e. mechanical and thermal, which make it easy to be broken. For more

investigation on direct ultrasonic consolidation, more attention should be given during the consolidation to keep continuous unbroken fiber for power light transmission test.

Regarding the powder metallurgy, the previous chapter - 5 showed the result of testing the functionality of the fiber embedded within aluminum-based powder material using cold compaction process. These results were compared with the 3D printing process of embedding using two different material i.e. Aluminum powder based structure had an intermediate result. But, unfortunately, the SPS did not produce a sample to be tested for in power light transmission test.

CHAPTER 7:

CONCLUSION AND RECOMMENDATIONS

7.1 Concluding Remarks

This work focused on defining the proper parameters of the process for proper embedding of optical fiber inside metal based material e.g. aluminum sheet using ultrasonic consolidation (UC), and powder based material e.g. aluminum powder using powder metallurgy (PM). This work was carried out based on extensive experiments starting from characterizing the fiber, investigating the process and the parameters affecting this process, and followed by repeated experiments to converge to suitable parameters of both methods. The functionality of the fiber was checked using the power light test through the fiber.

For the (UC), the numerical simulation validated the experimental tests, where almost the same embedding achieved in the tests was carried out using the simulation of the process.

7.2 Accomplishments

The related accomplishments are summarized as follow:

To investigate the process of fiber embedding for both methods and the effective parameters that govern building the structures.

To define the proper parameters of both methods to secure a suitable embedding for the fiber within the hosting material.

The functionality was checked partially for the embedding fiber.

7.3 Future Work

The main process of embedding i.e. Ultrasonic Consolidation could be extended to use the Fiber Bragg Gratings (FBG)s in the embedding process, and used a different type of materials i.e. plastics and other metals to host the fiber. Furthermore, investigating the proper parameters for embedding, opens the door to get a device dedicated to this process of embedding.

Once the process parameters are well defined from the previous investigation, a conceptual analysis would be carried out to come up with the best operating concept with defined functionalities needed to run the process of embedding properly. The design specifications will be defined from prior process investigation regarding the range of frequencies, welding time, the amplitude of wavelength and pressure force. The investigation of the embedding process in addition to the operating conditions of the machine will lead to a complete visualization of the concept to be selected and build a prototype of our machine to be initially tested and validated. For more validation, extensive assessment tests would be done for the machine to ensure the complete working with high efficiency. Other features e.g. mobility and safety conditions will be observed.

References

[1] S. Mekid and O. J. Kwon, “Nervous Materials: A New Approach for Better Control, Reliability and Safety of Structures,” *Sci. Adv. Mater.*, vol. 1, no. 3, pp. 276–285, 2009.

[2] K. Schabowicz, “State-of-the-art non-destructive methods for diagnostic testing of building structures – anticipated development trends,” vol. X, no. 3, pp. 8–9, 2010.

[3] R. D. Adams and P. Cawley, “A review of defect types and nondestructive testing techniques for composites and bonded joints,” vol. 21, no. 4, 1988.

[4] J. M. Ko and Y. Q. Ni, “Technology developments in structural health monitoring of large-scale bridges,” *Eng. Struct.*, vol. 27, no. 12 SPEC. ISS., pp. 1715–1725, 2005.

[5] X. P. Qing, S. J. Beard, A. Kumar, H. L. Chan, and R. Ikegami, “Advances in the development of built-in diagnostic system for filament wound composite structures,” *Compos. Sci. Technol.*, vol. 66, no. 11–12, pp. 1694–1702, 2006.

[6] S. Mekid, N. Saheb, S. M. A. Khan, and K. K. Qureshi, “Towards sensor array materials: can failure be delayed?,” *Sci. Technol. Adv. Mater.*, vol. 16, no. 3, p. 34607, 2015.

[7] N. Saheb and S. Mekid, “Fiber-embedded metallic materials: From sensing towards nervous behavior,” *Materials (Basel).*, vol. 8, no. 11, pp. 7938–7961, 2015.

[8] Http://www.mechengg.net/2015/01/introduction-to-engineering-material.html, “Material Classification.” .

[9] C. Budelmann and B. Krieg-Bruckner, “From sensorial to smart materials: Intelligent optical sensor network for embedded applications,” *J. Intell. Mater. Syst. Struct.*, vol. 24, no. 18, pp. 2183–2188, 2012.

[10] I. Chopra, “Review of State of Art of Smart Structures,” *Aiaa J.*, vol. 40, no. 11, pp. 16–19, 2002.

[11] G. Akhras, “Smart Materials and Smart Systems for the Future,” *Can. Mil. J.*, pp. 25–32, 2000.

[12] Https://www.slideshare.net/Biswajit_A/smart-materials-34678533, “Smart material classification.”

[13] M. L. Sabolinski, O. Alvarez, M. Auletta, G. Mulder, and N. L. Parenteau, “Cultured skin as a ‘smart material’ for healing wounds: Experience in venous ulcers,” *Biomaterials*, vol. 17, no. 3, pp. 311–320, 1996.

[14] S. Kamila, “Introduction, classification and applications of smart materials: An overview,” *Am. J. Appl. Sci.*, vol. 10, no. 8, pp. 876–880, 2013.

[15] D. S. Levi, N. Kusnezov, and G. P. Carman, “Smart materials applications for pediatric cardiovascular devices,” *Pediatr. Res.*, vol. 63, no. 5, pp. 552–558, 2008.

[16] K. Address, “Fiber optic sensors and their applications,” no. May, pp. 1–6, 2009.

[17] P. Information, “SMF-28 ™ Fiber,” *Coating*.

[18] F. Type, “Multimode vs . Singlemode – Fiber Bandwidth,” no. Mm, 2000.

[19] R. Leucht and H. J. Dudek, “Properties of SiC-fibre reinforced titanium alloys processed by fibre coating and hot isostatic pressing,” *Mater. Sci. Eng. A*, vol. 188, no. 1–2, pp. 201–210, 1994.

[20] X. Luo, Y. Q. Yang, Y. C. Liu, Z. J. Ma, M. N. Yuan, and Y. Chen, “The fabrication and property of SiC fiber reinforced copper matrix composites,” *Mater. Sci. Eng. A*, vol. 459, no. 1–2, pp. 244–250, 2007.

[21] N. P. Bansal, “CVD SiC fiber-reinforced barium aluminosilicate glass-ceramic matrix composites,” vol. 220, pp. 129–139, 1996.

[22] G. Jiang, M. Dawood, K. Peters, and S. Rizkalla, “Self-monitoring fiber reinforced polymer strengthening system for civil engineering infrastructures,” *Proc. SPIE*, vol. 6934, pp. 693406-693406–12, 2008.

[23] I. Paper, “Fiber Optic Smart Structures,” vol. 84, 1996.

[24] C. Wu, Y. Zhang, and B. Guan, “Simultaneous Measurement of Temperature and Hydrostatic Pressure Using Bragg Gratings in Standard and Grapefruit Microstructured Fibers,” vol. 11, no. 2, pp. 489–492, 2011.

[25] Güemes A, Fernandez-Lopez A and Hernandez-Crespo B 2013 Monitoring damage growth in composite materials by FBG sensors Proc. 5th Int. Conf. on NDT in Aerospace (Singapore,)

[26] A. Platforms, “Fiber Optic Sensors for Structural Health Monitoring of Air Platforms,” pp. 3687–3705, 2011.

[27] I. Transactions and O. N. Microwave, “Fiber-Optic Fabry-Perot Interferometer Sensor Applications,” pp. 1612–1621, 1982.

[28] M. Majumder, T. K. Gangopadhyay, A. K. Chakraborty, K. Dasgupta, and D. K. Bhattacharya, “Sensors and Actuators A : Physical Fibre Bragg gratings in structural health monitoring — Present status and applications,” vol. 147, pp. 150–164, 2008.

[29] S. Minakuchi and N. Takeda, “Photonic Sensors Recent Advancement in Optical Fiber Sensing for Aerospace Composite Structures [redacted] vol. 3, no. 4, pp. 345–354, 2013.

[30] G. Luyckx, E. Voet, N. Lammens, and J. Degrieck, “Strain measurements of composite laminates with embedded fibre bragg gratings: Criticism and opportunities for research,” *Sensors*, vol. 11, no. 1, pp. 384–408, 2011.

[31] D. Kinet, P. Mégret, K. W. Goossen, L. Qiu, D. Heider, and C. Caucheteur, “Fiber Bragg grating sensors toward structural health monitoring in composite materials: challenges and solutions,” *Sensors*, vol. 14, no. 4, pp. 7394–7419, 2014.

[32] G. Rajan, M. Ramakrishnan, Y. Semenova, E. Ambikairajah, G. Farrell, G. Peng, and L. Member, “Experimental Study and Analysis of a Polymer Fiber Bragg Grating Embedded in a Composite Material,” vol. 32, no. 9, pp. 1726–1733, 2014.

[33] G. Rajan, Y. Mohd, B. Liu, E. Ambikairaja, D. J. Webb, and G. Peng, “Sensors and Actuators A : Physical A fast response intrinsic humidity sensor based on an etched singlemode polymer fiber Bragg grating,” *Sensors Actuators A. Phys.*, vol. 203, pp. 107–111, 2013.

[34] X. Zhang, “Sensitivity alteration of fiber Bragg grating sensors through on-fiber metallic coatings produced by a combined laser-assisted maskless microdeposition and electroless plating process,” 2013.

[35] Y. Li, W. Liu, Y. Feng, and H. Zhang, “Ultrasonic embedding of nickel-coated fiber Bragg grating in aluminum and associated sensing characteristics,” *Opt. Fiber Technol.*, vol. 18, no. 1, pp. 7–13, 2012.

[36] O. Engineering, “Effect of metalizing nickel on the spectrum of fiber Bragg grating Effect of metalizing nickel on the spectrum of fiber Bragg grating,” no. May, 2013.

[37] G. D. Janaki Ram, Y. Yang, and B. E. Stucker, “Effect of process parameters on bond formation during ultrasonic consolidation of aluminum alloy 3003,” *J. Manuf. Syst.*, vol. 25, no. 3, pp. 221–238, 2006.

[38] S. ichi Matsuoka and H. Imai, “Direct welding of different metals used ultrasonic vibration,” *J. Mater. Process. Technol.*, vol. 209, no. 2, pp. 954–960, 2009.

[39] K. Graff, C. Albright, A. Benatar, and S. Rokhlin, “Mechanics and Mechanisms of Ultrasonic Metal Welding Dissertation Presented in Partial Fulfillment of the Requirements for the Degree Doctor of Philosophy In the Graduate School of The Ohio State University By,” 2004.

[40] P. Taylor and N. Biernadskij, “Ultrasonic welding of non-ferrous metals,” *Weld. Int.*, vol. 3, no. September, pp. 37–41, 2014.

[41] C. Y. Kong, R. C. Soar, and P. M. Dickens, “Optimum process parameters for ultrasonic

consolidation of 3003 aluminium," vol. 146, pp. 181–187, 2004.

[42] V. N. Khmelev, A. N. Slivin, and A. D. Abramov, "Model of process and calculation of energy for a heat generation of a welded joint at ultrasonic welding polymeric thermoplastic materials," - *Proc.*, pp. 316–322, 2007.

[43] J. R. Baer, W. Zhu, L. V Reatherford, A. J. Grima, D. J. Scholl, D. E. Wilkosz, S. Fatima, and S. M. Ward, "Robustness in Aluminum Automotive Body."

[44] Kerry's (Ultrasonics) Limited, UK, "Ultrasonic welding," *Vacuum*, vol. 16, no. 4, p. 210, 1966.

[45] Z. Al-Sarraf, M. Lucas, and P. Harkness, "A numerical and experimental study of ultrasonic metal welding," *IOP Conf. Ser. Mater. Sci. Eng.*, vol. 42, p. 12015, 2012.

[46] J. Tsujino, T. Ueoka, K. Hasegawa, Y. Fujita, T. Shiraki, T. Okada, and T. Tamura, "New methods of ultrasonic welding of metal and plastic materials," *Ultrasonics*, vol. 34, no. 2–5, pp. 177–185, 1996.

[47] S. M. Allameh, C. Mercer, D. Popoola, and W. O. Soboyejo, "Microstructural characterization of ultrasonically welded aluminum," *J. Eng. Mater. Technol.*, vol. 127, no. 1, p. 65, 2005.

[48] C. Y. Kong, R. C. Soar, and P. M. Dickens, "Characterisation of aluminium alloy 6061 for the ultrasonic consolidation process," vol. 363, pp. 99–106, 2003.

[49] C. Y. Kong, R. C. Soar, and P. M. Dickens, “Ultrasonic consolidation for embedding SMA fibres within aluminium matrices,” *Compos. Struct.*, vol. 66, no. 1–4, pp. 421–427, 2004.

[50] C. Y. Kong and R. C. Soar, “Fabrication of metal-matrix composites and adaptive composites using ultrasonic consolidation process,” *Mater. Sci. Eng. A*, vol. 412, no. 1–2, pp. 12–18, 2005.

[51] C. Mou, P. Saffari, D. Li, K. Zhou, L. Zhang, R. Soar, and I. Bennion, “Embedded fibre Bragg grating array sensors in aluminium alloy matrix by ultrasonic consolidation,” *Proc. SPIE*, vol. 7004, p. 70044B–70044B–4, 2008.

[52] A. R. Akisanya, A. C. F. Cocks, and N. A. Fleck, “The yield behaviour of metal powders,” *Int. J. Mech. Sci.*, vol. 39, no. 12, pp. 1315–1324, 1997.

[53] I. Sridhar and N. A. Fleck, “Yield behaviour of cold compacted composite powders,” *Acta Mater.*, vol. 48, no. 13, pp. 3341–3352, 2000.

[54] H. A. Al-Qureshi, M. R. F. Soares, D. Hotza, M. C. Alves, and A. N. Klein, “Analyses of the fundamental parameters of cold die compaction of powder metallurgy,” *J. Mater. Process. Technol.*, vol. 199, no. 1, pp. 417–424, 2008.

[55] O. Skrinjar and P. L. Larsson, “Cold compaction of composite powders with size ratio,” *Acta Mater.*, vol. 52, no. 7, pp. 1871–1884, 2004.

[56] H. A. Al-Qureshi, A. Galiotto, and A. N. Klein, “On the mechanics of cold die compaction for powder metallurgy,” *J. Mater. Process. Technol.*, vol. 166, no. 1, pp. 135–143, 2005.

[57] C. L. Martin, “Elasticity, fracture and yielding of cold compacted metal powders,” *J. Mech. Phys. Solids*, vol. 52, no. 8, pp. 1691–1717, 2004.

[58] P. R. Heyliger and R. M. McMeeking, “Cold plastic compaction of powders by a network model,” *J. Mech. Phys. Solids*, vol. 49, no. 9, pp. 2031–2054, 2001.

[59] N. Saheb, Z. Iqbal, A. Khalil, A. S. Hakeem, N. Al Aqeeli, T. Laoui, A. Al-Qutub, and R. Kirchner, “Spark plasma sintering of metals and metal matrix nanocomposites: A review,” *J. Nanomater.*, vol. 2012, 2012.

[60] S. Mekid, AM.Butt and KK. Qureshi, “Characterization of Fiber Optics Integrity Under Several Embedding Parameters in Smart Materials Characterization of Fiber Optics Integrity Under Several,” no. October, pp. 0–6, 2015.

[61] A. Abubakar, S. Khan, S. Mekid, “On the modeling of fibers embedding In aluminum using ultrasonic consolidation,” J. Eng. Mater. Technol., Vol. 139 (3) (2017)

Vitae

Name :Hammam Saeed Rizq Daraghma

Nationality :Palestinian

Date of Birth :8/24/1989

Email :hammamsaied1989@hotmail.com

Address :KSA-Dhahran-King Fahd university of Petroleum and Minerals

Academic Background :2012: Bachelor Degree in Mechanical Engineering/ An-Najah National University-Nablus-Palestine

Publications:

Conferences:

1. Samir Mekid, Nouari Saheb, **Hammam Daraghma**, Asad Butt and Khurram Qureshi. "Upscaling Sensing Materials with Challenges of Sensors Embedding in Powder Based Materials and Polymers", ASME 2015 Conference on Smart Materials, Adaptive Structures and Intelligent Systems
2. S. Mekid, **H. Daraghma**. "Experimental Ultrasonic Consolidation of FBGs in Aluminum", Advances in Manufacturing Technology/ Advances in Transdisciplinary Engineering, Volume 6, 84 – 89

Journals:

1. S. Mekid, **H. Daraghma.** “Experimental ultrasonic sub-surface consolidation of fiber bragg grating for sensorial materials”, Journal of Materials Processing Tech. 252 (2018) 673–679.